McGILL UNIVERSITY

Josephson tunneling in unconventional and topological superconductors

Rosa Rodríguez Mota

Department of Physics

December 2017

McGill University, Montreal, Quebec

A thesis submitted to McGill University in partial fulfillment of the requirements of the degree of Doctor of Philosophy

A mi abuelo y mi tía Vero

Abstract

The phase sensitivity of the Josephson effect makes it a powerful tool to probe superconductors with unusual properties. In this thesis, we study three different setups that highlight the usefulness of the Josephson effect to find experimental signatures of unconventional and topological superconductivity. The first studied setup consist of a tunnel junction between an s-wave and an unconventional $s_{\pm}$ superconductor. The second studied setup is a topological version of a Josephson junction ring coupled to a quantum dot. The third and final setup is a topological Josephson junction in the presence of phase fluctuations caused by charging effects. While this thesis comprises of studies of different materials, the results from the three projects presented here exhibit: a) how the Josephson tunneling can be used to probe superconductors with unusual properties and b) the need for theoretical models of Josephson tunneling that account for variations and fluctuations of the superconducting order parameter.

Résumé

La sensibilité de phase de l'effet Josephson en fait un outil puissant pour étudier les supraconducteurs aux propriétés anormales. Dans cette thèse, nous étudions trois contextes qui mettent en valeur les bienfaits de l'utilisation de l'effet Josephson pour détecter la signature expérimentale d'une supraconductivité non conventionnelle et topologique. La première situation étudiée correspond à une jonction en tunnel entre un supraconducteur de symétrie s-wave et un supraconducteur non conventionnel de symétrie $s_{\pm}$. La deuxième situation étudiée est une version topologique d'un anneau de jonctions Josephson couplée à une boîte quantique. La troisième et dernière situation représente une jonction Josephson topologique en présence de fluctuations de phase causées par des effets de charge. Cette thèse regroupe l'étude de matériaux différents, mais les résultats présentés démontrent tous que a) l'effet tunnel Josephson peut être utilisé pour étudier des supraconducteurs aux propriétés anormales et b) qu'il est nécessaire de créer des modèles théoriques de l'effet tunnel Josephson qui puissent prendre en compte les variations et fluctuations du paramètre d'ordre supraconducteur.

Acknowledgments

This work is the combination of several projects that have been a very important part of my life for the last five years. As a result, I find myself with a long list of people to thank and acknowledge.

First of all, this work would not have been possible without the apt supervision of Prof. Tami Pereg-Barnea. Tami, I really thank you for believing in me and in my ideas. I also thank you for all the support and guidance that I received from you throughout these years both professionally and personally.

I also want to thank our collaborators: Prof. Smitha Vishveshwara and Prof. Erez Berg. Your insights and contributions were extremely valuable for the completion of this work. Likewise, I want to thank my supervisory Committee members, Prof. Bill Coish and Prof. Dave Cooke, for their support.

I want to thank my office-mates for achieving the insurmountable task of making an office in the horrible Rutherford Physics Building a great place to work. Yony, Grace, Aaron Farrell, Jan, Kunal and Aaron McClendon, there are so many things to thank you for! From proof-reading my work (a.k.a correcting all of my English prepositions) to providing moral support and much needed distraction with cute animals videos to writing the thesis template I am using at this moment. I am so happy I met you and, even more so, that I got to share a space with you.

I also want to thank all of my other group members that I, sadly, did not get to share an office with. Olivier, Alexandre, Geremia and Etienne, I truly enjoyed working with you. I am also very thankful for you questions, insights and interest regarding my work.

There are many great people in McGill Physics Department, and I am very happy to count some of you as friend and colleagues. Erika, I particularly want to thank you for existing and for being my friend. I love you. You are really fun and hardworking and I admire you so much. I also want to thank all of the people I worked in with from the Department in not research related projects. Maddy, Paula, Hannah and Auriane, you ladies are absolutely amazing!

During my time in Montreal, I have had the pleasure of having many Mexican friends who have supported me. Sandra, I can not even begin to tell you how grateful I am to count you as a friend. You have provided me with all of the love and support of a life partner despite being married to someone else. Diego, I am probably not being very objective here but, I truly believe you are the best roommate that ever existed. I really appreciate all of your support, and I also think you are an amazing person. I am really happy to have shared an apartment with you. Mario and Sonia, I want to thank you for providing me with a small family in Montreal. I really appreciate that you are always there when I need you or when I need some distraction. I am so grateful that I, so very randomly, met you. Manuel and Lilia, I really want to thank you for still inviting me to your house, despite me being competitive at board games and always making Hugo cry.

I also want to thank my physics friend that are not in Montreal. La Pandilla, I want to thank you for encouraging me from afar, making me laugh and providing company during travels. Roi, I truly appreciate that you always manage to Skype in on my birthday, you have no idea how happy you have made me. Arturo, thank you for encouraging me to write papers via Gmail chat. Emilio, I also thank you for your encouragement and support and for your visit. Yunuen and Gabrielle, I am so happy you are in Montreal. And that I get to hang out, eat quesadillas and drink mezcal with you.

John, I want to thank you for feeding and taking care of me during the last weeks of writing. Saying that this could not have been done without you is an understatement.

Last but not least, I want to thank all of my family for their encouragement and support. I am incredibly thankful to have received support form my parents, my siblings, my cousins, my grandparents and my aunts and uncles. *Pa, te agradezco muchísimo todo tu apoyo y toda tu confianza. Mami, muchas gracias por cuidarnos a todos. A los dos, les agradezco tanto que siempre me hayan empujado a desarrollar mis propias ideas. Los quiero y los admiro mucho! Javier y Cony, muchas gracias por sacarme a pasear, ponerme a ver películas y discutir conmigo en todas mis visitas. Jorge y Lucy, gracias por recibirme en su casa y dejarme jugar con Marinita. Abuelita Rosita, aprecio infinitamente que seas mi fan y que creas en mi. Abue Lucy, gracias por todo, admiro mucho la fortaleza que has mostrado estos últimos años.*

Finally, this work would not have been possible without the financial support that my research and I received. I thank the *Fonds de Recherche du Québec - Nature et Technologies* (FQRNT) for the support I received through the Merit scholarship program for foreign students. I also acknowledge financial support from the Secretary of Public Education and the Government of Mexico through the program *Becas de Excelencia Académica para Estudios de Posgrado en el Extranjero*. Additionally, my research benefited from grants from the Natural Sciences and Engineering Research Council of Canada (NSERC) and the FQRNT, and from Calcul Québec computing resources.

Contributions of authors

This thesis is written in a manuscript based format. The main chapters of this dissertation (2, 3 and 4) are self-contained and each contains its own introduction and conclusion. All of these papers have been written during my candidature. I am the main author of each these chapters and the only author of this thesis. The contributions of each author to the manuscripts contained in this dissertation are listed below.

Effects of order parameter self-consistency in a $s_{\pm}$-s junction

Rosa Rodríguez-Mota:

Performed the numerical simulations presented in this work, compiled and interpreted the simulation results and wrote the manuscript.

Erez Berg:

Proposed the original idea for the work, provided key insights and revised the manuscript.

T. Pereg-Barnea:

Proposed the original idea for the work, supervised its execution, provided insights and context for the interpretation of the results and revised the manuscript.

Detecting Majorana modes through Josephson junction ring-quantum dot hybrid architectures

Rosa Rodríguez-Mota:

Proposed the orginal idea for the work, performed the numerical simulations and analytical calculations presented in this work, interpreted the results and wrote the manuscript.

Smitha Vishveshwara:

Provided key insights and context for the interpretation of the results and revised the manuscript.

T. Pereg-Barnea:

Proposed the original idea for the work and supervised its execution, assisted in the interpretation of the results and revised the manuscript.

Revisiting 2π phase slip suppression in topological Josephson junctions

Rosa Rodríguez-Mota:

Proposed the orginal idea for the work, performed the numerical simulations and analytical calculations presented in this work, interpreted the results and wrote the manuscript.

Smitha Vishveshwara:

Provided key insights and context for the interpretation of the results and revised the manuscript.

T. Pereg-Barnea:

Supervised the work, assisted in the interpretation of the results and revised the manuscript.

Contents

List of Figures

1

Introduction

The Josephson effect refers to the ability to conduct current across a tunnel barrier between two superconductors without the need for a voltage. This super-current is, instead, driven by a difference in the phase of the macroscopic wave-function between the two superconductors. As a macroscopic quantum phenomena, the Josephson effect has a variety of applications. Due to its phase sensitivity, the shape of the current/phase difference relation can often provide useful clues to the microscopic behavior of the superconductors. This thesis discusses how the Josephson effect is modified by the properties of unconventional and topological superconductors and how it can used as an experimental probe for these types of superconductors. This chapter provides a brief introduction to the Josephson effect (Sec. 1.1) and the two kinds of materials that motivate the following chapters: the unconventional iron-based superconductors (Sec. 1.2) and topological superconductors (Sec. 1.3).

1.1 Josephson effect

To begin our discussion of the Josephson effect, we will derive this effect from a simple microscopic model of tunneling between two identical s-wave superconductors. We describe this using a Hamiltonian $H = H_1 + H_2 + T$. H_1 and H_2 are BCS mean field Hamiltonians describing the superconductors and are given by the following expressions:

$$\begin{aligned} H_1 &= \sum_{\mathbf{k}\sigma} \xi_{\mathbf{k}} c^\dagger_{\mathbf{k}\sigma} c_{\mathbf{k}\sigma} - |\Delta| e^{i\phi_1} \sum_{\mathbf{k}} c^\dagger_{\mathbf{k}\uparrow} c^\dagger_{-\mathbf{k}\downarrow} - |\Delta| e^{-i\phi_1} \sum_{\mathbf{k}} c_{-\mathbf{k}\downarrow} c_{\mathbf{k}\uparrow} \\ H_2 &= \sum_{\mathbf{k}\sigma} \xi_{\mathbf{k}} d^\dagger_{\mathbf{k}\sigma} d_{\mathbf{k}\sigma} - |\Delta| e^{i\phi_2} \sum_{\mathbf{k}} d^\dagger_{\mathbf{k}\uparrow} d^\dagger_{-\mathbf{k}\downarrow} - |\Delta| e^{-i\phi_2} \sum_{\mathbf{k}} d_{-\mathbf{k}\downarrow} d_{\mathbf{k}\uparrow}, \end{aligned} \tag{1.1.1}$$

where the fermionic operators $c^\dagger_{\mathbf{k}\sigma}$ and $d^\dagger_{\mathbf{k}\sigma}$ create a particle with momentum $\mathbf{k}$ and spin σ in the first and second superconductor, respectively, and ϕ_1 and ϕ_2 are the superconducting phases. The tunneling part of the Hamiltonian between the two superconductors could be generally described by

$$T = \sum_{\mathbf{k},\mathbf{q},\sigma} (t_{\mathbf{k},\mathbf{q}} c^\dagger_{\mathbf{k}\sigma} d_{\mathbf{p}\sigma} + t^*_{\mathbf{k},\mathbf{q}} d^\dagger_{\mathbf{q}\sigma} c_{\mathbf{k}\sigma}). \tag{1.1.2}$$

To keep the derivation simple, we assume $t_{\mathbf{k},\mathbf{q}} \approx t$ with t real.

The ground-state and excitations of the BCS Hamiltonians H_1 and H_2 can be obtained by diagonalizing the Hamiltonians using Bogoliubov transformations. The resulting ground-state, e.g. for H_1, can be written as

$$|\phi_1\rangle_{BCS} = \prod_{\mathbf{k}} (|u_{\mathbf{k}}| + |v_{\mathbf{k}}| e^{i\phi_1} c^\dagger_{\mathbf{k}\uparrow} c^\dagger_{-\mathbf{k}\downarrow}) \left|0\right\rangle, \tag{1.1.3}$$

where $|u_{\mathbf{k}}|^2 + |v_{\mathbf{k}}|^2 = 1$ and $|u_{\mathbf{k}}|^2 = (E_{\mathbf{k}} + \xi_{\mathbf{k}})/(2E_{\mathbf{k}})$ and $E_{\mathbf{k}} = \sqrt{\xi^2_{\mathbf{k}} + |\Delta|^2}$. The BCS ground-state contains only paired momentum, and it does not have a well defined particle number.

For the purpose of this derivation we will also need to understand the excitations of a BCS superconductor. The excited eigenstates of the BCS Hamiltonian contain unpaired electrons with well defined spin and momentum. The energy cost of breaking the pairing between $\mathbf{k}$ and $-\mathbf{k}$ is $E_{\mathbf{k}}$. For example, an excited state containing three spin up electrons can written as

$$\prod_{\mathbf{p}\neq\mathbf{k},\mathbf{k}',\mathbf{k}''}(u_{\mathbf{p}}+v_{\mathbf{p}}c^\dagger_{\mathbf{p}\uparrow}c^\dagger_{-\mathbf{p}\downarrow})c^\dagger_{\mathbf{k}\uparrow}c^\dagger_{\mathbf{k}'\uparrow}c^\dagger_{\mathbf{k}''\uparrow}\left|0\right\rangle \tag{1.1.4}$$

and has an energy $E_{\mathbf{k}}+E_{\mathbf{k}'}+E_{\mathbf{k}''}$ above the ground-state. Crucially, $E_{\mathbf{k}}\geq\Delta$ so as long as the superconducting pairing is present, there will be a gap between the ground-state and the excitations.

In the absence of tunneling between the two superconductors, i.e. for $H=H_1+H_2$, the ground-state of the system is given by

$$\left|\phi_1,\phi_2\right\rangle=\prod_{\mathbf{k}}(|u_{\mathbf{k}}|+|v_{\mathbf{k}}|e^{i\phi_2}d^\dagger_{\mathbf{k}\uparrow}d^\dagger_{-\mathbf{k}\downarrow})\prod_{\mathbf{q}}(|u_{\mathbf{q}}|+|v_{\mathbf{q}}|e^{i\phi_1}c^\dagger_{\mathbf{q}\uparrow}c^\dagger_{-\mathbf{q}\downarrow})\left|0\right\rangle. \tag{1.1.5}$$

Our derivation of the Josephson effect will focus on the effect that the tunneling Hamiltonian T has on this ground-state. Considering T as a perturbation, the modification of T to the original ground-state energy of $\left|\phi_1,\phi_2\right\rangle$ up to second order is given by

$$E(\phi_1,\phi_2)=E_{gs}+\left\langle\phi_1,\phi_2\right|T\left|\phi_1,\phi_2\right\rangle+\sum_\lambda\frac{|\left\langle\lambda\right|T\left|\phi_1,\phi_2\right\rangle|^2}{E_{gs}-E_\lambda}, \tag{1.1.6}$$

where $\left|\lambda\right\rangle$ are the excited eigenstates of the H_1+H_2 system and E_λ the energy of such states. The action of the tunneling T on the ground-state is to create an unpaired particle in each superconductor. This means that the first order in T contribution cancels. In addition, T conserves spin, so the only excited states that contribute to the second order expansion are of the form:

$$
\begin{aligned}
|\mathbf{k}\uparrow\phi_1,-\mathbf{q}\downarrow\phi_2\rangle &= \prod_{\mathbf{q}'\neq\mathbf{q}}(|u_{\mathbf{q}'}|+e^{i\phi_2}|v_{\mathbf{q}'}|d^\dagger_{\mathbf{q}'\uparrow}d^\dagger_{-\mathbf{q}'\downarrow})\times \\
&\quad \prod_{\mathbf{k}\neq\mathbf{k}'}(|u_{\mathbf{k}}|+e^{i\phi_1}|v_{\mathbf{k}'}|c^\dagger_{\mathbf{k}'\uparrow}c^\dagger_{-\mathbf{q}'\downarrow})d^\dagger_{-\mathbf{q}\downarrow}c^\dagger_{\mathbf{k}\uparrow}|0\rangle \\
|-\mathbf{k}\downarrow\phi_1,\mathbf{q}\uparrow\phi_2\rangle &= \prod_{\mathbf{q}'\neq\mathbf{q}}(|u_{\mathbf{q}'}|+e^{i\phi_2}|v_{\mathbf{q}'}|d^\dagger_{\mathbf{q}'\uparrow}d^\dagger_{-\mathbf{q}'\downarrow})\times \\
&\quad \prod_{\mathbf{k}\neq\mathbf{k}'}(|u_{\mathbf{k}}|+e^{i\phi_1}|v_{\mathbf{k}'}|c^\dagger_{\mathbf{k}'\uparrow}c^\dagger_{-\mathbf{q}'\downarrow})d^\dagger_{\mathbf{q}\uparrow}c^\dagger_{-\mathbf{k}\downarrow}|0\rangle\,.
\end{aligned}
\tag{1.1.7}
$$

The energies of these excited states are $E_{gs}+E_{\mathbf{k}}+E_{\mathbf{q}}$.

In terms of the above states the action of T on the ground-state $|\phi_1,\phi_2\rangle$ is described by

$$
\begin{aligned}
T\,|\phi_1,\phi_2\rangle &= -t\sum_{\mathbf{k},\mathbf{q}}(|u_{\mathbf{k}}||v_{\mathbf{q}}|e^{i\phi_2}+|u_{\mathbf{q}}||v_{\mathbf{k}}|e^{i\phi_1})\,|\mathbf{k}\uparrow\phi_1,-\mathbf{q}\downarrow\phi_2\rangle \\
&\quad +t\sum_{\mathbf{k},\mathbf{q}}(|u_{\mathbf{q}}||v_{\mathbf{k}}|e^{i\phi_1}+|u_{\mathbf{k}}||v_{\mathbf{q}}|e^{i\phi_2})\,|-\mathbf{k}\downarrow\phi_1,\mathbf{q}\uparrow\phi_2\rangle\,.
\end{aligned}
\tag{1.1.8}
$$

This results in an energy shift that depends on the phase difference between the two superconductors:

$$
E(\phi_1,\phi_2) = -4t^2\cos(\phi_2-\phi_1)\sum_{\mathbf{k},\mathbf{q}}\frac{|u_{\mathbf{k}}||v_{\mathbf{k}}||u_{\mathbf{q}}||v_{\mathbf{q}}|}{E_{\mathbf{k}}+E_{\mathbf{q}}}+C. \tag{1.1.9}
$$

In the above equation, C is a constant which we will disregard as it arises from second order tunneling processes that do not transfer charge from one superconductor to the other.

Defining θ as the phase difference between the two superconductors $\theta=\phi_2-\phi_1$, and taking $E_J = 4t^2 \sum_{\mathbf{k},\mathbf{q}} \frac{|u_\mathbf{k}||v_\mathbf{k}||u_\mathbf{q}||v_\mathbf{q}|}{E_\mathbf{k}+E_\mathbf{q}}$ the above result can written in a simple form

$$E(\theta) = -E_J \cos(\theta). \tag{1.1.10}$$

$E(\theta)$ is known as the Josephson energy and E_J as the Josephson coupling. The energy of the junction will then be minimized when the two superconductors have the same phase.

The BCS ground-state energy is independent of the phase of the superconducting order parameter. Hence, for two superconductors we can consider a space of superconducting ground-states span by all possible order parameter phases. In the absence of tunneling, all such states are degenerate. Following the above results, the junction Hamiltonian $H = H_1 + H_2 + T$ in such space can be approximated by:

$$H \approx -E_J \sum_{\phi_1,\phi_2} \cos(\phi_2 - \phi_1) \left|\phi_1, \phi_2\right\rangle \left\langle\phi_1, \phi_2\right| = -E_J \cos(\hat{\phi}_2 - \hat{\phi}_1). \tag{1.1.11}$$

So far, we have established that when a tunneling junction exists between two superconductors there is an energy cost if the phase of the order parameter changes across the junction. We will now obtain the tunneling current across the junction. The current through the junction would be given by the rate of charge transferred from superconductor 1 to 2 which can be calculated as the change in the number of pairs times the charge of the pairs, i.e.

$$I = (-2e) \left\langle\phi_1, \phi_2\right| \frac{d}{dt}\hat{N}_2 \left|\phi_1, \phi_2\right\rangle = \frac{(-2e)i}{\hbar} \left\langle\phi_1, \phi_2\right| [\hat{N}_2, H] \left|\phi_1, \phi_2\right\rangle, \tag{1.1.12}$$

where $\hat{N}_2 = \sum_{\mathbf{k}\sigma} d^\dagger_{\mathbf{k}\sigma} d_{\mathbf{k}\sigma}$ and e is the electron charge. We proceed to calculate the commutator $[\hat{N}_2, H]$. We start by noting that although for a well-defined superconducting phase the corresponding BCS ground-state does not have a well defined number of particles, it is possible to obtain states with well-defined particle number from them.

For instance, a combination of BCS ground-states with N pairs, or $2N$ particles, can be obtained through:

$$|N\rangle = \frac{1}{2\pi}\int_0^{2\pi} d\phi e^{-i\phi N} |\phi\rangle \, . \tag{1.1.13}$$

Hence, in the space of BCS ground-states, there is a canonical commutation relation between the number of pairs and the superconducting phase:

$$[\hat{\phi}, \hat{N}] = i. \tag{1.1.14}$$

Using this relation it is straightforward to calculate $[\hat{N}_2, H]$, which leads to

$$I = \frac{2e}{\hbar} E_J \sin(\phi_2 - \phi_1) = \frac{2e}{\hbar}\frac{dE(\theta)}{d\theta} = I_c \sin(\theta) \tag{1.1.15}$$

where $I_c = 2eE_J/\hbar$ is known as the critical current, and $E(\theta)$ is the Josephson energy given in Eq. (1.1.10).

Hence, current may flow between two superconductors without a need for a voltage to drive such current. The maximum amount of current occurs when the phase difference between the superconductors is $\pi/2$ and it is I_c. That is the maximum current that can be driven between the two superconductors without dissipation, hence the name critical current.

A voltage V between the two superconductors can be modeled by adding a difference in chemical potential into our effective model:

$$H = -E_J \cos(\hat{\phi}_2 - \hat{\phi}_1) + \mu_2(2\hat{N}_2) + \mu_1(2\hat{N}_1), \tag{1.1.16}$$

with $\mu_2 - \mu_1 = eV$. This leads to the following phase difference evolution:

$$\frac{d}{dt}\hat{\theta} = \frac{i}{\hbar}[\hat{\phi}_2 - \hat{\phi}_1, H] = \frac{2eV}{\hbar}. \tag{1.1.17}$$

In the presence of a DC voltage, the current obtained from Eqs. (1.1.15) and (1.1.17) is an AC current. This phenomenon is known as the AC Josephson effect. If the voltage between the superconductors is large enough to break a pair, i.e. $eV > 2\Delta$, a DC quasi-particle current will also be present [1].

We have derived the Josephson effect using a simplified tunnel barrier between two conventional s-wave superconductors. In realistic situations, there can be important modifications from this simplified version of the Josephson effect. For instance, when the transparency of the contact increases, higher order terms in perturbation theory become important. This leads to the presence of higher harmonics in the current vs phase difference relation of Eq. 1.1.15. Also due to higher order effects, a DC quasi-particle current appears in the presence of a voltage V even for $eV < 2\Delta$. [2] The type of barrier, temperature effects and the characteristics of the superconductors can also lead to important deviations from the sinusoidal behavior of Eq. 1.1.15. [3] The following Chapters consider deviations from this behavior arising due to an unconventional pairing symmetry or due to exotic bound states close to the junction that result from a non-trivial topology.

Before moving on to discuss some applications of the Josephson effect, a few remarks about the description of the Josephson effect are in order. The Josephson effect and superconductivity in general can be described following a microscopic BCS theory. In this derivation, Eqs. (1.1.10) and (1.1.14) were obtained from the microscopic BCS ground-state. However for many of its applications the equations describing the behavior of the macroscopic collective variables (the superconducting phase and number) are

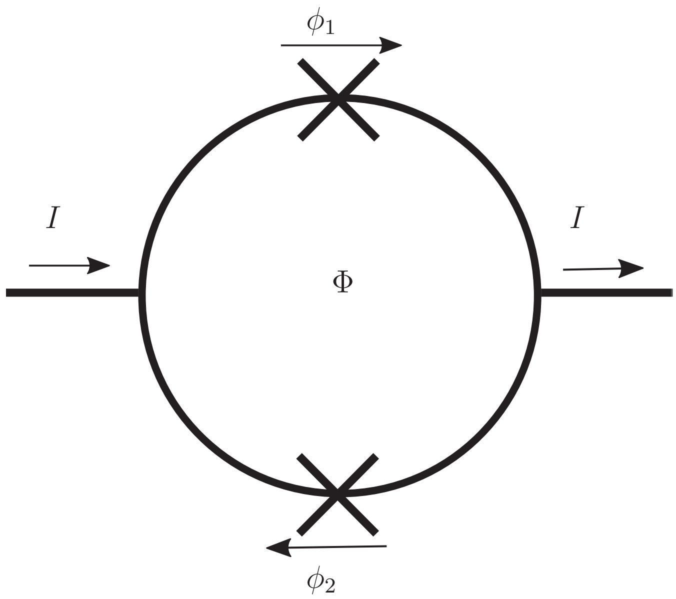

Figure 1.1: A DC-SQUID consist of a superconducting loop interrupted by two Josephson junctions. The dependence of the critical current of the SQUID on the magnetic flux threading the loop makes the SQUID a sensitivity magnetometer.

sufficient to describe the system. [4, 5] That was the procedure we used in this derivation to obtain Eqs. (1.1.15) and (1.1.17). In this thesis, Chapter 2 will favor a microscopic description of the Josephson effect while Chapters 3 and 4 favor a macroscopic one.

1.1.1 Applications of the Josephson effect

In this section, we discuss some applications of the Josephson effect. This list of applications is by no means exhaustive. We focus on examples of applications that illustrate the usefulness of the Josephson effect and that bear some relation to the themes that will be discussed in the rest of this thesis.

Superconducting Interference Devices (SQUID)

Superconducting Interference Devices (SQUIDs) are examples of powerful devices that takes advantage of the Josephson effect. For simplicity, here we will only discuss

DC-SQUIDs. As shown in Fig. 1.1, a DC-SQUID consists of a superconducting loop interrupted by two Josephson junctions. The loops is threaded by some flux Φ, the phase difference across the junctions are ϕ_1 and ϕ_2 and I is the current through the loop, as signaled in Fig. 1.1. We will now show how the critical current of a DC-SQUID depends on the magnetic flux through the loop. Since the macroscopic wave-function of the superconductors needs to be single valued, we have the following relation for the phases ϕ_1 and ϕ_2:

$$\phi_1 + \phi_2 + 2\pi\frac{\Phi}{\Phi_0} = 2\pi m, \tag{1.1.18}$$

with m an integer and $\Phi_0 = h/(2e)$ is the superconducting flux quantum. In the above equation, $2\pi\frac{\Phi}{\Phi_0}$ corresponds to the contribution to the superconducting phase from the magnetic flux [1]. Then the current across the SQUID I is given by:

$$I = I_1 + I_2 = I_c \sin(\phi_1) + I_c \sin(-\phi_2) = 2I_c \cos\left(\frac{\pi\Phi}{\Phi_0}\right)\sin(\delta\phi) \tag{1.1.19}$$

with $\delta\phi = \phi_1 + \frac{\pi\Phi}{\Phi_0} = -\phi_2 - \frac{\pi\Phi}{\Phi_0}$ the gauge invariant phase difference. The maximum current flowing through the loop is then $2I_c \cos\left(\frac{\pi\Phi}{\Phi_0}\right)$. This makes SQUIDs very sensitive magnetometers with a wide arrange of applications. For instance, in condensed matter physics SQUIDs can be used to map the magnetic structure of a material [6–9]. In addition, the current vs. $\delta\phi$ relation from Eq. (1.1.19) can also be thought of as a junction with a tunable parameter. This construction of a tunable junction is widely used for superconducting qubits, in which case the SQUID is normally refered to as a split junction. An extensive discussion of SQUIDs and their applications can be found in Ref. [10].

Josephson effect as a probe for d-wave pairing symmetry

A useful example of the applications of the Josephson effect as a probe for unconventional superconductors comes from the identification of the d-wave pairing symmetry of the cuprates superconductors [11, 12]. In a d-wave superconductor, the phase of the order parameter exhibits shifts of π that depends on the momentum direction. Due to this internal π shift, junction structures with certain geometries show spontaneous magnetization of half quantum flux. Examples of structures in which this has been measured are corner SQUIDs [13], corner junctions [14] between s and d-wave superconductors and tri-crystal junctions between three d-wave superconductors [15]. These experiments took advantage of the phase sensitivity of the Josephson effect to provide an unambiguous identification of the d-wave pairing symmetry in cuprate superconductors.

Superconducting qubits: the Cooper pair box

Josephson junctions are a crucial ingredient for the three main kinds of superconducting qubits: flux qubits, charge qubits and phase qubits. [16, 17] For example, a Cooper pair box [18, 19] consists of a tiny superconducting island coupled to a superconducting reservoir using a Josephson junction. The island is small enough that the cost of adding a pair to the island E_C is much greater than the thermal energy. The Hamiltonian of the island becomes:

$$H = E_C(\hat{N} - n_g)^2 + E_J \cos\hat{\theta}, \tag{1.1.20}$$

where the phase difference $\hat{\theta}$ and the number of pairs in the island $\hat{N}$ follow the usual commutation relation. The charge offset n_g can be tuned using a gate voltage. For $E_C \gg E_J$ and $n_g = n + 1/2$ with n integer, the states with well defined number of pairs $|n\rangle$ and $|n+1\rangle$ form a two level system. The superposition of these Cooper pairs states was shown experimentally twenty years ago. [18]

1.2 Iron-based superconductors

Discovered in the last decade [20, 21], the iron-based superconductors (FeSC) have high superconducting transition temperatures (T_c) [22, 23] and a rich phase diagram. It was soon realized that their high T_c could not be accounted for by the conventional electron-phonon coupling of BCS theory. [24] The common feature in all FeSC is a corrugated layer Fe-As(Se) layer in which the Fe ions form a square lattice with As(Se) atoms located above or below the center of each face. The typical electronic structure of the FeSC consist of a Fermi surface made of two electron band and two hole bands. [25] However there are notable exceptions to this typical electronic structure [26, 27], mainly the absence of hole bands in the Fermi surface of some iron selenides. Overall, the FeSC are characterized by their multi-band nature, a bad metal normal state and a strong coupling between their magnetic, structural and electronic degrees of freedom. [28, 29] The superconducting phase appears in close proximity to an anti-ferromagnetic order, a structural transition and a nematic order. Because of these intertwined phases and degrees of freedom it is hard to pin down the origin of superconductivity in these materials, but most results point towards it being driven by anti-ferromagnetic fluctuations. This picture results in a pairing symmetry often refered to as $s_{\pm}$, in which the order parameter changes sign between the electron-like and hole-like part of the Fermi surface. [30, 31] The dependence of the sign change on the amplitude of momentum, rather that in its direction makes it challenging to detect this pairing symmetry experimentally. Chapter 2 of this thesis focuses on studying a tunnel junction between a superconductor with $s_{\pm}$ pairing symmetry and a conventional s superconductor.

1.3 Topological superconductors

Since Chapters 3 and 4 of this thesis deal with Josephson tunneling in topological superconductors, we give a brief introduction to topological superconductors and Majorana modes in this section assuming no prior knowledge of topology in condensed matter. The section is organized as follows. In Sec. 1.3.1, we introduce some of the properties of topological superconductors through an overview of a toy model for a topological superconductor known as the Kitaev chain. Later, in Sec. 1.3.2, we discuss the effects of topological superconductivity in the Josephson effect. The final two subsections are devoted to motivate the interest in topological superconductivity by: discussing the non-Abelian statistics of Majorana modes and its possible applications in Quantum Computation (Sec. 1.3.3) and introducing an experimentally realizable model of a 1D topological superconductor (Sec. 1.3.4).

1.3.1 Kitaev chain

The Kitaev chain is a simple model of a 1D spinless p-wave superconductor introduced by A. Kitaev in Ref. [32]. As the discussion in A. Kitaev's original work assumes no prior knowledge of topology, we will follow it closely. We consider a chain of L fermionic sites, labeled by $j = 1, ..., L$. Associated with the j-site of the chain, we have the fermion annihilation operator c_j which removes a particle from this site. Because of their fermionic nature, these operators follow the commutation relations:

$$\{c_j, c_m\} = 0, \quad \{c_j, c_m^\dagger\} = \delta_{j,m} \tag{1.3.1}$$

In terms of the above operators, the Hamiltonian of the Kitaev chain can be written as:

$$H = \sum_{j=1}^{L} \left[-\mu \left(c_j^\dagger c_j - 1/2 \right) - w c_j^\dagger c_{j+1} - w c_{j+1}^\dagger c_j + \Delta c_j c_{j+1} + \Delta^* c_{j+1}^\dagger c_j^\dagger \right], \quad (1.3.2)$$

where $\Delta = |\Delta| e^{i\phi}$ is the superconducting pairing, w, the nearest-neighbor hopping amplitude and μ, the chemical potential.

Alternatively, the chain can be described in terms of $2L$ *Majorana operators* defined by

$$\begin{aligned} c_j &= \frac{e^{-i\phi/2}}{2} \left(\gamma_{2j-1} + i\gamma_{2j} \right) \\ c_j^\dagger &= \frac{e^{i\phi/2}}{2} \left(\gamma_{2j-1} - i\gamma_{2j} \right). \end{aligned} \quad (1.3.3)$$

These operators are called Majorana operators in honor of the fermions theorized by E. Majorana [33] as they follow:

$$\gamma_j = \gamma_j^\dagger, \quad \{\gamma_j, \gamma_m\} = 2\delta_{j,m}. \quad (1.3.4)$$

Note that the above relations result exclusively from the definition of the operators (1.3.3) and the fermion commutation relations (1.3.1). Furthermore, the occupation of each site can be easily described using the Majorana operators through its parity:

$$\mathcal{P}_j = (-1)^{c_j^\dagger c_j} = 1 - 2c_j^\dagger c_j = -i\gamma_{2j-1}\gamma_{2j}. \quad (1.3.5)$$

Hence, for a state $|\Psi\rangle$ the fermion site j is occupied if $-i\gamma_{2j-1}\gamma_{2j} |\Psi\rangle = |\Psi\rangle$ and empty if $-i\gamma_{2j-1}\gamma_{2j} |\Psi\rangle = - |\Psi\rangle$. In terms of the Majorana operators, the Kitaev chain

Hamiltonian is

$$H = \frac{i}{2}\sum_{j=1}^{L}\left[-\mu\gamma_{2j-1}\gamma_{2j} + (|\Delta| + w)\gamma_{2j}\gamma_{2j+1} + (|\Delta| - w)\gamma_{2j-1}\gamma_{2j+2}\right]. \quad (1.3.6)$$

The properties of the model are best illustrated by considering two special cases. First, we consider the trivial case with $\mu < 0$, $|\Delta| = w = 0$. The Hamiltonian of the system becomes:

$$H = -\frac{i\mu}{2}\sum_{j=1}^{L}\gamma_{2j-1}\gamma_{2j}. \quad (1.3.7)$$

The ground-state of such system would be given by a state $|\Psi\rangle$ such that $-i\gamma_{2j-1}\gamma_{2j}|\Psi\rangle = |\Psi\rangle$. In terms of the fermionic sites, this corresponds to all sites being empty (see Eq. 1.3.5) which is consistent with what we expect by setting $\mu < 0$, $|\Delta| = w = 0$ in Eq. 1.3.2. We can also think of the ground-state of this system as a state in which all of the Majorana operators are paired. Regardless of which description we use for the system, the ground-state of the chain for this choice of parameters is unique.

The ground-state properties of the second special case we will consider, $\mu = 0$ and $w = |\Delta|$, are remarkably different. For this choice of parameters, the Hamiltonian becomes

$$H = i\sum_{j=1}^{L}|\Delta|\gamma_{2j}\gamma_{2j+1}. \quad (1.3.8)$$

The Majorana operators at the edges of the chain, i.e. γ_1 and γ_{2L}, do not appear in the Hamiltonian. Hence, we can think of this system as having unpaired Majoranas at its edges. Since γ_1 and γ_{2L} are *unpaired* by the Hamiltonian, there are two possible ground-states $|\Psi_\pm\rangle$ such that

$$-i\gamma_{2j}\gamma_{2j+1}|\Psi_\pm\rangle = |\Psi_\pm\rangle \text{ for } j = 1, ..., L-1 \text{ and } -i\gamma_1\gamma_{2L}|\Psi_\pm\rangle = \pm|\Psi_\pm\rangle. \quad (1.3.9)$$

We can further argue that these two ground-states are orthogonal by noting that these states differ by their fermionic parity:

$$\begin{aligned}\prod_{j=1}^{L}\mathcal{P}_j\left|\Psi_\pm\right\rangle &= \prod_{j=1}^{L}(-i\gamma_{2j-1}\gamma_{2j})\left|\Psi_\pm\right\rangle = -i\gamma_1\prod_{j=1}^{L-1}(-i\gamma_{2j}\gamma_{2j+1})\gamma_{2L}\left|\Psi_\pm\right\rangle \\ &= -i\gamma_1\gamma_{2L}\prod_{j=1}^{L-1}(-i\gamma_{2j}\gamma_{2j+1})\left|\Psi_\pm\right\rangle = \pm\left|\Psi_\pm\right\rangle.\end{aligned} \tag{1.3.10}$$

Unlike the previous case, the ground-state for this choice of parameters is doubly degenerate. Furthermore, the two different ground-states of the system can be distinguished by the occupancy of a fermionic mode $d = (\gamma_1 + i\gamma_{2L})/2$ which is split between two different sites.

The next step is to argue that the properties at these two special cases are not a result of fine tuning the parameters, but rather they are representative of two phases of the chain with different topology. To do this, we first assume periodic boundary conditions, i.e. $c_1 = c_{L+1}$, to transform our system from a real space description to a momentum space description:

$$\begin{aligned}H_p = \sum_{0<k<\pi}\begin{pmatrix} c_k^\dagger & c_{-k}\end{pmatrix}\begin{pmatrix} -2w\cos k - \mu & -2i\Delta^*\sin k \\ 2i\Delta\sin k & 2w\cos k + \mu\end{pmatrix}\begin{pmatrix} c_k \\ c_{-k}\end{pmatrix} \\ + (-2w-\mu)c_0^\dagger c_0 + (2w-\mu)c_\pi^\dagger c_\pi.\end{aligned} \tag{1.3.11}$$

In the above equation, the momentum space operators are given by $c_k = \sum_j e^{ikj}c_j/\sqrt{L}$, and, for simplicity, we have assumed that the number of sites in the chain L is even. The ground-state parity of H_p depends only on whether the $k = 0, \pi$ modes are occupied as all other k values are paired, so it will be given by the sign of $\mu^2 - 4w^2$.

If instead we transform the system to momentum space assuming anti-periodic boundary conditions, i.e. $c_1 = -c_{L+1}$, the Hamiltonian becomes

$$H_{ap} = \sum_{0<k<\pi} \begin{pmatrix} c_k^\dagger & c_{-k} \end{pmatrix} \begin{pmatrix} -2w\cos k - \mu & -2i\Delta^* \sin k \\ 2i\Delta \sin k & 2w \cos k + \mu \end{pmatrix} \begin{pmatrix} c_k \\ c_{-k} \end{pmatrix}. \quad (1.3.12)$$

In this case, the ground-state parity is always even as 0 and π are no longer allowed momentum values. Then, the ground-state parity of the system changes between the periodic and anti-periodic boundary conditions if $|\mu| < 2|w|$. This conclusion does not rest on the assumption that L is even. In the odd L case, 0 is an allowed momenta for periodic boundary conditions while π is allowed for anti-periodic boundary conditions.

For $L \gg 1$, we expect the bulk of the chain to be independent of the chosen boundary conditions. Yet, we find that for $|\mu| < 2|w|$, the bulk states found from periodic and anti-periodic boundary conditions have different parities. This apparent contradiction could be solved by the existence of a boundary state similar to the one formed by the unpaired Majorana operators for $\mu = 0$ and $w = |\Delta|$.

We can put the above speculation on a somewhat firmer footing by noting that we can deform the periodic boundary Hamiltonian to the anti-periodic boundary Hamiltonian. For instance, if we take

$$H(t) = H - t(wc_L^\dagger c_1 + wc_1^\dagger c_L - \Delta c_L c_1 - \Delta^* c_1^\dagger c_L^\dagger). \quad (1.3.13)$$

with H given by Eq. (1.3.2), we have $H(1) = H_p$, $H(0) = H$ and $H(-1) = H_{ap}$. If $|\mu| < 2|w|$, the ground-state parity is different for $t = -1$ to $t = 1$, so the ground-state must be degenerate at some point of the trajectory. Otherwise, we could invoke adiabaticity to argue that the ground-state parity cannot change throughout the trajectory if we follow it slow enough. This is because the ground-state parity is a topological invariant. A topological invariant cannot change under a continuous transformation of

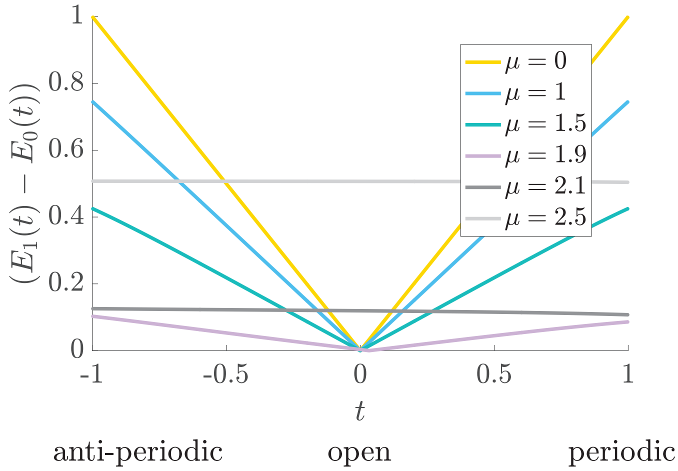

Figure 1.2: Energy gap between the ground-state and the first excited state for the Hamiltonian of Eq. (1.3.13) for a chain of 80 sites with $w = \Delta = 1$ and different values of μ. For $t = -1, 0, +1$, this system corresponds to a Kitaev chain with anti-periodic, open and periodic boundary conditions, respectively. Since the Hamiltonian of Eq. (1.3.13) continuously interpolates between periodic and anti-periodic boundary conditions, in the topological phase ($\mu < 2$), the gap must close at some point of the trajectory. For $\mu = 1.9$ (purple line) finite size effects shift the gap closing from $t = 0$. In the non-topological phase ($\mu > 2$), the gap does not need to close throughout the trajectory as the ground-state parity does not change between the end points of the trajectory.

the Hamiltonian unless the gap (the energy difference between the 1st excited state and the ground-state) closes. This gap closing is shown in Fig. 1.2. For $L \gg 1$, or for the special choice $\mu = 0$ and $w = |\Delta|$, the gap closes at $t = 0$. Otherwise, finite size effects move the gap closure and the open chain shows a small gap which is proportional to e^{-L}. [32]

Note that the existence of these boundary modes can be revealed by looking at the behavior of the bulk of the chain only. In the continuum limit, the ground-state parity of the chain would be

$$\mathcal{P} = \text{sign}(\mu^2 - 4w^2), \tag{1.3.14}$$

as we have established that the only unpaired momenta are 0 and π. At the end of the chain, the parity is that of the trivial vacuum $+1$. Hence, if $\mathcal{P} = -1$, the difference in the parity at the bulk of the chain and the vacuum guarantees the appearance of the boundary modes. This is commonly referred to as the *bulk-boundary correspondence*. In this case in particular, it was sufficient to look at the behavior of the system at the k values of 0 and π. This is because the symmetries of the chain constrain the k-values in which the topological invariant, in this case the parity can change. The Kitaev chain with $|\mu| < 2|w|$ is a 1D topological superconductor which is an example of a Symmetry Protected Topological Phase (SPT). [34–36]

1.3.2 4π periodic Josephson effect

Majoranas modes have striking consequences for Josephson tunneling between topological superconductors. In our discussion of the Josephson effect, we saw that pairs of electrons can tunnel between two superconductors without the need for a voltage. We will see now that for topological superconductors, the Majorana end modes allow for single particle tunneling with the same coherent properties as the Josephson pair tunneling. This phenomenon is known as the 4π Josephson effect. [32, 37–42]

For simplicity, we will illustrate this phenomenon by considering tunneling between two Kitaev chains, with superconducting phases ϕ_1 and ϕ_2, at the topological special point ($w = |\Delta|$, $\mu = 0$) joined by a weak link. The Hamiltonian of the system is $H = H_1 + H_2 + T$ with $H_1 = i\sum_{j=1}^{L-1} |\Delta_1|\gamma_{2j}\gamma_{2j+1}$, $H_2 = i\sum_{j=L+1}^{L-1} |\Delta_2|\gamma_{2j}\gamma_{2j+1}$ and $T = -\lambda c_L^\dagger c_{L+1} - \lambda c_{L+1}^\dagger c_L$. The tunneling part of the Hamiltonian can be rewritten in terms of the Majorana operators:

$$\begin{aligned} T =& \frac{\lambda}{2}\cos\left(\frac{\theta}{2}\right)(i\gamma_{2L}\gamma_{2L+1} - i\gamma_{2L-1}\gamma_{2L+2}) \\ &- \frac{\lambda}{2}\sin\left(\frac{\theta}{2}\right)(i\gamma_{2L+1}\gamma_{2L-1} + i\gamma_{2L+2}\gamma_{2L}), \end{aligned} \tag{1.3.15}$$

where $\theta = \phi_2 - \phi_1$ is the phase difference in the order parameter of the superconductors. The operators γ_{2L} and γ_{2L-1} do not take the chains out of the $H_1 + H_2$ ground-state manifold. Then taking T as a perturbation, to first order we obtain

$$T \approx \frac{\lambda}{2}\cos\left(\frac{\theta}{2}\right) i\gamma_{2L}\gamma_{2L+1}. \tag{1.3.16}$$

The other terms from Eq. (1.3.15) do not contribute to the first order expansion of T as their action on one of the $H_1 + H_2$ ground-states does not overlap with any $H_1 + H_2$ ground-state. In terms of the fermion operators, the above result is given by

$$\begin{aligned} T \approx -\frac{\lambda}{2}\cos\left(\frac{\theta}{2}\right) \Big(& e^{-\frac{i\phi_2}{2}+\frac{i\phi_1}{2}} c^\dagger_{L+1}c_L + e^{-\frac{i\phi_1}{2}+\frac{i\phi_2}{2}} c^\dagger_L c_{L+1} \\ & + e^{\frac{i\phi_2}{2}+\frac{i\phi_1}{2}} c_{L+1}c_L + e^{-\frac{i\phi_1}{2}-\frac{i\phi_2}{2}} c^\dagger_L c^\dagger_{L+1}\Big). \end{aligned} \tag{1.3.17}$$

Eq. (1.3.16) describes the 4π Josephson effect. It is generally interpreted as the unpaired Majorana at the edges of the junction hybridizing to form a bound-state whose energy is 4π periodic with respect to the phase difference between the superconductors. If we assume that the occupation of the bound-state does not change, then the resulting energy and current between the superconductors are 4π periodic instead of 2π periodic. The 4π periodicity and the fact that Eq. (1.3.16) was obtained to first order in perturbation theory indicate that 4π Josephson effect is a single particle tunneling process.

We obtained Eq. 1.3.16 for a very idealized system. However, we can note that our main assumptions were 1) that the action of the Majorana operators γ_{2L} and γ_{2L-1} do not take the superconductors out of their ground-state and 2) that the creation of a particle at the edge of the superconductors overlaps with these Majorana operators, e.g. $c^\dagger_L = e^{i\phi_1/2}(-i\gamma_{2L}/2 + ...)$. The 4π Josephson effect then relies only on the existence of Majorana modes localized at the edges of the superconductors.

From what we have seen so far, Josephson tunneling can be used to probe Majorana modes experimentally. We will now discuss some potential caveats. The first is that the tunneling current is only 4π periodic if the occupation of the bound-state formed by the Majoranas is conserved. [38] In realistic settings, there might be quasi-particles present that can tunnel into the bound-state. Because of this, most proposals for detection of Majoranas rely on the AC version of the 4π Josephson effect, where the rate at which the superconducting phase changes can be made faster than the rate at which quasi-particles can tunnel into the bound-state or the change in the bound-state occupation can be detected in the noise current. Also, in our idealized system the 4π Josephson effect is the main component in the tunneling current. While this is true as long as localized Majorana modes are present in a conducting channel, in a realistic system there might be more conducting channels present. Thus, the 4π terms may only be a small part of the overall tunneling current. The final caveat that we will mention is that the 4π Josephson effect can be mimicked in non-topological junctions by Landau-Zener tunneling through Andreev bound-states. [37, 43, 44]. Note that in this case, the 4π periodicity arises when the junction bound-state occupation is not conserved.

1.3.3 Majorana modes and quantum computation

Although topological superconductors are interesting materials in their own right, part of the motivation for creating topological superconductors resides in their potential use for quantum computation. [32, 45, 46] Quantum computation using Majorana modes follows many of the original ideas of topological quantum computation. [47] Quantum information is stored in topologically degenerated states, which can be manipulated through braiding operations. For instance information stored in the delocalized state formed by the two Majoranas at the edges of the chain is protected from local perturbations. Furthermore, Majorana modes are non-Abelian anyons, i.e. exchanges of Majorana modes are non-trivial operations which in general do not commute [48], allowing the state to be manipulated. Although the ideas behind topological quantum computation have been around for a long time, progress has been hindered by the difficulty of realizing topological states of matter. As we will see in the next subsection, recent experimental progress has made the possibility of realizing topological superconductors seem tangible. There are two main problems faced by quantum computation using Majorana modes. The first is that information stored in Majorana modes can be destroyed by quasi-particle poisoning. The second is that the universal quantum computation cannot be achieved using only braiding operations. However there are different strategies that can be used to solve these caveats (see Ref. [49] for a recent proposal).

1.3.4 Majorana modes in proximitized structures

The Kitaev chain is clearly a theoretical construction as it assumes the existence of unrealistic spinless fermions. Considering a spinful version of the Kitaev chain would lead to two copies of the chain (one for spin up and one for spin down) which would result in two Majorana modes at each of the edges. The Majoranas at each edge would couple resulting in two fermion modes localized at each edge, rather than one delocalized fermion mode. Realistic realizations of Majorana modes need to find a way around the spin degeneracy, not to mention that most common superconductors are singlet, mainly s-wave, superconductors. Nonetheless, it is possible to realize an effective continuum version of the Kitaev chain in proximitized semi-conducting wires [40, 41], sometimes referred to as Majorana wires. The prescription followed by these proposals consists of: 1) using strong spin-orbit coupling to break the spin degeneracy, 2) inducing superconductivity through proximity effect and 3) using a Zeeman field to open up a gap.

The proposals in Refs. [40] and [41] are by no means the only, or the first, realistic proposals to obtain Majorana modes. Majorana modes are also expected to appear the following proximitized structures: chains of magnetic atoms deposited on the surface of superconductors [50, 51], the interface of a topological insulator with a superconductor [52], semiconducting thin films proximitized by an s-wave superconductor and a ferromagnetic insulator [53] and quantum wells with Rashba and Dresselhaus spin-orbit coupling proximitized by an s-wave superconductor under an applied magnetic field [54]. In addition, Majorana modes can also occur in other types of structures such as vortices of $p + ip$ superconductors and the $\nu = 5/2$ fractional quantum Hall state. However, proximitized structures, particularly Majorana wires, have seen considerable experimental progress in recent years. Presently, there is encouraging experimental evidence that Majorana modes can be physically realized. [55–64]

1.4 Thesis outline

The remainder of this thesis is organized as follows. Chapter 2 starts with a microscopic calculation of the energy/phase difference relation of a tunnel junction between an $s_\pm$ superconductor and an s-wave superconductor. After discussing the energy/phase difference relation of a single junction, Chapter 2 also explores how to probe the different found types of energy/phase difference relations using a magnetic flux threaded loop. Chapter 3 moves away from microscopic calculations, and focuses on probing the manifestations of the 4π periodic Josephson effect on a ring made of N topological superconductors. The topological superconductors of the system studied in Chapter 3 interact through tunneling and through electrostatic repulsion. We also study the effects of coupling the ring to a quantum dot as a way for breaking the parity of the ring in a controlled manner. Finally, in Chapter 4, we focus on studying the effects of charging induced phase fluctuations in a single topological junction.

This thesis is written as a manuscript-based thesis. Chapters 2, 3 and 4 can be read independently and they each include their own introduction and conclusion. To make this thesis a cohesive work, there is a preface at the beginning of each chapter.

References

[1]M. Tinkham, Dover Books on Physics Series (Dover Publications, 1996).

[2]D. Averin, and A. Bardas, Phys. Rev. Lett. **75**, 1831–1834 (1995).

[3]A. A. Golubov, M. Y. Kupriyanov, and E. Il'ichev, Rev. Mod. Phys. **76**, 411–469 (2004).

[4]A. J. Leggett, Progress of Theoretical Physics Supplement **69**, 80–100 (1980).

[5]B. Yurke, and J. S. Denker, Phys. Rev. A **29**, 1419–1437 (1984).

[6]J. R. Kirtley, Reports on Progress in Physics **73**, 126501 (2010).

[7]L. N. Vu, and D. J. V. Harlingen, IEEE Transactions on Applied Superconductivity **3**, 1918–1921 (1993).

[8]J. R. Kirtley, M. B. Ketchen, K. G. Stawiasz, J. Z. Sun, W. J. Gallagher, S. H. Blanton, and S. J. Wind, Applied Physics Letters **66**, 1138–1140 (1995).

[9]R. C. Black, A. Mathai, F. C. Wellstood, E. Dantsker, A. H. Miklich, D. T. Nemeth, J. J. Kingston, and J. Clarke, Applied Physics Letters **62**, 2128–2130 (1993).

[10]J. Clarke, and A. I. Braginski, (Wiley-VCH, Weinheim, 2006).

[11]C. C. Tsuei, and J. R. Kirtley, Rev. Mod. Phys. **72**, 969–1016 (2000).

[12]D. J. Van Harlingen, Rev. Mod. Phys. **67**, 515–535 (1995).

[13]D. A. Wollman, D. J. Van Harlingen, W. C. Lee, D. M. Ginsberg, and A. J. Leggett, Phys. Rev. Lett. **71**, 2134–2137 (1993).

[14]D. A. Wollman, D. J. Van Harlingen, J. Giapintzakis, and D. M. Ginsberg, Phys. Rev. Lett. **74**, 797–800 (1995).

[15]C. C. Tsuei, J. R. Kirtley, C. C. Chi, L. S. Yu-Jahnes, A. Gupta, T. Shaw, J. Z. Sun, and M. B. Ketchen, Phys. Rev. Lett. **73**, 593–596 (1994).

[16] J. Clarke, and F. K. Wilhelm, Nature **453**, 1031 (2008).

[17] Y. Makhlin, G. Schön, and A. Shnirman, Rev. Mod. Phys. **73**, 357–400 (2001).

[18] Y. Nakamura, C. D. Chen, and J. S. Tsai, Phys. Rev. Lett. **79**, 2328–2331 (1997).

[19] V. Bouchiat, D. Vion, P. Joyez, D. Esteve, and M. H. Devoret, Physica Scripta **1998**, 165 (1998).

[20] Y. Kamihara, H. Hiramatsu, M. Hirano, R. Kawamura, H. Yanagi, T. Kamiya, and H. Hosono, Journal of the American Chemical Society **128**, PMID: 16881620, 10012–10013 (2006).

[21] Y. Kamihara, T. Watanabe, M. Hirano, and H. Hosono, Journal of the American Chemical Society **130**, PMID: 18293989, 3296–3297 (2008).

[22] Z. A. REN, Chin. Phys. Lett. **25**, 2215 (2008).

[23] J.-F. Ge, Z.-L. Liu, C. Liu, C.-L. Gao, D. Qian, Q.-K. Xue, Y. Liu, and J.-F. Jia, Nature Materials **14**, (2014).

[24] L. Boeri, O. V. Dolgov, and A. A. Golubov, Phys. Rev. Lett. **101**, 026403 (2008).

[25] M. Yi, D. H. Lu, J. G. Analytis, J.-H. Chu, S.-K. Mo, R.-H. He, R. G. Moore, X. J. Zhou, G. F. Chen, J. L. Luo, N. L. Wang, Z. Hussain, D. J. Singh, I. R. Fisher, and Z.-X. Shen, Phys. Rev. B **80**, 024515 (2009).

[26] T. Qian, X.-P. Wang, W.-C. Jin, P. Zhang, P. Richard, G. Xu, X. Dai, Z. Fang, J.-G. Guo, X.-L. Chen, and H. Ding, Phys. Rev. Lett. **106**, 187001 (2011).

[27] T. Sato, K. Nakayama, Y. Sekiba, P. Richard, Y.-M. Xu, S. Souma, T. Takahashi, G. F. Chen, J. L. Luo, N. L. Wang, and H. Ding, Phys. Rev. Lett. **103**, 047002 (2009).

[28] Q. Si, R. Yu, and E. Abrahams, Nature Reviews Materials **1**, (2016).

[29] R. M. Fernandes, A. V. Chubukov, and J. Schmalian, Nature Physics **10**, (2014).

[30]P. J. Hirschfeld, M. M. Korshunov, and I. I. Mazin, Reports on Progress in Physics **74**, 124508 (2011).

[31]A. Chubukov, Annual Review of Condensed Matter Physics **3**, 57–92 (2012).

[32]A. Y. Kitaev, Physics-Uspekhi **44**, 131 (2001).

[33]E. Majorana, Il Nuovo Cimento (1924-1942) **14**, 171 (2008).

[34]C.-K. Chiu, J. C. Y. Teo, A. P. Schnyder, and S. Ryu, Rev. Mod. Phys. **88**, 035005 (2016).

[35]A. P. Schnyder, S. Ryu, A. Furusaki, and A. W. W. Ludwig, Phys. Rev. B **78**, 195125 (2008).

[36]A. Kitaev, AIP Conference Proceedings **1134**, 22–30 (2009).

[37]H.-J. Kwon, K. Sengupta, and V. M. Yakovenko, The European Physical Journal B - Condensed Matter and Complex Systems **37**, 349–361 (2004).

[38]L. Fu, and C. L. Kane, Phys. Rev. B **79**, 161408 (2009).

[39]H.-J. Kwon, V. M. Yakovenko, and K. Sengupta, Low Temperature Physics **30**, 613–619 (2004).

[40]R. M. Lutchyn, J. D. Sau, and S. Das Sarma, Phys. Rev. Lett. **105**, 077001 (2010).

[41]Y. Oreg, G. Refael, and F. von Oppen, Phys. Rev. Lett. **105**, 177002 (2010).

[42]D. M. Badiane, L. I. Glazman, M. Houzet, and J. S. Meyer, Comptes Rendus Physique **14**, 840–856 (2013).

[43]J. D. Sau, E. Berg, and B. I. Halperin, ArXiv e-prints (2012).

[44]J. D. Sau, and F. Setiawan, Phys. Rev. B **95**, 060501 (2017).

[45]C. Nayak, S. H. Simon, A. Stern, M. Freedman, and S. Das Sarma, Rev. Mod. Phys. **80**, 1083–1159 (2008).

[46]J. Alicea, Y. Oreg, G. Refael, F. von Oppen, and M. P. A. Fisher, NATURE PHYSICS **7**, 412–417 (2011).

[47]A. Kitaev, Annals of Physics **303**, 2–30 (2003).

[48]D. A. Ivanov, Phys. Rev. Lett. **86**, 268–271 (2001).

[49]T. Karzig, C. Knapp, R. M. Lutchyn, P. Bonderson, M. B. Hastings, C. Nayak, J. Alicea, K. Flensberg, S. Plugge, Y. Oreg, C. M. Marcus, and M. H. Freedman, Phys. Rev. B **95**, 235305 (2017).

[50]S. Nadj-Perge, I. K. Drozdov, B. A. Bernevig, and A. Yazdani, Phys. Rev. B **88**, 020407 (2013).

[51]F. Pientka, Y. Peng, L. Glazman, and F. von Oppen, Physica Scripta **2015**, 014008 (2015).

[52]L. Fu, and C. L. Kane, Phys. Rev. Lett. **100**, 096407 (2008).

[53]J. D. Sau, R. M. Lutchyn, S. Tewari, and S. Das Sarma, Phys. Rev. Lett. **104**, 040502 (2010).

[54]J. Alicea, Phys. Rev. B **81**, 125318 (2010).

[55]S. Nadj-Perge, I. K. Drozdov, J. Li, H. Chen, S. Jeon, J. Seo, A. H. MacDonald, B. A. Bernevig, and A. Yazdani, Science **346**, 602–607 (2014).

[56]H. O. H. Churchill, V. Fatemi, K. Grove-Rasmussen, M. T. Deng, P. Caroff, H. Q. Xu, and C. M. Marcus, Phys. Rev. B **87**, 241401 (2013).

[57]A. D. K. Finck, D. J. Van Harlingen, P. K. Mohseni, K. Jung, and X. Li, Phys. Rev. Lett. **110**, 126406 (2013).

[58]V. Mourik, K. Zuo, S. M. Frolov, S. R. Plissard, E. P. A. M. Bakkers, and L. P. Kouwenhoven, Science **336**, 1003–1007 (2012).

[59]M. T. Deng, C. L. Yu, G. Y. Huang, M. Larsson, P. Caroff, and H. Q. Xu, Nano Letters **12**, PMID: 23181691, 6414–6419 (2012).

[60]L. P. Rokhinson, X. Liu, and J. K. Furdyna, NATURE PHYSICS **8**, 795–799 (2012).

[61]M. T. Deng, C. L. Yu, G. Y. Huang, M. Larsson, P. Caroff, and H. Q. Xu, SCIENTIFIC REPORTS **4** (2014).

[62]J. Wiedenmann, E. Bocquillon, R. S. Deacon, S. Hartinger, O. Herrmann, T. M. Klapwijk, L. Maier, C. Ames, C. Bruene, C. Gould, A. Oiwa, K. Ishibashi, S. Tarucha, H. Buhmann, and L. W. Molenkamp, NATURE COMMUNICATIONS **7** (2016).

[63]A. Das, Y. Ronen, Y. Most, Y. Oreg, M. Heiblum, and H. Shtrikman, NATURE PHYSICS **8**, 887–895 (2012).

[64]R. S. Deacon, J. Wiedenmann, E. Bocquillon, F. Domínguez, T. M. Klapwijk, P. Leubner, C. Brüne, E. M. Hankiewicz, S. Tarucha, K. Ishibashi, H. Buhmann, and L. W. Molenkamp, ArXiv e-prints (2016).

Preface to Chapter 2

In this first manuscript, we study Josephson tunneling between a conventional (single band s-wave) and an unconventional (two band $s_{\pm}$) superconductor. We use a microscopic tight-binding model of the junction in which the order parameter close to the junction is determined using self-consistent mean-field theory. Since in the $s_{\pm}$ superconductor the order parameter has different signs in each of the two Fermi surfaces, the system will be frustrated if both of the Fermi surfaces interact comparably with the s superconductor. We find that if the s-$s_{\pm}$ junction is highly frustrated allowing the order parameter to be self-consistently determined has important consequences on the junction behavior. Particularly, one of types of energy/phase relation found for this system, the “double-minimum" junction, can only be found when spatial variations of the order parameter are considered. The results presented in this chapter show that Josephson tunneling can be used as a probe of unconventional superconductivity and highlight the need of theoretical models of Josephson tunneling that take into account variations in the superconducting order parameter.

2

Effects of order parameter self-consistency in a $s_{\pm}$-s junction

Rosa Rodríguez-Mota[1], Erez Berg[2] and T. Pereg-Barnea[1]

[1]Department of Physics and the Centre for Physics of Materials, McGill University, Montreal, Quebec, Canada H3A 2T8
[2]Department of Condensed Matter Physics, Weizmann Institute of Science, Rehovot, Israel 76100

This chapter has been published in Physical Review B.
Journal Reference: Physical Review B 93, 214507 (2016)

Abstract

The properties of Josephson tunneling between a single band s-wave superconductor and a two band $s_{\pm}$ superconductor are studied, in relation to recent experiments involving iron-based superconductors. We study both a single junction and a loop consisting of two junctions. In both cases, the relative phase between the order parameters of the two superconductors is tuned and the energy of the system is calculated. In a single junction, we find four types of behaviors characterized by the location of minima in the energy/phase relations. These phases include a newly found double minimum junction which appears only when the order parameters are treated self-consistently. We analyze the loop geometry setup in light of our results for a single junction, where the phase difference in the junctions is controlled by a threaded flux. We find four types of energy/flux relations. These include states for which the energy is minimized when the threaded flux is an integer or half integer number of flux quanta, a time reversal broken state and a meta-stable state.

2.1 Introduction

The experimental determination of the pairing symmetry of an unconventional superconductor is an important tool for narrowing down the microscopic theories which suggest different origins for superconductivity in the system. Shortly after the discovery of the iron-based superconductors (FeSCs)[1, 2], spin fluctuations were proposed as the pairing mechanism in this family. This mechanism results in a novel pairing symmetry, called $s_{\pm}$[3, 4]. The $s_{\pm}$ order parameter is finite on both the hole and electron Fermi pockets but changes sign between the Brillouin zone Γ point, where the hole pockets are, and the M point, where the electron pockets reside. Although most evidence point towards spin fluctuations as the pairing mechanism, superconductivity on FeSCs could also arise from orbital fluctuations, in which case, the order parameter on electron and hole pockets would have the same phase[3, 4]. It is therefore crucial to pin down the possible sign difference between the two types of pockets. The sign difference has proven challenging to detect[5–12], and despite experimental evidence in favor of $s_{\pm}$[13–16], the pairing symmetry of FeSCs has not been unequivocally determined.

One important tool for detecting the order parameter structure is the Josephson effect, due to its sensitivity to the order parameter phase difference across the junction. The Josephson effect played a key role in determining the d-wave nature of the order parameter of the high T_c cuprate superconductors[17, 18]. There, the phase of the order parameter is tied to the crystallographic direction and one can engineer a π corner junction by piecing together samples in different orientations. In contrast, identifying a sign change in the case of the iron based superconductors is more challenging. This is because the sign change is expected between Fermi pockets at low momenta (at the Γ point) and Fermi pockets at high momenta (at the M point). Therefore, a rotation of the physical lattice does not result in a sign change.

In iron based superconductors (FeSCs), some evidence in favor of $s_{\pm}$ order parameter symmetry was provided by a loop-flux experiment by Chen *et al.*[16]. The setup consisted of a niobium fork making two contacts with a sample of $\mathrm{NdFeAsO_{0.88}F_{0.12}}$. This amounts to a loop made of a conventional s-wave superconductor which is connected in two points to an FeSC sample. This loop was subjected to a pulse of magnetic flux after which the flux in the loop was measured over time. Flux jumps of integer and half integer units of the superconducting flux quantum were observed. As explained in Ref. [19], this can be interpreted as a meta-stable $1/2$-flux loop, possible in the case of $s_{\pm}$-s-wave loop.

The problem of a junction between an s-wave superconductor and an $s_{\pm}$-superconductor was considered by several authors previously[12, 19–34]. Those include different approaches such as the Ginzburg-Landau (GL) formalism[19, 25, 34], calculating Josephson current from Andreev levels[24], or through Usadel quasiclassical equation[28–30], among others.

The literature points at two possible types of contacts: (i) the s-wave superconductor couples predominantly to either the electron or hole pockets or (ii) the couplings between the s-wave and the electron and hole pockets are comparable leading to Josephson frustration. One type of proposals to experimentally determine the $s_{\pm}$ symmetry rely on the ability to produce different types of contacts in which the s-wave predominantly couples to one type of pocket or another[24, 28, 35–38]. Other experimental proposals assume comparable coupling to both pockets and conclude that the Josephson frustration can lead to a time reversal symmetry breaking phase (TRB) in a loop setup[19, 22, 25–27].

It has been argued[12, 22, 24], and will be argued in this work, that higher order harmonics in the Josephson current, which are often neglected, for instance within the Ginzburg-Landau[19, 25, 34] and the Usadel quasiclassical equation[28–30, 39] approaches, become very important in this scenario. At low temperatures, this is especially crucial in the case of comparable coupling between the s-wave superconductor and the hole/electron pockets.

In the current paper we work with a microscopic model on a lattice in an $s_{\pm}$-s-wave junction setup. While our model is similar to that investigated by previous authors[12, 20, 21] our treatment is different as we solve the Bogoliubov deGennes equations *self-consistently*. The self-consistently causes the order parameters of the superconductors on both sides of the junction to be a function of the distance from the junction, both their amplitude and phase. This helps the system relieve some of its Josephson frustration and leads to important differences from the non self-consistent treatment. Namely, we find that a double minimum structure in the energy/phase difference relation is obtained only when the Bogoliubov-deGennes equations are solved self-consistently.

In the next section, we present our model and method for a single $s_{\pm}$-s-wave junction (section 2.2.1). The results are presented in section 2.2.2 and discussed in section 2.2.3. Section 2.3 discusses the combination of two $s_{\pm}$-s junctions into a loop and its possible states.

2.2 $s_{\pm}$-s junction

2.2.1 The model

We study the Josephson junction depicted in Fig. 2.1 within a tight-binding formalism. In this arrangement, we consider both superconductors to be two dimensional, and the tunneling between them is planar and directed along the (1 0) direction. For simplicity, the lattice constant of both superconductors is taken to be equal and will be set to 1 for the remainder of this paper. In order to provide a better understanding of our model, we first write the Hamiltonian for each superconductor separately without tunneling between

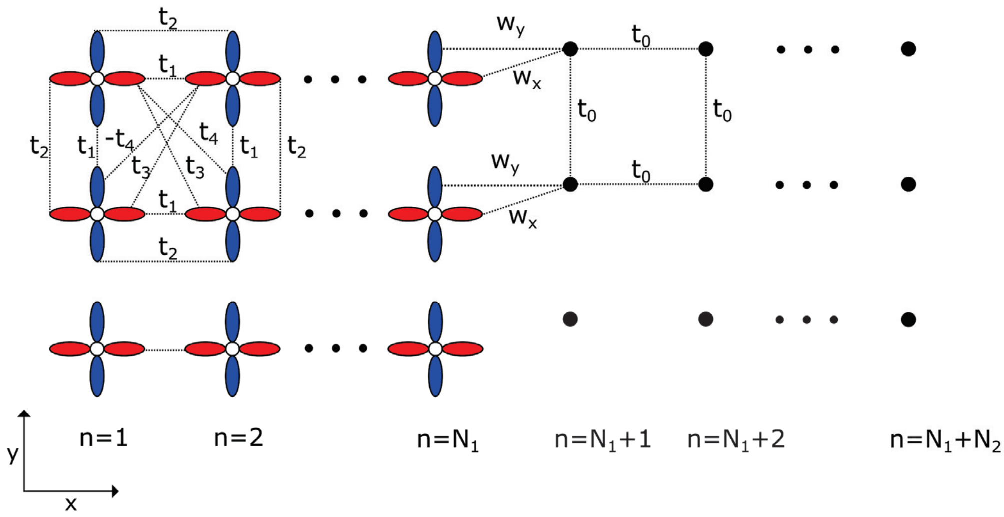

Figure 2.1: Illustration of the planar junction studied in this work showing the different hopping parameters. The $s_{\pm}$ superconductor (left) has two orbitals per site and the s superconductor (right) one.

them.

$s_{\pm}$ Superconductor

For the $s_{\pm}$ superconductor, we use a minimal two orbital model[40] in which the two orbitals correspond to the $3d_{xz}$ and $3d_{yz}$ iron orbitals illustrated by red/blue lobes in Fig. 2.1. In this model, there are four different types of hopping: t_1 is the amplitude of nearest neighbor intra-orbital hopping in the direction in which the orbitals maximally overlap, t_2 is the nearest neighbor intra-orbital hopping amplitude in the direction in which the orbitals minimally overlap, t_3 is the next-nearest neighbor intra-orbital hopping amplitude, and t_4 is the next-nearest neighbor inter-orbital hopping. We add Cooper pairing with $s_{\pm}$ symmetry in the form of an intra-orbital pairing[21, 41] with the momentum structure $\cos k_x \cos k_y$. We define the operators $d^{\dagger}_{x,\mathbf{k},\sigma}$ and $d^{\dagger}_{y,\mathbf{k},\sigma}$ which create an electron in the d_{xz}, d_{yz} orbital with momentum $\mathbf{k}$ and spin σ. Using these operators we write the Hamiltonian $H_{s_{\pm}}$ in the form $H_{s_{\pm}} = \sum_{\mathbf{k}} \Psi^{\dagger}(\mathbf{k}) A(\mathbf{k}) \Psi(\mathbf{k})$, where $\Psi^{\dagger}(\mathbf{k}) = \left(d^{\dagger}_{x,\mathbf{k},\uparrow}, d_{x,-\mathbf{k},\downarrow}, d^{\dagger}_{y,\mathbf{k},\uparrow}, d_{y,-\mathbf{k},\downarrow}\right)$, and

$$A(\mathbf{k}) = \begin{pmatrix} \epsilon_x(\mathbf{k}) & \Delta_x(\mathbf{k}) & \epsilon_{xy}(\mathbf{k}) & 0 \\ \Delta_x^*(\mathbf{k}) & -\epsilon_x(\mathbf{k}) & 0 & -\epsilon_{xy}(\mathbf{k}) \\ \epsilon_{xy}(\mathbf{k}) & 0 & \epsilon_y(\mathbf{k}) & \Delta_y(\mathbf{k}) \\ 0 & -\epsilon_{xy}(\mathbf{k}) & \Delta_y^*(\mathbf{k}) & -\epsilon_y(\mathbf{k}) \end{pmatrix} \tag{2.2.1}$$

$$\begin{aligned} \epsilon_x(\mathbf{k}) &= -2t_1 \cos k_x - 2t_2 \cos k_y - 4t_3 \cos k_x \cos k_y - \mu \\ \epsilon_y(\mathbf{k}) &= -2t_2 \cos k_x - 2t_1 \cos k_y - 4t_3 \cos k_x \cos k_y - \mu \\ \epsilon_{xy}(\mathbf{k}) &= -4t_4 \sin k_x \sin k_y \\ \Delta_{x,y}(\mathbf{k}) &= \Delta_{x,y} \cos k_x \cos k_y \end{aligned} \tag{2.2.2}$$

where μ is the chemical potential, $\Delta_{x,y}$ is the pairing amplitude and ϵ_i are the Fourier transforms of the hoping amplitudes.

Close to the junction we expect the order parameter of both superconductors to become dependent on position. A mean-field Hamiltonian cannot account for the effects of this order parameter modification, therefore it is necessary to write down interaction terms which lead to superconductivity in our system. The position dependence of the order parameter is then determined self-consistently.

We consider the $s_{\pm}$ order parameter to arise from a $J_1 - J_2$ nearest neighbors and next nearest neighbors anti-ferrromagnetic Heisenberg interaction. The mean-field decoupling of this interaction leads to four possible pairing symmetries. The dominant pairing symmetry for this model is $s_{\pm}$ in the relevant region of parameters[41]. For simplicity, we only consider the terms of the interaction that lead to an intra-orbital $s_{\pm}$ pairing.

Hence we write the interaction term as:

$$\sum_{\mathbf{k},\mathbf{k}',\mathbf{q},\alpha} V\left(\mathbf{k},\mathbf{k}',\mathbf{q}\right) d^{\dagger}_{\alpha,\mathbf{k},\uparrow} d^{\dagger}_{\alpha,-\mathbf{k}+\mathbf{q},\downarrow} d_{\alpha,-\mathbf{k}'+\mathbf{q},\downarrow} d_{\alpha,\mathbf{k}',\uparrow} \tag{2.2.3}$$

where

$$\begin{aligned} V\left(\mathbf{k},\mathbf{k}',\mathbf{q}\right) = -\frac{8J_2}{N} \cos\left(k_x - \frac{q_x}{2}\right) \cos\left(k_y - \frac{q_y}{2}\right) \times \\ \cos\left(k'_x - \frac{q_x}{2}\right) \cos\left(k'_y - \frac{q_y}{2}\right), \end{aligned} \tag{2.2.4}$$

and $\alpha = x, y$ here and throughout the paper. This interaction is decoupled as:

$$\sum_{\mathbf{k},\mathbf{q},\alpha} \Delta_{\alpha}(\mathbf{q}) f\left(\mathbf{k},\mathbf{q}\right) d^{\dagger}_{\alpha,\mathbf{k},\uparrow} d^{\dagger}_{\alpha,-\mathbf{k}+\mathbf{q},\downarrow} + h.c. \tag{2.2.5}$$

with the structure factor

$$f\left(\mathbf{k},\mathbf{q}\right) = \cos\left(k_x - \frac{q_x}{2}\right) \cos\left(k_y - \frac{q_y}{2}\right), \tag{2.2.6}$$

and

$$\Delta_{\alpha}(\mathbf{q}) = -\frac{8J_2}{N} \sum_{\mathbf{k}'} f\left(\mathbf{k}',\mathbf{q}\right) \left\langle d_{\alpha,-\mathbf{k}'+\mathbf{q},\downarrow} d_{\alpha,\mathbf{k}',\uparrow} \right\rangle. \tag{2.2.7}$$

In a system with translation invariance, the ground state corresponds to zero momentum pairing, i.e. $\Delta_{\alpha}(\mathbf{q}) = \Delta_{\alpha}\delta_{\mathbf{q},0}$ resulting in the mean field Hamiltonian, Eq. (2.2.1). Furthermore, the self-consistent solution in the translational invariant system gives $\Delta_x = \Delta_y$, which corresponds to electron-electron and hole-hole pairing with opposite signs.

s-wave Superconductor

The s-wave superconductor is modeled using one orbital per site, nearest neighbors hopping t_0, and momentum independent pairing Δ_0. The operator $c^{\dagger}_{\sigma\mathbf{k}}$ creates an electron with momentum $\mathbf{k}$ and spin σ on the s-wave superconductor side. The system is described by $H_s = \sum_{\mathbf{k}} \Phi^{\dagger}_{\mathbf{k}} B_{\mathbf{k}} \Phi_{\mathbf{k}}$, where $\Phi^{\dagger}_{\mathbf{k}} = \begin{pmatrix} c^{\dagger}_{\mathbf{k},\uparrow} & c_{-\mathbf{k},\downarrow} \end{pmatrix}$,

$$B_{\mathbf{k}} = \begin{pmatrix} \epsilon_0(\mathbf{k}) - \mu_0 & \Delta_0 \\ \Delta_0^* & -\epsilon_0(\mathbf{k}) + \mu_0 \end{pmatrix}, \tag{2.2.8}$$

$\epsilon_0(\mathbf{k}) = -2t_0(\cos(k_x) + \cos(k_y))$, μ_0 is the chemical potential, and Δ_0 the pairing amplitude.

To account for superconductivity in the s-wave side of the system, we use an attractive Hubbard-U term:

$$-\frac{U}{N} \sum_{\mathbf{k},\mathbf{k}',\alpha} c^{\dagger}_{\mathbf{k},\uparrow} c^{\dagger}_{-\mathbf{k}+\mathbf{q},\downarrow} c_{-\mathbf{k}'+\mathbf{q},\downarrow} c_{\mathbf{k}',\uparrow}, \tag{2.2.9}$$

with $U > 0$. In a translation-invariant system, the mean-field decoupling of this interaction leads to the Hamiltonian H_s mentioned above and the self-consistency equation:

$$\Delta_0 = -\frac{U}{N} \sum_{\mathbf{k}} \langle c_{-\mathbf{k},\downarrow} c_{\mathbf{k},\uparrow} \rangle . \tag{2.2.10}$$

Junction

The model of the $s_{\pm}$-s junction considered in this work consists of the two superconductors previously described connected through a tunneling contact along the (1 0) direction. We consider N_1 lattice sites in the x-direction in the $s_{\pm}$ superconductor and N_2 in the s-wave superconductor. The contact breaks the translation symmetry along the x-direction, but since the y-direction is still periodic, the momentum k_y is well defined. The natural description of the system is in terms of the operator $d^{\dagger}_{\alpha,k_y,\sigma}(n)$ which create an electron whose momentum component in the y-direction is k_y, on a site with x-coordinate index n, with spin σ in the α orbital, and $c^{\dagger}_{k_y,\sigma}(n)$ which creates an electron whose momentum component in the y-direction is k_y, on a site with x-coordinate n, with spin σ in the s-wave superconductor. In order to write the Hamiltonian, we define the vectors

$$\begin{aligned} d^{\dagger}_{\alpha,\sigma}(k_y) &= \begin{pmatrix} d^{\dagger}_{\alpha,k_y,\sigma}(1) & ... & d^{\dagger}_{\alpha,k_y,\sigma}(N_1) \end{pmatrix}, \text{and} \\ c^{\dagger}_{\sigma}(k_y) &= \begin{pmatrix} c^{\dagger}_{k_y,\sigma}(N_1+1) & ... & c^{\dagger}_{k_y,\sigma}(N_1+N_2) \end{pmatrix} \end{aligned} \tag{2.2.11}$$

which contain all the possible creation operators for a given k_y, spin and orbital. Combining them into Nambu vectors

$$\begin{aligned} &\Psi^{\dagger}_{s\pm}(k_y) = \begin{pmatrix} d^{\dagger}_{x,\uparrow}(k_y) & d^{\dagger}_{y,\uparrow}(k_y) & d^{T}_{x,\downarrow}(-k_y) & d^{T}_{y,\downarrow}(-k_y) \end{pmatrix} \\ &\Psi^{\dagger}_{s}(k_y) = \begin{pmatrix} c^{\dagger}_{\uparrow}(k_y) & c^{T}_{\downarrow}(-k_y) \end{pmatrix}, \end{aligned} \tag{2.2.12}$$

allows us to write the Hamiltonian in the following compact form:

$$H = \sum_{k_y} \Psi^{\dagger}(k_y) \begin{pmatrix} H_{s\pm}(k_y) & T \\ T^{\dagger} & H_s(k_y) \end{pmatrix} \Psi(k_y) + C, \tag{2.2.13}$$

where C is defined below and

$$\Psi^{\dagger}(k_y) = \begin{pmatrix} \Psi^{\dagger}_{s\pm}(k_y) & \Psi^{\dagger}_{s}(k_y) \end{pmatrix}.$$

The matrices $H_{s_\pm}(k_y)$ and $H_s(k_y)$ are given by the following BCS form:

$$H_{s\pm(s)}(k_y) = \begin{pmatrix} K_{s\pm(s)}(k_y) & \Delta_{s\pm(s)}(k_y) \\ \Delta_{s\pm(s)}(k_y)^\dagger & -K_{s\pm(s)}(-k_y)^* \end{pmatrix} \tag{2.2.14}$$

For the s-wave part of the Hamiltonian $H_s(k_y)$, $K_s(k_y)$ and $\Delta_s(k_y)$, are $N_2 \times N_2$ matrices given by:

$$\begin{aligned} (\Delta_s(k_y))_{m,n} =& \Delta_s(N_1 + n)\delta_{m,n} \\ (K_s(k_y))_{m,n} =& -(2t_0 \cos(k_y) + \mu_0)\,\delta_{m,n} \\ & - t_0\left(\delta_{m,n+1} + \delta_{m,n-1}\right). \end{aligned} \tag{2.2.15}$$

For the $s_\pm$ part of the Hamiltonian the matrices $K_{s_\pm}(k_y)$ and $\Delta_{s\pm(s)}(k_y)$ can be further decomposed as:

$$K_{s_\pm}(k_y) = \begin{pmatrix} K_x(k_y) & K_{xy}(k_y) \\ K_{xy}(k_y) & K_y(k_y) \end{pmatrix}, \tag{2.2.16}$$

and

$$\Delta_{s_\pm}(k_y) = \begin{pmatrix} \Delta_x(k_y) & 0 \\ 0 & \Delta_y(k_y) \end{pmatrix}, \tag{2.2.17}$$

where the above sub-blocks are the following $N_1 \times N_1$ matrices:

$$\begin{aligned}
(K_x(k_y))_{m,n} =& -(2t_2\cos(k_y)+\mu)\,\delta_{m,n} \\
& -(t_1+2t_3\cos(k_y))\,(\delta_{m,n+1}+\delta_{m,n-1}) \\
(K_y(k_y))_{m,n} =& -(2t_1\cos(k_y)+\mu)\,\delta_{m,n} \\
& -(t_2+2t_3\cos(k_y))\,(\delta_{m,n+1}+\delta_{m,n-1}) \\
(K_{xy}(k_y))_{m,n} =& -2it_4\sin(k_y)\,(\delta_{m,n+1}-\delta_{m,n-1}) \\
(\Delta_\alpha(k_y))_{m,n} =& \Delta_\alpha(n+1,n)\cos(k_y)\delta_{m,n+1} \\
& +\Delta_\alpha(n-1,n)\cos(k_y)\delta_{m,n-1}
\end{aligned} \tag{2.2.18}$$

The matrix T describes the tunneling contact between the two superconductors. As shown in Figure 2.1, we consider hopping an electron in the $3d_{xz}$ ($3d_{yz}$) orbital of the last site of the $s_{\pm}$ superconductor to the first site of the s-wave superconductor with an amplitude w_x (w_y). Hence, T is given by:

$$T = \begin{pmatrix} T_x & 0 \\ T_y & 0 \\ 0 & -T_x \\ 0 & -T_y \end{pmatrix}, \tag{2.2.19}$$

with,

$$(T_\alpha)_{m,n} = -w_\alpha \delta_{m,N_1}\delta_{n,1} \tag{2.2.20}$$

here T_x and T_y are $N_1 \times N_2$ matrices.

Finally C in Eq. (2.2.13) is equal to:

$$C = \frac{N_y}{2J_2} \sum_{\alpha,n=1}^{N_1-1} |\Delta_\alpha(n,n+1)|^2 - \frac{N_y}{U} \sum_{n=N_1+1}^{N_1+N_2} |\Delta_0(n)|^2 \tag{2.2.21}$$

Since superconductivity arises from the spin interaction terms given in Eqs. 2.2.3-2.2.4,2.2.9, the following self-consistency equations should be satisfied:

$$\begin{aligned} \Delta_\alpha(n,n+1) = &- \frac{2J_2}{N_y} \sum_{k_y} \cos k_y \left(g_{\alpha,k_y}(n+1,n)\right. \\ &\left.+ g_{\alpha,k_y}(n,n+1)\right) \\ \Delta_s(n) = &-\frac{U}{N_y} \sum_{k_y} \left\langle c_{-k_y,\downarrow}(n) c_{k_y,\uparrow}(n) \right\rangle, \end{aligned} \tag{2.2.22}$$

with $g_{\alpha,k_y}(m,n) = \left\langle d_{\alpha,-k_y,\downarrow}(m) d_{\alpha,k_y,\uparrow}(n) \right\rangle$.

We study how the energy of the system and the current depend on the phase difference between the two superconductors. In an infinite system, this can be modeled by fixing the order parameter at $\pm\infty$ and imposing a phase difference between the two ends. The self-consistency equations of our lattice model are complicated and must be solved numerically, on a finite lattice. Therefore, we model the composite system by dividing each superconductor into a bulk part and a junction. In the bulk of the $s_\pm$ superconductor, we set $\Delta_x(n,n+1) = \Delta_y(n,n+1) = \Delta_\pm$, where $\Delta_\pm$ is real, positive and equal to the pairing amplitude that is obtained self-consistently in a translation invariant system, ignoring the contact. In the bulk part of the s-wave superconductor, $\Delta_0(n) = |\Delta_0|e^{i\phi}$, with $|\Delta_0|$ self-consistently determined in the absence of the interface. ϕ is the phase difference between the s-wave order parameter away from the contact and the $s_\pm$ order parameter away from the contact on the other side. In the part near the junction, $\Delta_x(n,n+1)$, $\Delta_y(n,n+1)$ and $\Delta_0(n)$ are determined by the self-consistency equations, Eq. (2.2.22). Once the order parameters of the system are determined self-consistently, the energy of the system can be found. The current across the contact can be obtained from the energy dependence on the phase difference as $I\left(\phi\right) = \frac{2\mathrm{e}}{\hbar}\frac{dE}{d\phi}$. For simplicity, we ignore the small phase gradient in the bulk in situations where a supercurrent is flowing through the junction.

2.2.2 Results

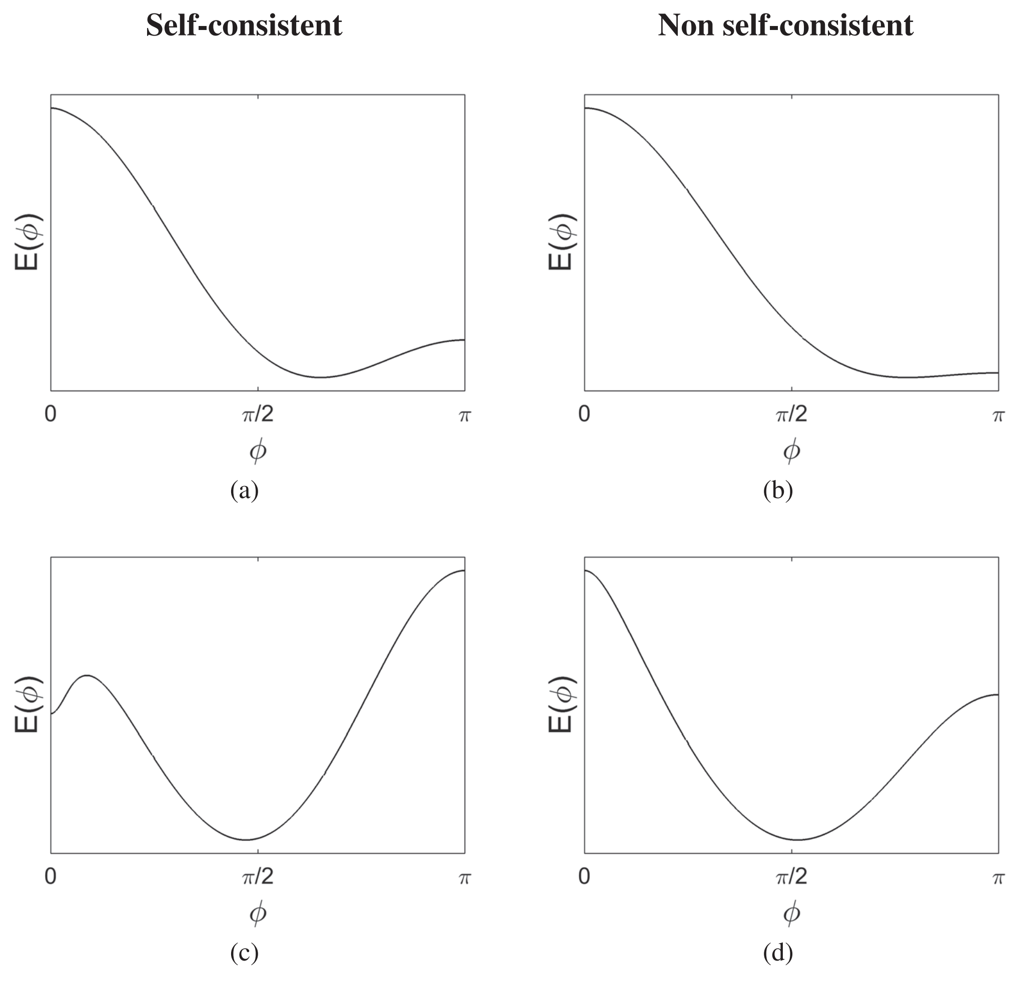

Figure 2.2: LEFT: Examples of energy vs. phase behavior calculated self-consistently for (a) a 0-Junction and (c) a Double Minimum Junction. RIGHT: Panels (b) and (d) show the energy vs. phase behavior obtained from non self-consistent calculations for the same parameters used in (a) and (c), respectively.

We have performed junction simulations on a 20 by 20 lattice for each of the s-wave and the $s_{\pm}$ superconductors, allowing the order parameters of the system to be determined self-consistently on up to 5 lattice sites from the contact. In order to elucidate the effects of the self-consistent determination of the order parameter, we also perform non-self-consistent energy and current calculations in which the order parameters are fixed.

All of the energy relations found in our model are 2π periodic and inversion symmetric ($E(\phi) = E(-\phi)$). We therefore present the energy-phase relation in the $[0, \pi]$ interval. For the studied parameter space, we find four types of junctions: a) 0-junctions where the energy is minimized when the phase difference between the order parameter of the s-wave superconductor and the hole pockets is 0 (corresponding to a phase difference of π between the s-wave and the electron pockets), b) π-junctions, where the energy is minimized for phase difference π, c) ϕ-junctions, see Fig. 2.2a, where the energy is minimized for a phase value ϕ, with $0 < \phi < \pi$ and d) double minimum junctions, see Fig. 2.2c, which present two minima in the $[0, \pi]$ interval, a local minimum at 0 and a global minimum at $0 < \phi \leq \pi$. In the following text we use the term π-junction in the sense that the junction energy is minimized for a phase difference of π between the s-wave and the $s\pm$-wave order parameter of the hole pockets, as described above.

Phase diagram

Our model contains parameters that characterize the properties of both superconductors and the contact between them. In order to study some representative phase diagrams we fix the bulk properties of the $s_{\pm}$ superconductor, and focus on varying the properties of the contact and the s-wave superconductor. Following Ref. [40] we set: $t_1 = -|t_1|$, $t_2 = 1.3|t_1|$ and $t_3 = t_4 = -0.85|t_1|$. For this choice of parameters, half filling corresponds to $\mu = 1.54|t_1|$. Since doping is a common way to tune the superconducting

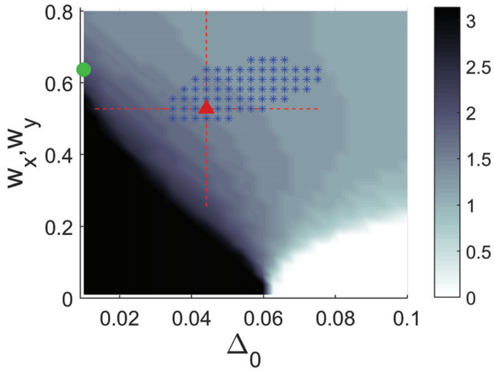

(a)

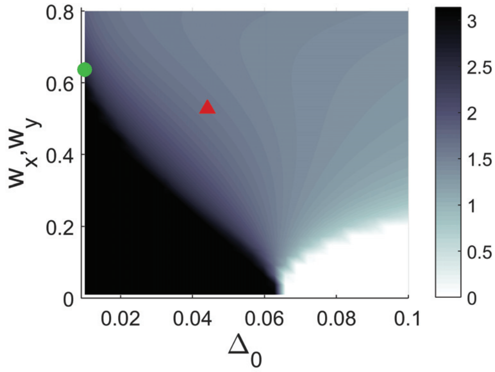

(b)

Figure 2.3: Value of the phase difference that minimizes the energy of an s-$s_{\pm}$ junction at zero temperature for $\mu_0 = -1.3$ when (a) the order parameter is solved self-consistently for both superconductors close to the contact, and (b) the order parameter is constant on both sides. The areas marked by blue symbols represent a state with a double minimum energy/phase relation, where the global minimum is at $0 < \phi \leq \pi$ while the local minimum is at 0 phase difference. All the parameters are given in units of $|t_1|$. The green circle corresponds to the parameters used in Fig. 2.2(a) and Fig. 2.2(b), and the red triangle to those of Fig. 2.2(c) and Fig. 2.2(d).

phase in FeSCs, we choose to work away from half-filling and set $\mu = 1.805|t_1|$. This value of μ corresponds to a doping of 0.18 electrons per Fe site. Following the measurements from Refs. [42, 43] and the estimates for $|t_1|$ found in Ref. [44], we set the bulk pairing amplitudes $\Delta_x(n, n+1) = \Delta_y(n, n+1) = 0.08|t_1|$. In the subsequent text we work in units such that $|t_1| = 1$. On the s-wave superconductor, we fix $t_0 = |t_1|$ to get a similar band width on the two sides of the junction. The other parameters of the s-wave superconductor, i.e. the chemical potential μ_0 and the bulk pairing amplitude Δ_0, as well as the contact parameters are varied. Sample phase diagrams are shown in Fig. 2.3, 2.4 and 2.5.

Fig. 2.3 demonstrates the importance of treating the order parameter close to the junction self consistently. The phase of junctions with a double minimum in the energy-phase relation only appears when the model is treated self consistently. We also find that the phase boundaries between the π-junction, 0-junction and the ϕ-junction are shifted in the self-consistent treatment as compared with the non-self-consistent one.

Observing the energy/phase relations, $E(\phi)$ we see that the location of the global minimum changes continuously as the model parameters are varied. If we start in a phase where the minimum is at $\phi = 0$ and change the parameters the minimum changes continuously until it reaches π. Hence, the ϕ-junction is always between the 0-junction and the π-junction. When the tunneling parameters of the contact w_x, w_y are small, the transition between the 0- and π-junction is very sharp and the ϕ-junction phase occupies only a narrow sliver in parameter space. As the tunneling amplitudes are increased, the ϕ-junction takes up a larger portion of parameter space.

The parameter μ_0, the chemical potential of the s-wave superconductor has a dramatic effect on the phase diagram. We can relate this to the overlap between the hole and electron pockets with the Fermi surface underlying the s-wave superconductor. This relation is further demonstrated in Fig. 2.4, where we slice the phase diagram along the line $w_x = w_y$ and a constant order parameter Δ_0. In all panels of Fig. 2.4 there is a critical value of the chemical potential, μ_0 such that for $\mu_0 > \mu_c > 0$, the energy of the junction is minimized when the phase difference is π and for $\mu_0 < \mu_c$, small changes in μ_0 can lead to transitions from 0 to π minimum. This striking behavior with respect to the chemical potential, μ_0, is also found when the order parameter is not solved self-consistently.

We can also observe in Fig. 2.4 that for some values of μ_0 and Δ_0, transitions from 0 to π minimum can be driven by increasing the tunneling $w_x = w_y$. These transitions become more rare with increasing Δ_0.

The final insight that can be gained from Fig. 2.4 is that the double minimum behavior becomes more common as we increase Δ_0, as well as the tunneling strength $w_x = w_y$.

The role of the tunneling parameters w_x and w_y is further explored in Fig. 2.5. The phase diagrams at zero temperature for $\Delta_0 = 0.04$ and three different values of the

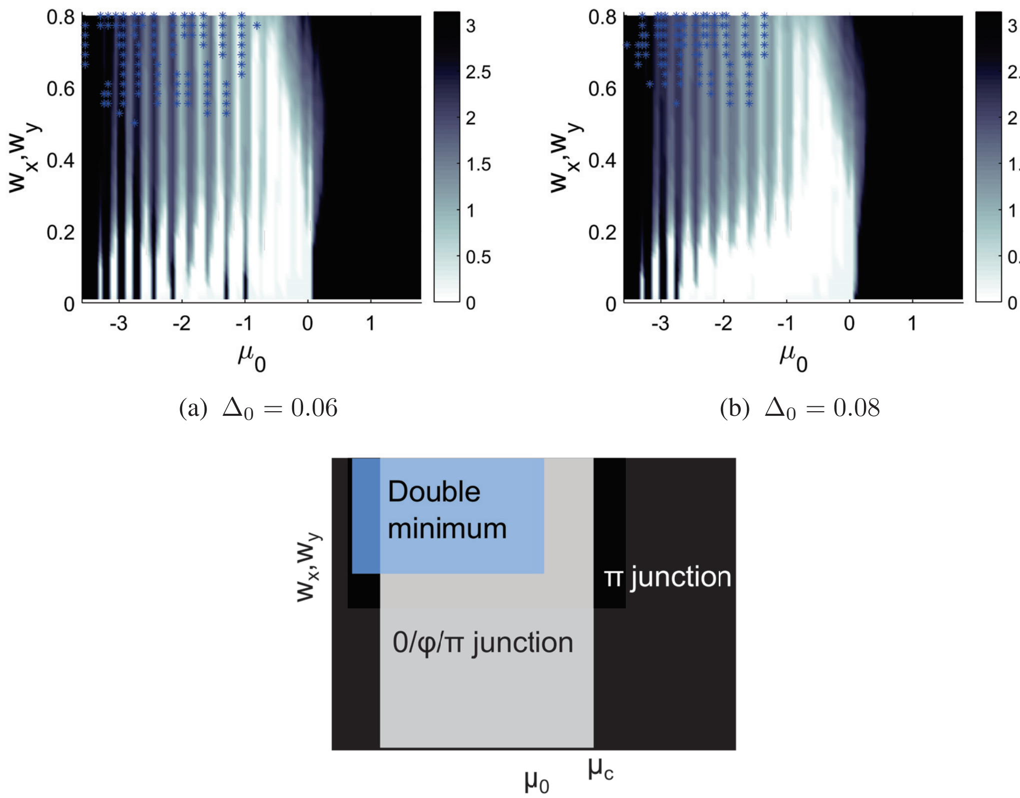

(a) $\Delta_0 = 0.06$ (b) $\Delta_0 = 0.08$

(c)

Figure 2.4: The panels (a) and (b) show the phase diagram by plotting the phase difference which minimizes the junction energy in color as a function of the tunneling amplitudes, $w_x = w_y$ and the chemical potential of the s-wave superconductor, μ_0. White regions correspond to a phase difference of 0 between the s-wave superconductor and the electron pocket order parameter while black color corresponds to a phase difference of π. The gray areas represent intermediate phase difference values and the blue symbols indicate areas with a double minimum energy/phase relation. Panel (c) is a schematic plot of the phase diagram. In the black areas the energy of the system is minimized by a phase difference of π, while in the gray area there is a close competition between the 0, ϕ and π junction phases. In the area marked by blue there is a possibility of finding an additional minimum at 0 phase difference.

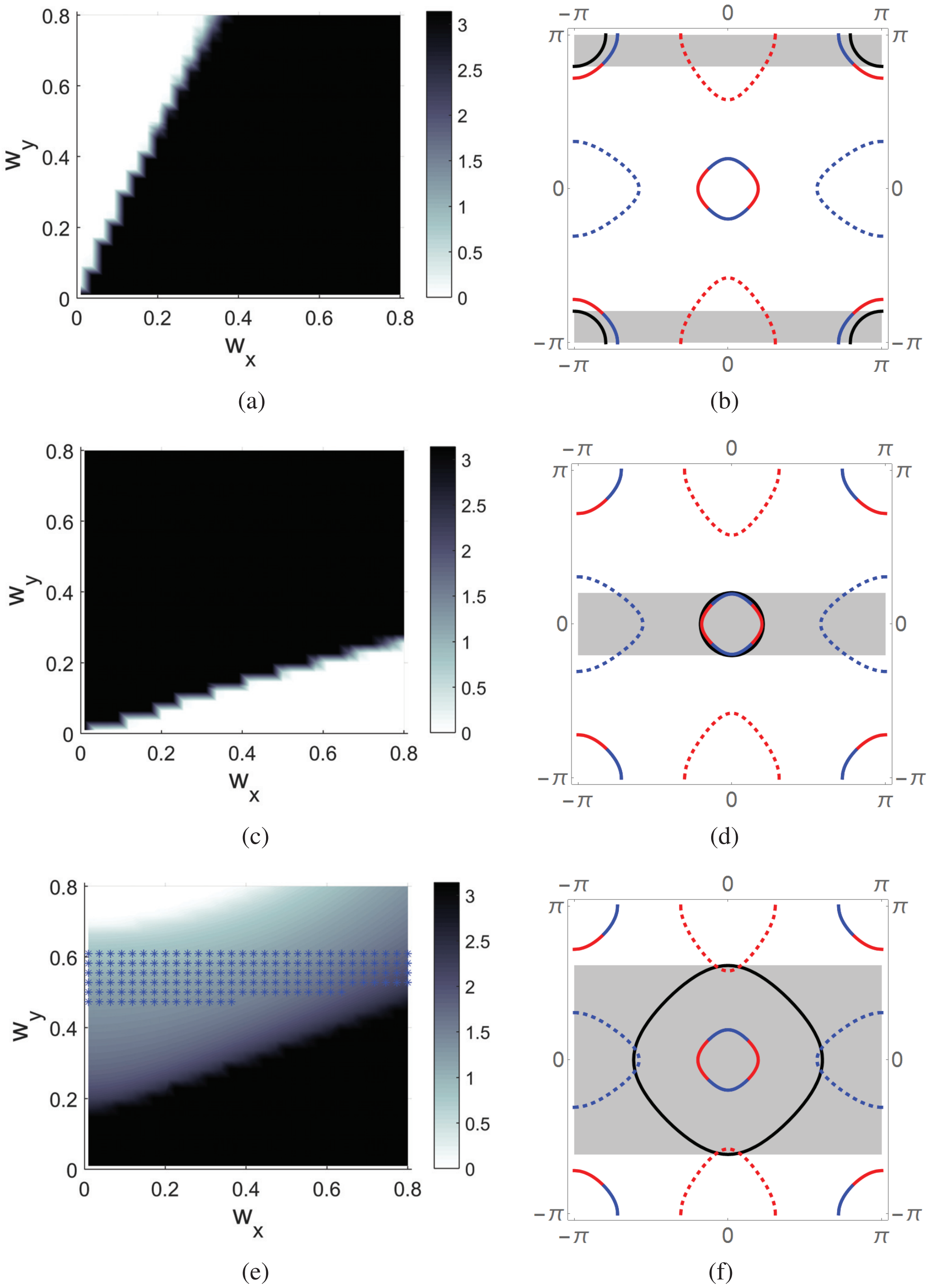

Figure 2.5: LEFT: The phase difference of the energy minimum as a function of w_x and w_y for (a) $\Delta_0 = 0.04$, $\mu_0 = 3.6$ and $U = 2.33$, (c) $\Delta_0 = 0.04$, $\mu_0 = -3.6$ and $U = 2.33$ and (e) $\Delta_0 = 0.04$, $\mu_0 = -1.3$ and $U = 1.45$. The areas marked by blue symbols represent a state with a double minimum energy/phase relation. RIGHT: Fermi surface of the two superconductors in the extended Brillouin zone centered around the Γ point for (b) $\mu_0 = 3.6$, (d) $\mu_0 = -3.6$ and (f) $\mu_0 = -1.3$. For the $s_{\pm}$ superconductor, the hole pockets marked by straight lines, and the electron pockets with dashed lines. The red/blue coloring indicates the portions of the Fermi surface whose main contribution comes from the d_{xz}/d_{yz} orbital. The Fermi surface of the s-wave system is shown with a solid black line. The shading marks the values of k_y for which there are s-wave Fermi surface states. Note that since the system is only invariant to translation in the y-direction k_y is the only relevant momentum. All the parameters are given in units of $|t_1|$.

chemical potential of the s-wave side, $\mu_0 = 3.6$, $\mu_0 = -3.6$, and $\mu_0 = -1.3$, are shown in Fig. 2.5a, Fig. 2.5c and Fig. 2.5e, respectively. The orbital composition of the Fermi surface for the $s_{\pm}$ superconductor together with the Fermi surface of the s-wave superconductor is shown in Fig. 2.5b for $\mu_0 = 3.6$, in Fig. 2.5d for $\mu_0 = -3.6$ and in Fig. 2.5f for $\mu_0 = -1.3$. The contact preserves the momentum in the y-direction, hence fixing the value of μ_0 will select the values of k_y for which Cooper pairs can tunnel through the contact. For $\mu_0 = 3.6$, as shown in Fig. 2.5a, a transition from an energy minimum at π to an energy minimum at 0 is driven by increasing the ratio w_y/w_x. It can be seen in Fig. 2.5b that for this value of μ_0 the pairs from the electron pockets that tunnel through the contact come from the d_{xz} orbital while the pairs that tunnel from the hole pockets come mostly from the d_{yz} orbital. The role of the parameters w_x and w_y for $\mu_0 = -3.6$ in Fig. 2.5c is the opposite of the one in Fig. 2.5a, an energy minimum at 0 is obtained when the ratio w_y/w_x is sufficiently small. The orbital composition of the pairs tunneling from the $s_{\pm}$ superconductor to the s superconductor for $\mu_0 = -3.6$ is shown in Fig. 2.5c. In this case, the electron-like pairs tunneling through the contact come from the d_{yz}, while the pairs coming from the hole pockets are evenly composed of d_{xz} and d_{yz} electrons.

For a large s-wave Fermi surface, the role of the parameters w_x and w_y is more difficult to understand. According to Fig. 2.5f, the electron-like pairs tunneling through the contact mainly come from the d_{yz} orbital, while the hole-like pairs are evenly composed of d_{xz} and d_{yz} electrons. Nonetheless, in Fig. 2.5e a 0-junction phase is found for large enough w_y, which cannot solely be explained by looking at the orbital composition of the $s_{\pm}$ superconductor. The close competition between electron- and hole-like pairs for a large s-wave Fermi surface is also evident in Fig. 2.5e by the wide area of ϕ-junction phase and the appearance of the double-minimum phase for large enough w_y.

Order parameter form

Since the $s_{\pm}$ order parameter is defined on the lattice links we define an on-site order parameter in the $s_{\pm}$ superconductor for the purpose of visualization:

$$\Delta_{\alpha}(n) = \frac{1}{2}\left(\Delta_{\alpha}(n, n+1) + \Delta_{\alpha}(n+1, n)\right). \tag{2.2.23}$$

In Fig. 2.6 we look at the various order parameters as a function of their position with respect to the contact. We set the parameters of the system to the double minimum regime and plot the amplitudes in Fig. 2.6a and Fig. 2.6c, and the order parameter phase in Fig. 2.6b and Fig. 2.6d for two phase difference values, 0 and $\pi/4$. The amplitudes of the various order parameters of the system for 0 and $\pi/4$ phase difference, shown in Fig. 2.6a and Fig. 2.6c respectively, presents only small differences. The variation of the phase of the order parameters from the bulk phase difference is imperceptible in Fig. 2.6b and small in Fig. 2.6d. Despite having only small quantitative differences in the shape of the self-consistent solution for different phases, determining the order parameter self-consistently has important consequences for this choice of parameters, as it leads to the double minimum phase.

In the different panels of Fig. 2.6 we observe the presence of sharp oscillations. This kind of oscillations has been previously found in microscopic models of s-wave superconductors close to an insulating boundary and has been attributed to Friedel-like oscillations[45–47]. The period of the oscillations seen here is dependent on the chemical potential as expected.

In order to further explore the relation between the self-consistent determination of the order parameter and the double minimum phase, it is necessary to quantify the dependence of Δ_x and Δ_y on the phase difference ϕ. To do this, we define the following

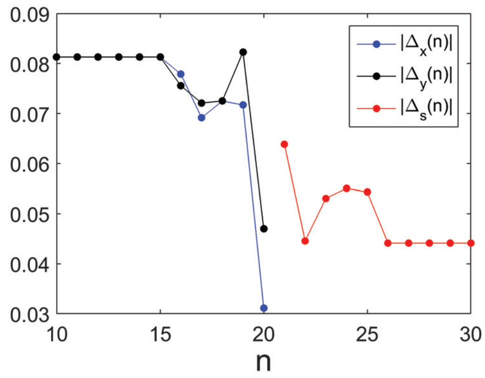

(a) $\phi = 0$

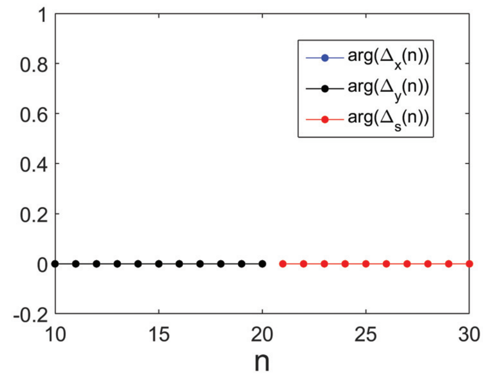

(b) $\phi = 0$

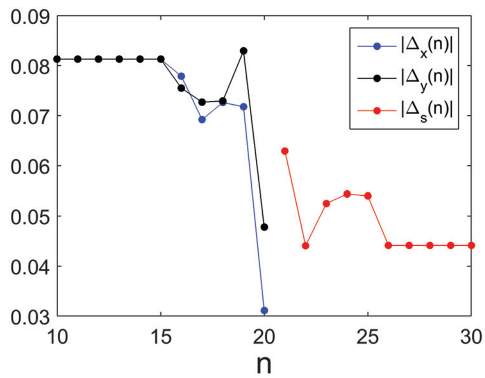

(c) $\phi = \pi/4$

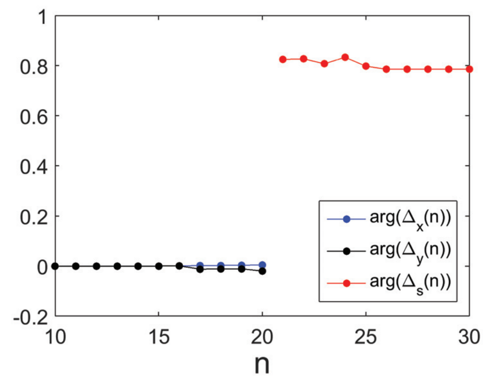

(d) $\phi = \pi/4$

Figure 2.6: LEFT: Amplitude (in units of $|t_1|$) of the order parameters of the system for two values of the phase difference (a) $\phi = 0$ and (c) $\phi = \pi/4$. RIGHT: Phase of the order parameters of the system for (b) $\phi = 0$ and (d) $\phi = \pi/4$. The set of parameters used corresponds to the red triangle in Fig. 2.3.

functions:

$$
\begin{aligned}
g_x &= |\Delta_x(N_1, \phi = \pi) - \Delta_x(N_1, \phi = 0)| \\
g_y &= |\Delta_y(N_1, \phi = \pi) - \Delta_y(N_1, \phi = 0)| \,.
\end{aligned}
\tag{2.2.24}
$$

The behavior of g_x and g_y for two different cuts of parameters around the double minimum phase is shown in Fig. 2.7. In both Fig. 2.7a and Fig. 2.7b, g_y is maximized in the double minimum regime, indicating that Δ_y has a greater dependence on the phase difference ϕ in the double minimum regime. On the other hand, the value of g_x in Figs. 2.7a and 2.7b is an order of magnitude smaller than that of g_y, signaling a much lower dependence of Δ_x with ϕ, and it increases slowly with increasing $w_x = w_y$ and Δ_0. The stronger dependence of Δ_y (compared to Δ_x) with ϕ is consistent with the greater role that w_y (compared to w_x) has in driving the transition to the double minimum regime exhibited in Fig. 2.5e. The critical current of a Josephson junction increases when increasing the order parameter of the superconductors and the tunneling through the interface. Hence, the energy cost of the Josephson frustration is higher when w_x, w_y or Δ_0 increase, leading the to a stronger dependence of the order parameter on the phase difference as a mechanism to relieve this frustration. Accordingly, the double minimum state is more likely to appear when w_x, w_y or Δ_0 are large.

2.2.3 Discussion

The problem of Josephson tunneling between an $s_{\pm}$ superconductor and a single band s-wave superconductor has been considered previously using different approaches. These previous studies point at two possible scenarios: (i) the s-wave superconductor couples predominantly to either the electron or hole pockets or (ii) the couplings between the s-wave and the electron and hole pockets are comparable leading to Josephson frustration.

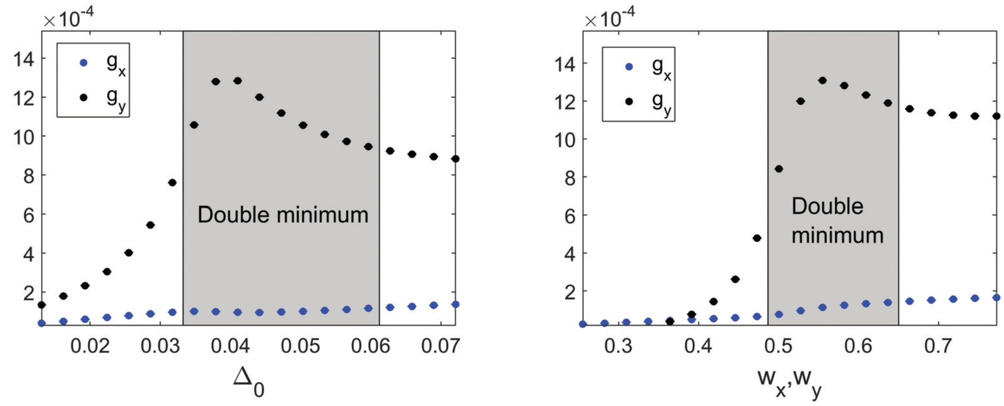

(a) (b)

Figure 2.7: Values of g_x and g_y (in units of $|t_1|$) for the parameters given by the (a) horizontal and (b) vertical cuts marked with red on Fig. 2.3. The quantities g_x and g_y, defined in Eqn. 2.2.24, measure the dependence of Δ_x and Δ_y with respect to the phase difference between the two superconductors.

The momentum space structure of the order parameter in our model is $\Delta_\alpha \cos(k_x)\cos(k_y)$, hence in the hole pockets the order parameter phase is the same phase as Δ_α while in the electron pockets the order parameter phase is shifted by π. Hence, we can interpret the 0-junction as a scenario in which the s-wave is interacting primarily with the hole pockets, the π-junction as one where the s-wave is interacting primarily with the electron pockets, and the other two cases (ϕ-junction and a double minimum junction) as resulting from competing interaction of the s-wave with electron an hole pockets.

In the current study, we find that the global minimum is at a phase difference of π, i.e. when the phase of the s-wave order parameter is equal to that of the electron-like pairs, for a large portion of the parameter space. This is consistent with the fact that we are working with an electron doped $s_\pm$ sample. Hence, the $s_\pm$ superconductor has more pairs that come from electron pocket states rather than from hole pocket states. Upon tuning of model parameters, the preferred phase difference may shift to 0. In both these cases the system minimizes its energy by matching the order parameter phase of the s-wave superconductor with either the hole or electron pockets. This tendency is strongly dependent on the overlap between Fermi surface states on both sides of the Junction. Figure 2.5 shows the orbital composition of different parts of the $s_{\pm}$ Fermi surface, at two different chemical potentials on the s-wave side and with varying tunneling amplitudes. It should be noted that while the hole pockets are composed of both the x and y orbitals, each electron pocket is dominated by one orbital. Moreover, since the contact conserves momentum only in the y-direction, the chemical potential of the s-wave part selects which parts of the $s_{\pm}$ Fermi surface participates in the tunneling. Depending on the value of μ_0, the electron-like and hole-like pairs involved in the tunneling process have a different orbital composition. Thus, the ratio of w_y/w_x at which the junction switches from the 0-junction to the π-junction phase depends on the value of μ_0 and the geometry of the junction.

Our phase diagrams suggest that a transition between a 0-junction and a π-junction does not occur directly. Instead, an intermediate ϕ-junction or double minimum phase appears (see Fig. 2.2a and 2.2c). Despite being a regime commonly found in theoretical models, there is no consensus on the mechanism behind these junction states. While Ref. [22] stresses that the extent of the ϕ-junction is related to the second Josephson harmonic, this phase is also obtained within a Ginzburg-Landau mechanism which only considers first order terms in the Josephson coupling. In this case, the mechanism that leads to the ϕ/double minimum phase is the possibility of twisting the relative phase between the hole-like and electron-like pairs.

In this work, we developed a model that considers both higher order Josephson terms and a self-consistently determined order parameter. Our results suggest that the higher order Josephson harmonics play a more important role in the realization of the ϕ state. This can be demonstrated by comparing the results of a self-consistent order parameter determination with the non-self consistent solutions. In the non-self-consistent case, the hole and electron pocket order parameters are given by the form of Eq. 2.2.2. Unlike in the self-consistent treatment, their amplitudes are related and their phase difference is always π. Comparing the two cases we see that the main difference is the appearance of the double minimum phase (Fig. 2.3). A secondary effect is a slight shift in the boundaries of the ϕ-junction state in the phase diagram. We therefore conclude that the main reason for the appearance of the ϕ-junction is the inclusion of higher harmonics in the Josephson tunneling. This is also supported by the fact that the tendency to develop a ϕ-junction is increased when the tunneling amplitude across the junction is increased.

To make this point clearer, let us look into the first two terms in the Josephson coupling. It has been pointed out in Ref. [24] that if the coupling between the hole-like pairs and the s-wave superconductor is similar to the coupling between the electron-like pairs and the s-wave superconductor, the first order terms on the Josephson energy tend to cancel each other, increasing the importance of the next order terms. This can be shown by writing the Josephson energy of the junction as $E = E_h + E_e$, where $E_{h(e)}$ is the Josephson energy associated to the coupling between the s-wave and the hole(electron) pockets. Then we have:

$$E_{h(e)} = E^{(1)}_{e(h)} \cos\left(\phi_{h(e)}\right) + E^{(2)}_{h(e)} \cos\left(2\phi_{h(e)}\right) + ..., \tag{2.2.25}$$

where $\phi_{h(e)}$ is the phase difference between the s-wave and the hole(electron) pairs. Since $\phi_e = \phi_h + \pi$, the energy of the contact is then

$$\begin{aligned} E = &\left(E^{(1)}_h - E^{(1)}_e\right) \cos\left(\phi_h\right) + \\ &\left(E^{(2)}_h + E^{(2)}_e\right) \cos\left(2\phi_h\right) + ... \end{aligned} \tag{2.2.26}$$

Hence, when $E^{(1)}_h \approx E^{(1)}_e$, the first Josephson harmonic cancels, and the second order term cannot be neglected.

Several theoretical models of an $s_{\pm}$-s junction can exhibit 0-junction, π-junction, or ϕ-junction behavior[12, 20–34]. On the other hand, a double minimum behavior has only been previously found in Ref. [19] within a Ginzburg-Landau formalism. There are important differences between our results and those of Ref. [19], namely, in the location of the two minima. The double minimum phase found in Ref. [19] is characterized by one global minimum at 0 phase difference across the junction and a local minimum at π phase difference. In our microscopic model, the 'double minimum' junction behavior also occurs when there is a global minimum at some phase $\phi \neq 0, \pi$ and a local minimum at 0 phase difference.

It is interesting to note the differences and similarities between this work and the phenomenological Ginzburg-Landau treatment of Ref. [19]. While the two models describe an interface between a single order parameter superconductor and a double order parameter superconductor the details are quite different. Most importantly, in the Ginzburg-Landau model the order parameters are defined on each band and are only coupled through their amplitudes (in a way that ensures their opposite sign is favored in the bulk). In our microscopic model, the order parameter is defined on the orbitals and due to inter-orbital hopping, the two bands are gapped. As a result, in the current work we can not easily control the gap magnitude on each band, nor can we directly control the effective coupling between the order parameters on the two bands. We should also note that while the Ginzburg-Landau model does not explicitly contain terms of higher harmonic Josephson tunneling, our model does. These differences make the comparison between the models difficult. However, we can speculate that the differences mentioned above are responsible for the different states found in the two models.

Overall, we find that for competing coupling between the electron and hole pockets and the s-wave it is important to consider higher order processes, such as higher order Josephson harmonics and the effect of the contact on the order parameters of the system.

At low tunneling strength, the contact phase diagram is dominated by the 0 -junction and π-junction phases. When the tunneling strength is increased higher order processes cause the TRB phase to widen and the double minimum phase appears.

2.3 Flux threaded $s_{\pm}$-s Loop

We now proceed to use the formalism developed for studying an $s_{\pm}$-s junction to treat the experimentally relevant problem of a flux threaded $s_{\pm}$-s loop. The system we study consists of bending the $s_{\pm}$-s junction along the x-direction and adding another planar contact to form a loop. Each of the contacts forming the loop is characterized by two tunneling parameters: $w_{\alpha}^{(1(2))}$, which describe the amplitude of tunneling an electron from the α orbital in the $s_{\pm}$ superconductor to an adjacent site in the s-wave superconductor across contact $1(2)$.

After the addition of the second contact, the Hamiltonian for the $s_{\pm}$-s junction can still be described by Eq. (2.2.13) if we modify T_{α} as:

$$(T_{\alpha})_{m,n} = -w_{\alpha}^{(1)}\delta_{m,N_1}\delta_{n,1} - w_{\alpha}^{(2)}\delta_{m,1}\delta_{n,N_2} \tag{2.3.1}$$

where the sites in the $s_{\pm}$ side of the loop are enumerated $1..N_1$ and the sites on the s-wave side are enumerated $1..N_2$. The self-consistency equations remain those given in Eq. (2.2.22).

Next, we proceed by threading the loop with a magnetic flux Φ. As shown in the Appendix, the flux dependence can be transferred to the contact by performing a gauge transformation. With the addition of magnetic flux the tunneling matrices become:

$$(T_{\alpha})_{m,n} = -w_{\alpha}^{(1)}e^{i\frac{\phi_1}{2}}\delta_{m,N_1}\delta_{n,1} - w_{\alpha}^{(2)}e^{i\frac{\phi_2}{2}}\delta_{m,1}\delta_{n,N_2} \tag{2.3.2}$$

Here, $\frac{\phi_1}{2}$ is the phase an electron acquires through a clockwise hopping across the tunneling contact 1 and $\frac{\phi_2}{2}$ the phase acquired by an anti-clockwise hopping across the contact 2. These two phases will fully account for the effect of the magnetic flux as long as ϕ_1 and ϕ_2 obey:

$$\phi_1 - \phi_2 = \frac{2\pi\Phi}{\Phi_0}, \tag{2.3.3}$$

where $\Phi_0 = \frac{hc}{2\mathrm{e}}$ is the superconducting flux quantum.

For long loops, $N_1, N_2 \gg 1$ the two junctions essentially decouple. The behavior of the order parameters near one contact is uninfluenced by the presence of the other contact and the energy cost of the two contacts is a simple sum. Moreover, by making an additional gauge transformation, the phase acquired by hopping between the two superconductors, $\frac{\phi_{1(2)}}{2}$, can be translated into a phase difference $\phi_{1(2)}$ between the two superconductor order parameters. Hence, the ground state energy of the loop is given by:

$$E\left(\Phi\right) = \min_{\phi_1-\phi_2=\frac{2\pi\Phi}{\Phi_0}} \left(E_1\left(\phi_1\right) + E_2\left(\phi_2\right)\right), \tag{2.3.4}$$

where $E_{1(2)}(\phi_{1(2)})$ is the energy of a single $s_{\pm}$-s junction where the phase difference between the superconductors is $\phi_{1(2)}$ with contact parameters $w_{\alpha}^{(1(2))}$.

If we denote the phase difference that minimizes the energy of junction 1(2) by $\phi_1^{min}(\phi_2^{min})$ then the values of flux that minimize $E(\Phi)$ are given by $\pm\frac{\Phi_0}{2\pi}\left(\phi_1^{min} + \phi_2^{min}\right)$, $\pm\frac{\Phi_0}{2\pi}\left(\phi_1^{min} - \phi_2^{min}\right)$. This allows us to deduce the energy of the flux threaded loop as a function of the flux.

We find four types of behavior of the energy vs. flux curve, shown in Fig. 2.8: 1) Integer-flux-loop with energy minima at integer flux quantum values, 2) $1/2$-flux-loop with energy minima at half integer flux quantum values, 3) Time reversal broken loop (TRB) with energy minima at fractional values of flux quantum and 4) Meta-stable, with

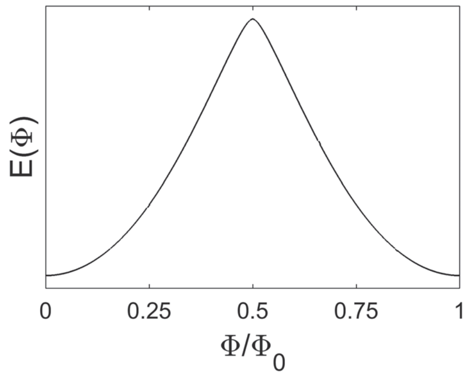

(a) 0-loop

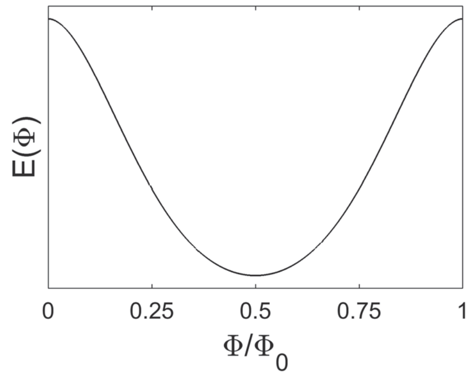

(b) π-loop

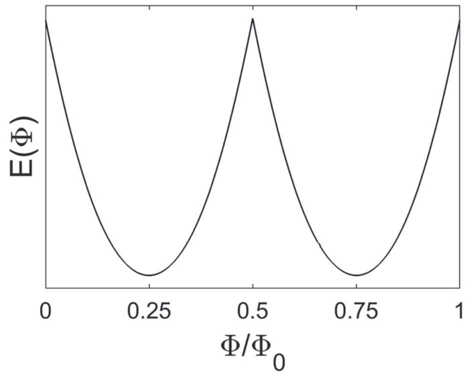

(c) TRB

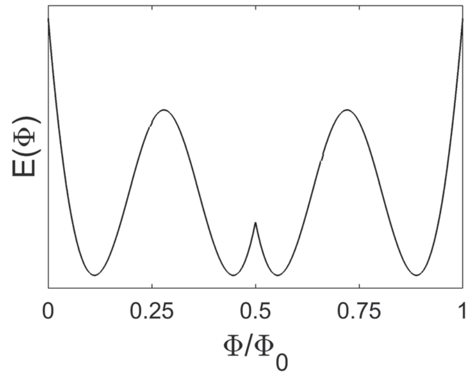

(d) TRB'

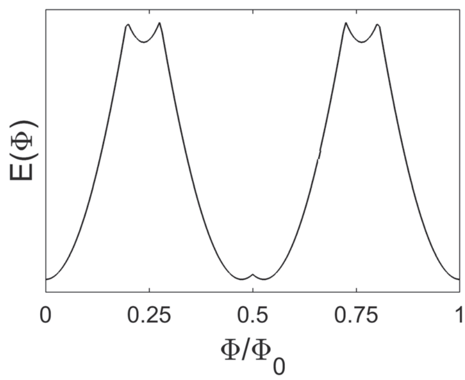

(e) Metastable

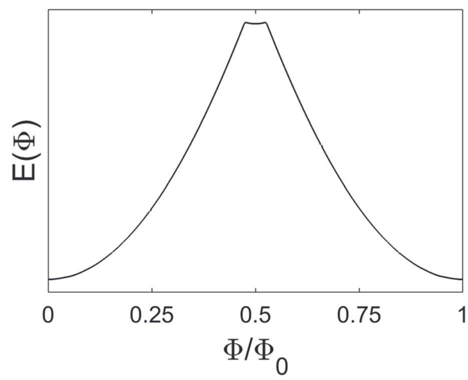

(f) Metastable'

Figure 2.8: Energy vs flux examples. In panels (a)-(e), the s-wave superconductor parameters are $\Delta_0 = 0.04$, $\mu_0 = -1.3$ and $U = 1.446$, while the junction parameters are: (a) $w_x^{(1)} = w_y^{(1)} = 0.146$, $w_x^{(2)} = 0.31$, and $w_y^{(2)} = 0.092$, (b) $w_x^{(1)} = w_y^{(1)} = w_x^{(2)} = 0.146$ and $w_y^{(2)} = 0.8$, (c) $w_x^{(1)} = w_y^{(1)} = w_x^{(2)} = 0.146$ and $w_y^{(2)} = 0.364$, (d) $w_x^{(1)} = w_y^{(1)} = 0.31$ and $w_x^{(2)} = w_y^{(2)} = 0.637$, and (e) $w_x^{(1)} = w_x^{(2)} = 0.5$ and $w_y^{(1)} = w_y^{(2)} = 0.528$. In panel (f), $\Delta_0 = 0.02$, $\mu_0 = 0.3438$, $U = 0.9341$, $w_x^{(1)} = w_y^{(1)} = 0.6638$, and $w_x^{(2)} = w_y^{(2)} = 0.6910$.

two types of energy minima. While the first three cases have been found by several authors[22, 24–28, 35–38], the possibility of an energy/flux relation with minima of different depth has not been seen in a microscopic theory before.

The case where the energy of the loop is minimized for integer values of flux quantum occurs whenever the energy of both of the contacts is minimized at a phase difference of 0 or π.

The energy of the loop is minimized for half-integer flux quantum values when the energy/phase relation one of the contacts has a minimum at 0 and the other has a minimum at π. Our analysis shows that it is possible to find this behavior without changing the bulk parameters of the superconductors if the tunneling parameters across each of the two contacts are different.

If the energy of one of the contacts is minimized for a phase difference $0 < \phi < \pi$, then the energy of the loop will be minimized for values of magnetic flux which are neither integer flux quantum nor half integer flux quantum. This causes supercurrent to flow in the loop and therefore the phase is named 'time reversal breaking'. The energy-flux relation shown in Fig. 2.8c results from having one of the contacts in the ϕ-junction phase, while the other is in the $0(\pi)$-junction phase. On the other hand, if the energy of both contacts is minimized for a phase difference $0 < \phi < \pi$ we obtain four degenerate minima: $\pm\frac{\Phi_0}{2\pi}\left(\phi_1^{min} + \phi_2^{min}\right)$, $\pm\frac{\Phi_0}{2\pi}\left(\phi_1^{min} - \phi_2^{min}\right)$. An example of this type of energy vs flux relation is shown in Fig. 2.8d. For a significant portion of the ϕ-junction phase, the value of the minimum is close to $\pi/2$. If this is the case for the two junctions forming the loop, we will find two energy minima close to integer flux quantum and two energy minima close to half integer flux quantum.

An energy/flux relation with minima of different depth such that one is a global minimum and the other is a (meta-stable) local minimum can occur when the loop is formed by two contacts that have a double minimum. As can be seen in Figure 2.8e, the energy/flux relation exhibits the four degenerate minima of Fig. 2.8d and two additional local minima. If one of the contacts is in a double minimum phase while the other is not, the resulting energy-flux behavior will be that of Fig. 2.8c or of Fig. 2.8d. In other words, in order to detect signatures of the double minimum regime in the energy-flux relation, both contacts must be in this regime. Therefore to obtain a loop with minima of different depth, it is necessary to have a) a large tunneling amplitude across the two contacts and b) a large pairing amplitude in the s-wave superconductor.

The local minima in the meta-stable relations found in this work are shallow (see Fig. 2.8e and Fig. 2.8f) and hence they would be very hard to detect experimentally. However, we find that these minima are considerably deeper for loops with large inductance. The ground state energy of a loop threaded by a total flux Φ and with inductance L is given by[48]:

$$E(\Phi) = \min_{\phi_1 - \phi_2 = \frac{2\pi\Phi}{\Phi_0}} \left(\sum_{i=1,2} \left(E_i(\phi_i) + \frac{L}{4} I_i^2(\phi_i) \right) \right) \tag{2.3.5}$$

where for simplicity we have considered an equal inductance in both arms of the loop. In Fig. 2.9, we show how the energy vs flux relations of Fig. 2.8e and Fig. 2.8f are modified for different values of the screening parameter $\beta_L = \frac{L(I_{0,1}+I_{0,2})}{\Phi_0}$, where $I_{0,1}$ and $I_{0,2}$ are the critical currents of the two junctions. As can be seen in Fig. 2.9, increasing the inductance of the loop has the effect of deepening the local energy minima.

2.4 Conclusions

We studied the Josephson tunneling between an $s_\pm$ superconductor and a single band s-wave superconductor within a microscopic formalism in which the order parameters of both superconductor are determined using self-consistent Bogoliubov-deGennes

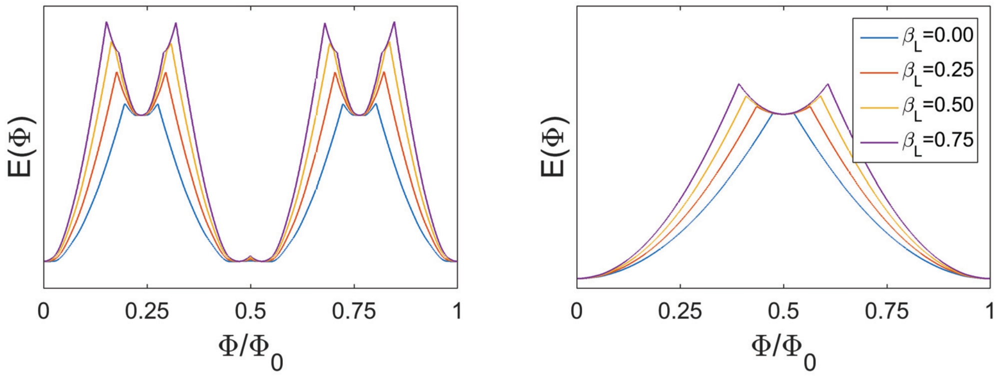

(a) Metastable (b) Metastable’

Figure 2.9: Effects of inductance in the Metastable and Metastable’ energy vs flux relations.

equations. We find four possible junction behaviors, characterized by their energy/phase difference relation. The possible states are: (i) 0-junction where the energy minimum is at zero phase difference, (ii) π-junction where the energy minimum occurs at π, (iii) ϕ-junction where $0 < \phi < \pi$, and (iv) a double minimum junctions where there are two minima, one of them global and the other local.

We find that allowing the order parameter to change its amplitude and phase self-consistently close to the junction has some important effects on the resultant phase diagram. Most notable - it is essential for the appearance of a new state, namely the double minimum junction.

We also use our results to study the energy of a flux threaded $s_{\pm}$-s loop. We find that the loop can have different types of unconventional energy/flux behavior such as, $1/2$-flux-loop, TRB and metastable.

2.5 Acknowledgments

R.R. acknowledges financial support from the FQRNT through Merit Scholarship Program for Foreign students and from the Secretary of Public Education and the Government of Mexico. T.P. acknowledges financial support from the NSERC and the FQRNT. E. B. was supported by the ISF under grant 1291/12, by the US-Israel BSF, and by a Minerva ARCHES prize. Numerical calculations for this work were performed using Calcul Québec computing resources.

2.A Magnetic flux

In this Appendix we explain how the magnetic flux is added to our microscopic model. For non-zero magnetic flux, we select a gauge in which the magnetic potential is parallel to the angular direction, i.e. $\mathbf{A} = A\hat{x}$. The magnetic flux enclosed by the loop Φ, must be equal to $\oint \mathbf{A} \cdot d\mathbf{l}$. This yields $\mathbf{A} = \frac{\Phi}{N_1+N_2}\hat{x}$, since the diameter of the circle is equal to the number of sites in the x-direction times the lattice constant $(N_1 + N_2)\,a$ and we have set $a = 1$. The hopping terms in the Hamiltonian are modified with the introduction of the magnetic potential according to Peierls substitution.

$$t \to t\exp\left(-\frac{ie}{\hbar c}\int_{r'}^{r} \mathbf{A} \cdot d\mathbf{l}\right) \tag{2.A.1}$$

For nearest neighbor hopping around the loop this leads to $t \to te^{-i\phi}$ with ϕ given by:

$$\phi = \frac{\pi}{N_1 + N_2}\left(\frac{\Phi}{\Phi_0}\right) \tag{2.A.2}$$

where $\Phi_0 = \frac{hc}{2e}$ is the superconducting flux quantum. The system can still be described by equation (2.2.13) with the appropriate modification of the matrices $K_{s_\pm}$, K_s, T_x and T_y which become dependent on the phase ϕ.

In order to simplify the Hamiltonian we use the transformation $c_{k_y,\sigma}(n) \to e^{i\frac{\phi_1}{2}-in\phi}c_{k_y,\sigma}(n)$, $d_{\alpha,k_y,\sigma}(n) \to e^{-in\phi}d_{\alpha,k_y,\sigma}(n)$, which accordingly modifies the self consistent order parameters defined by Eq. (2.2.22) as $\Delta_0\left(n\right) \to e^{i\phi_1-2in\phi}\Delta_0\left(n\right)$, $\Delta_\alpha\left(n, n+1\right) \to$

$e^{-i(2n+1)\phi}\Delta_\alpha(n, n+1)$.

It is easy to see that under this transformation the flux dependence is transferred to the contacts. This can be seen in the transformed Hamiltonian with the definitions in Eq. (2.2.13) as $K_{s_\pm}$ and K_s loose their dependence and the pairing matrices $\Delta_{s_\pm}$ and Δ_s are invariant while the T_α matrices are now given by:

$$(T_\alpha)_{m,n} = -w_\alpha^{(1)} e^{i\frac{\phi_1}{2}} \delta_{m,N_1}\delta_{n,1} - w_\alpha^{(2)} e^{i\frac{\phi_2}{2}} \delta_{m,1}\delta_{n,N_2} \tag{2.A.3}$$

where ϕ_1 and ϕ_2 are solutions of

$$\phi_1 - \phi_2 = \frac{2\pi\Phi}{\Phi_0} \tag{2.A.4}$$

2.B Numerical Methods

2.B.1 Finding the relation between the superconducting coupling constants and the bulk pairing amplitudes

In this work, we set the bulk pairing amplitudes $\Delta_x(n, n+1) = \Delta_y(n, n+1) = 0.081$. In a translationally invariant system, this corresponds to the Hamiltonian given by equations (2.2.1) and (2.2.2) with $\Delta_x = \Delta_y = 0.162$. The value of J_2 is then set such that the solution of the self-consistency equation (2.2.7) for $\mathbf{q} = 0$ is $\Delta_x = \Delta_y = 0.162$. The self-consistent equation (2.2.7) can be solved numerically, iterating from an initial guess. In a 100×100 lattice, the coupling $J_2 = 0.624$ leads to the desired value of the bulk $s_\pm$ pairing amplitude. The iteration loop was stopped when the difference between the input and the calculated order parameters was less than 1×10^{-5}.

The bulk pairing amplitude Δ_0 corresponding to given values of μ_0 and U can be

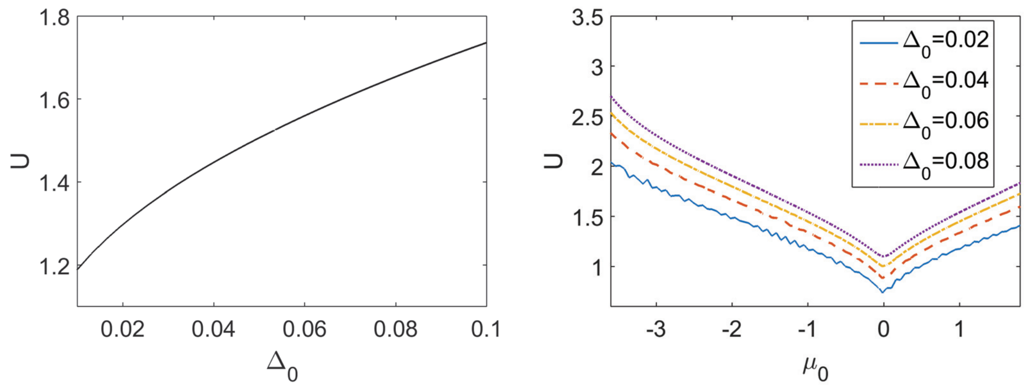

Figure 2.10: Values of the superconducting coupling U used in (a) Fig. 2.3 and (b) Fig. 2.4.

calculated by solving the self-consistency equation (2.2.10). This was done iterating equation (2.2.10) in a 100×100 lattice with periodic boundary conditions until the input and the calculated order parameters was less than 1×10^{-5}. To obtain the value of U corresponding to given values of μ_0 and Δ_0, we used a numerical solver to solve the equation $\Delta_0(\mu_0, U) - \Delta_0 = 0$ with the function $\Delta_0(\mu_0, U)$ defined as the (numerical)solution of the self-consistency equation. The values of U obtained for Figures 2.3 and 2.4 are shown in Fig. 2.10, some finite size effects can be appreciated in the solution for $\Delta_0 = 0.02$.

2.B.2 Self-consistent solution of the BdG equations - calculating the order parameter magnitude close to the junction

The self-consistency equations 2.2.22 were solved in the vicinity of the interface, using the bulk values of the order parameters, i.e $\Delta_x(n, n+1) = \Delta_y(n, n+1) = 0.081$ and $\Delta_0(n) = |\Delta_0|e^{i\phi}$, as a starting point of the iteration loop. The iteration loop is stopped when the difference in the order parameters obtained in two consecutive iterations is less than 1×10^{-6}. We consider periodic boundary conditions on the y-direction and a 20×20 lattice for each superconductor.

When changing the momentum resolution in the direction along the junction cross section (k_y) we find some sensitivity of our results to the resolution. However, the main findings are not altered. In the phase diagram the nature of the different phases is not sensitive to the k_y resolution but the phase boundaries may shift slightly.

2.B.3 Energy/flux curves

The energy/flux relation for the array in Sec. 2.3 can be easily found from the energy/phase profile of the two interfaces following Eqn. 2.3.4. The energy/ phase relation is found by solving the order parameter self-consistently and the energy using exact diagonalization for 41 evenly spaced values of the phase difference between 0 and 2π. Afterwards, we can define the energy/phase relations $E_{1(2)}(\phi)$ for any value of ϕ using cubic Hermite spline interpolation. Finally, the energy vs flux curve is given by:

$$E\left(\Phi\right) = \min_{0\leq\phi\leq 2\pi} E_1\left(\phi + \frac{2\pi\Phi}{\Phi_0}\right) + E_2\left(\phi\right), \tag{2.B.1}$$

Since the value of ϕ is bounded and the minima of $E_1\left(\phi + \frac{2\pi\Phi}{\Phi_0}\right) + E_2\left(\phi\right)$ are very sharp for the metastable cases, the most practical way to do the minimization is by brute force, i.e. by directly evaluating the function for a grid of points in the $[0, 2\pi]$ interval. The curves is Fig. 2.8 were obtained using a grid of 1000 points.

References

[1] Y. Kamihara, H. Hiramatsu, M. Hirano, R. Kawamura, H. Yanagi, T. Kamiya, and H. Hosono, Journal of the American Chemical Society **128**, PMID: 16881620, 10012–10013 (2006).

[2] Y. Kamihara, T. Watanabe, M. Hirano, and H. Hosono, Journal of the American Chemical Society **130**, PMID: 18293989, 3296–3297 (2008).

[3] P. J. Hirschfeld, M. M. Korshunov, and I. I. Mazin, Reports on Progress in Physics **74**, 124508 (2011).

[4] A. Chubukov, Annual Review of Condensed Matter Physics **3**, 57–92 (2012).

[5] C. W. Hicks, T. M. Lippman, M. E. Huber, Z.-A. Ren, J. Yang, Z.-X. Zhao, and K. A. Moler, Journal of the Physical Society of Japan **78**, 013708 (2009).

[6] J. E. Hoffman, Reports on Progress in Physics **74**, 124513 (2011).

[7] Y. Yin, M. Zech, T. L. Williams, X. F. Wang, G. Wu, X. H. Chen, and J. E. Hoffman, Phys. Rev. Lett. **102**, 097002 (2009).

[8] C.-L. Song, Y. Yin, M. Zech, T. Williams, M. M. Yee, G.-F. Chen, J.-L. Luo, N.-L. Wang, E. W. Hudson, and J. E. Hoffman, Phys. Rev. B **87**, 214519 (2013).

[9] X. Zhang, Y. S. Oh, Y. Liu, L. Yan, K. H. Kim, R. L. Greene, and I. Takeuchi, Phys. Rev. Lett. **102**, 147002 (2009).

[10] P. Seidel, Superconductor Science and Technology **24**, 043001 (2011).

[11] D. Daghero, M. Tortello, G. A. Ummarino, and R. S. Gonnelli, Reports on Progress in Physics **74**, 124509 (2011).

[12] A. V. Burmistrova, I. A. Devyatov, A. A. Golubov, K. Yada, Y. Tanaka, M. Tortello, R. S. Gonnelli, V. A. Stepanov, X. Ding, H.-H. Wen, and L. H. Greene, Phys. Rev. B **91**, 214501 (2015).

[13] A. D. Christianson, E. A. Goremychkin, R. Osborn, S. Rosenkranz, M. D. Lumsden, C. D. Malliakas, I. S. Todorov, H. Claus, D. Y. Chung, M. G. Kanatzidis, R. I. Bewley, and T. Guidi, Nature **456**, 930–932 (2008).

[14] D. S. Inosov, J. T. Park, P. Bourges, D. L. Sun, Y. Sidis, A. Schneidewind, K. Hradil, D. Haug, C. T. Lin, B. Keimer, and V. Hinkov, Nature Physics **6**, 178–181 (2010).

[15] T. Hanaguri, S. Niitaka, K. Kuroki, and H. Takagi, Science **328**, 474–476 (2010).

[16] C.-T. Chen, C. C. Tsuei, M. B. Ketchen, Z.-A. Ren, and Z. X. Zhao, Nature Physics **6**, 260–264 (2010).

[17] C. C. Tsuei, and J. R. Kirtley, Rev. Mod. Phys. **72**, 969–1016 (2000).

[18] D. A. Wollman, D. J. Van Harlingen, W. C. Lee, D. M. Ginsberg, and A. J. Leggett, Phys. Rev. Lett. **71**, 2134–2137 (1993).

[19] E. Berg, N. H. Lindner, and T. Pereg-Barnea, Phys. Rev. Lett. **106**, 147003 (2011).

[20] A. V. Burmistrova, and I. A. Devyatov, EPL (Europhysics Letters) **107**, 67006 (2014).

[21] A. V. Burmistrova, I. A. Devyatov, A. A. Golubov, K. Yada, and Y. Tanaka, Superconductor Science and Technology **27**, 015010 (2014).

[22] A. E. Koshelev, Phys. Rev. B **86**, 214502 (2012).

[23] A. Moor, A. F. Volkov, and K. B. Efetov, Phys. Rev. B **87**, 100504 (2013).

[24] I. B. Sperstad, J. Linder, and A. Sudbø, Phys. Rev. B **80**, 144507 (2009).

[25] T. K. Ng, and N. Nagaosa, EPL (Europhysics Letters) **87**, 17003 (2009).

[26] V. Stanev, and Z. Tešanović, Phys. Rev. B **81**, 134522 (2010).

[27]S.-Z. Lin, Phys. Rev. B **86**, 014510 (2012).

[28]J. Linder, I. B. Sperstad, and A. Sudbø, Phys. Rev. B **80**, 020503 (2009).

[29]V. G. Stanev, and A. E. Koshelev, Phys. Rev. B **86**, 174515 (2012).

[30]S. Apostolov, and A. Levchenko, Phys. Rev. B **86**, 224501 (2012).

[31]W. Da, L. Hong-Yan, and W. Qiang-Hua, Chinese Physics Letters **30**, 077404 (2013).

[32]W.-F. Tsai, D.-X. Yao, B. A. Bernevig, and J. Hu, Phys. Rev. B **80**, 012511 (2009).

[33]D. F. Agterberg, E. Demler, and B. Janko, Phys. Rev. B **66**, 214507 (2002).

[34]Y. Tanaka, Journal of the Physical Society of Japan **70**, 2844–2847 (2001).

[35]W.-Q. Chen, F. Ma, Z.-Y. Lu, and F.-C. Zhang, Phys. Rev. Lett. **103**, 207001 (2009).

[36]A. A. Golubov, and I. I. Mazin, Applied Physics Letters **102**, 032601 (2013).

[37]D. Parker, and I. I. Mazin, Phys. Rev. Lett. **102**, 227007 (2009).

[38]J. Wu, and P. Phillips, Phys. Rev. B **79**, 092502 (2009).

[39]K. D. Usadel, Phys. Rev. Lett. **25**, 507–509 (1970).

[40]S. Raghu, X.-L. Qi, C.-X. Liu, D. J. Scalapino, and S.-C. Zhang, Phys. Rev. B **77**, 220503 (2008).

[41]K. Seo, B. A. Bernevig, and J. Hu, Phys. Rev. Lett. **101**, 206404 (2008).

[42]R. Jin, M. H. Pan, X. B. He, G. Li, D. Li, R.-w. Peng, J. R. Thompson, B. C. Sales, A. S. Sefat, M. A. McGuire, D. Mandrus, J. F. Wendelken, V. Keppens, and E. W. Plummer, Superconductor Science and Technology **23**, 054005 (2010).

[43]Y. Fasano, I. Maggio-Aprile, N. D. Zhigadlo, S. Katrych, J. Karpinski, and Ø. Fischer, Phys. Rev. Lett. **105**, 167005 (2010).

[44]A. Moreo, M. Daghofer, J. A. Riera, and E. Dagotto, Phys. Rev. B **79**, 134502 (2009).

[45]K. Tanaka, and F. Marsiglio, Physica C: Superconductivity **384**, 356–368 (2003).

[46]B. P. Stojković, and O. T. Valls, Phys. Rev. B **47**, 5922–5930 (1993).

[47]G. Litak, P. Miller, and B. L. Györffy, Physica C: Superconductivity and its applications **251**, 263–273 (1995).

[48]B. Chesca, R. Kleiner, and D. Koelle, in *The squid handbook* (Wiley-VCH Verlag GmbH & Co. KGaA, 2005), pp. 29–92.

Preface to Chapter 3

In the previous chapter we studied how unusual energy/phase difference relations can arise in tunnel junctions between a conventional s-wave superconductor and an unconventional $s_{\pm}$ superconductor. In this chapter we study another kind of unsual energy/phase different relation: the 4π Josephson effect between two topological superconductors. In the previous chapter, the main focus was on obtaining the energy/phase difference relation from the microscopic behavior. Then in Sec. 2.3, the effects of the energy/phase difference of a junction were probed by considering the behavior of a flux threaded loop. This chapter follows a similar direction to Sec. 2.3–we study the consequences an energy/phase difference relation, which has been previously justified in the literature, in an specific setup. The setup considered is a flux threaded ring made of a series of topological superconductors.

3

Detecting Majorana modes through Josephson junction ring-quantum dot hybrid architectures

Rosa Rodríguez-Mota[1], Smitha Vishveshwara[2] and T. Pereg-Barnea[1]

[1]Department of Physics and the Centre for Physics of Materials, McGill University, Montreal, Quebec, Canada H3A 2T8

[2]Department of Physics, University of Illinois at Urbana-Champaign, Urbana, Illinois 61801-3080, USA

This chapter has been accepted for publication in 'Spin-Orbit Coupled Materials' topical issue of Journal of Physics and Chemistry of Solids. Preprint available at arXiv:1706.08181

Abstract

Unequivocal signatures of Majorana zero energy modes in condensed matter systems and manipulation of the associated electron parity states are highly sought after for fundamental reasons as well as for the prospect of topological quantum computing. In this paper, we demonstrate that a ring of Josephson coupled topological superconducting islands threaded by magnetic flux and attached to a quantum dot acts as an excellent parity-controlled probe of Majorana mode physics. As a function of flux threading through the ring, standard Josephson coupling yields a $\Phi_0 = h/(2e)$ periodic features corresponding to 2π phase difference periodicity. In contrast, Majorana mode assisted tunneling provides additional features with $2\Phi_0$ (4π phase difference) periodicity, associated with single electron processes. We find that increasing the number of islands in the ring enhances the visibility of the desired 4π periodic components in the groundstate energy. Moreover as a unique characterization tool, tuning the occupation energy of the quantum dot allows controlled groundstate parity changes in the ring, enabling a toggling between Φ_0 and $2\Phi_0$ periodicity.

3.1 Introduction

Majorana zero modes (MZM) have captivated condensed matter theorists and experimentalists alike of late [1–4] from the fundamental perspective as well as for their potential application in topological quantum computation [5–7]. Progress toward the realization of MZM has been made by several theoretical proposals [8–11] as well as experimental work [12–21]. While most experiments involving topological superconductors present zero bias conductance peaks as evidence for the existence of MZM [12–16, 18, 20], this alone can not serve as proof for their existence [22–35]. Another manifestation of the existence of MZM is the presence of 4π periodic components in the Josephson current between two topological superconductors [5, 8, 9, 36–39]. Despite encouraging experimental evidence [19–21], interpreting the presence of 4π periodic tunneling as an unequivocal sign of MZM remains problematic for three main reasons. The first is that the 4π periodicity can only be observed when the time scale over which the phase difference in the junction changes is smaller than the time scale for quasi-particle poisoning [37]. The second problem is that the 4π periodic components in the Josephson current are generally accompanied by other, possibly much larger, 2π periodic components. Finally, the presence of 4π periodic components can be caused by Andreev bound states rather than MZM [36, 40, 41].

Our proposal to address these problems is to study the signatures of 4π periodic tunneling due to MZM in Josephson junction ring-quantum dot hybrid architectures. As will be shown, the setup we propose in this paper controls quasiparticle tunneling by tuning the capacitance of the superconducting islands and suppresses the 2π periodic Josephson contribution by connecting a number of junctions in a ring. While single particle tunneling through bound states in the junctions can only be eliminated by producing very clean junctions, our setup is able to distinguish their contribution from

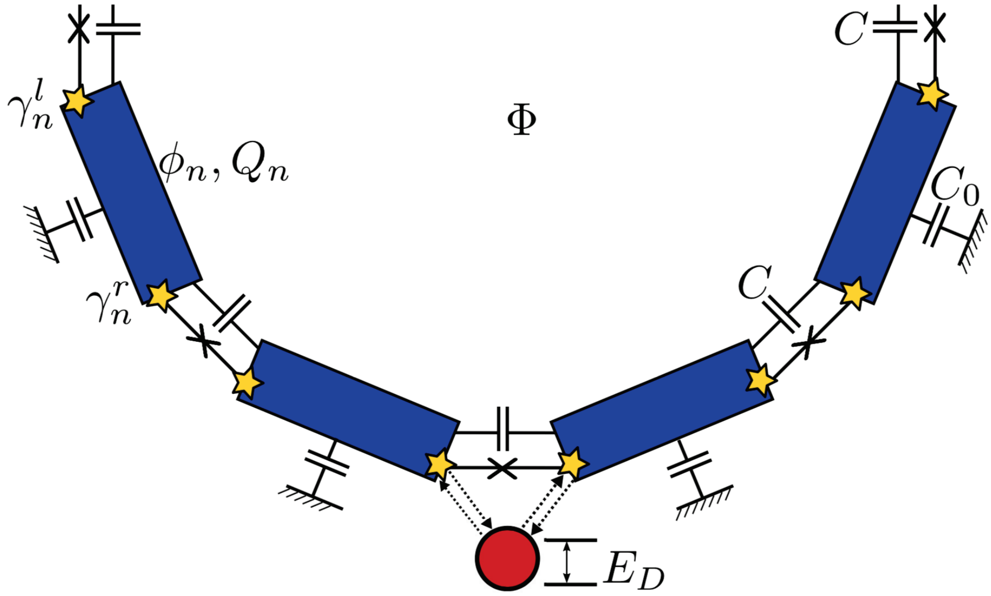

Figure 3.1: The setup consists of a ring made of N topologically superconducting islands (blue rectangles) coupled to a quantum dot (red circle) and threaded by magnetic flux Φ. The islands present Majorana modes (stars) at their edges leading to single particle tunneling in addition to the usual Josephson tunneling. Electrostatic effects in the ring are modeled by self and nearest-neighbor capacitances, C_0 and C, respectively.

Majorana assisted tunneling by connecting with a quantum dot.

Here, we combine two promising MZM settings to obtain a powerful and controlled means of MZM detection - Josephson junction arrays and quantum dot geometries. Josephson junction arrays provide a rich playground for studying the interplay between superconductivity and electrostatic repulsion [42]. These are appealing experimental systems since the relevant energy scales are relatively easy to tune, especially in one dimension [43–46]. Understanding such interplay in networks of multiply-connected 1D topological superconductors is particularly important, as it is a key ingredient in proposals to detect and manipulate MZM [47–53]. Another approach to detect and control MZM is by coupling to quantum dots and enabling single-electron hopping [18, 54–62]. Our setup builds on previous work to integrate 1D Josephson junction arrays made of topological superonconductors and quantum dots into a single architecture.

Majorana nanowires[8, 9] provide the most natural path to physically assemble the setup studied on this work. Although more technically challenging, another possible path for physical realization could be through assembling chains of magnetic atoms on the surface of superconductors[11, 63].

The setup we study is shown in Fig. 3.1. It consists of a topological Josephson junction ring (TJJ ring) formed by N topological superconducting islands threaded by magnetic flux and coupled to a quantum dot. Our key results are summarized in Fig. 3.2. Assuming the absence of quasiparticle poisoning, the net parity of the ring (odd or even number of electrons) $\mathcal{P}_{TJJ}$ is conserved when it is decoupled from the quantum dot. Without phase fluctuations its low energy spectrum as a function of flux is a collection of parabolas centered around integer flux quanta. These parabolas corresponds to different angular momentum states for which the winding of the superconducting phase across the TJJ ring is a multiple of 2π. The contours are essentially the same as those obtained for non-topological rings with one crucial difference. When $\mathcal{P}_{TJJ} = 1(-1)$, only parabolas which are centered around odd(even) integer flux quanta are possible. This is shown for $\mathcal{P}_{TJJ} = 1$ in Fig. 3.2a. Once phase fluctuations, induced by the charging energy, are included, quantum phase slips occur, creating avoided crossings in the spectrum as shown in Fig. 3.2b. While in the non-topological rings phase slips create a Φ_0 periodic spectrum, the spectrum of the TJJ ring in the presence of phase slips is $2\Phi_0$ periodic. This is a consequence of parity conservation forbidding the existence of either the even or the odd parabolas. Upon coupling to the quantum dot, the TJJ ring can violate parity conservation by accepting or donating an electron to the dot, thus hybridizing the odd and even parity sectors and tuning the periodicity of the ring from $2\Phi_0$ to Φ_0. The associated energy spectrum as a function of flux, measurable via persistent current, then takes on a characteristic form depending on quantum dot parameters, as shown in Figs. 3.2c and 3.2d.

As we show in what follows, several features of this architecture together yield distinct advantages in isolating MZM physics. In contrast to a single topological junction, in the TJJ ring the effects of the $2\Phi_0$ periodic tunneling are amplified by increasing the number of islands, N. Due to the charging energy of the islands, $E_0 = \mathrm{e}^2/(2C_0)$, and the occupation energy of the dot, E_D, there is an energy shift ΔE between the even and odd parity spectrum of the ring. The characteristic dependence of the energy spectrum on ΔE rules out the possibility of this effect being caused by Andreev boundstates. A large value of the self-charging energy E_0 helps suppress quasi-particle poisoning arising from undesired electron and hole excitations. The dot's affinity to accept or donate an electron is easily controlled via applying a gate voltage and altering E_D. Tuning ΔE in this setup allows toggling between the two different TJJ ring parity sectors and thus pinpointing the effect of MZM via the associated tuning of the periodicity of the ring between $2\Phi_0$ and Φ_0.

3.2 Topological Josephson junction (TJJ) ring

To analyze the scenario in detail, let us begin by considering the TJJ ring in Fig. 3.1 uncoupled to the quantum dot. Each of the N islands in the ring is characterized by a superconducting order parameter phase ϕ_n and a charge Q_n. The islands' topological nature leads to two Majorana modes, γ_n^l and γ_n^r, localized around the left and the right edge of the nth island. Neighboring islands interact through tunneling and electrostatic repulsion. To lowest order in the interaction, only tunneling processes that keep the superconductors in their ground state contribute. These correspond to Josephson tunneling of pairs and Majorana assisted single electron tunneling. The tunneling as well as the capacitance of the islands make up the TJJ ring Hamiltonian:

$$
\begin{aligned}
H_{TJJ} &= H_J + H_M + H_C \\
H_J &= -\sum_n E_J \cos(\phi_{n+1} - \phi_n + \delta_\Phi) \\
H_M &= \sum_n E_M \left(c_n^\dagger c_n - \frac{1}{2}\right) \cos\left(\frac{\phi_{n+1} - \phi_n + \delta_\Phi}{2}\right) \\
H_C &= \frac{1}{2}\sum_{n,m} Q_n C^{-1}_{nm} Q_m,
\end{aligned}
\tag{3.2.1}
$$

where $\phi_{n+1} - \phi_n + \delta_\Phi$ corresponds to the gauge invariant phase difference between the islands, with $\delta_\Phi = 2\pi\Phi/(N\Phi_0)$. H_J describes the Josephson tunneling, with amplitude E_J. H_M describes the tunneling enabled by MZM with the energy scale E_M and fermionic operators $c_n = (\gamma_n^r + i\gamma_{n+1}^l)/2$. H_C describes the electrostatic repulsion with the capacitance $C_{nm} = (C_0 + 2C)\delta_{n,m} - C\,(\delta_{n+1,m} + \delta_{n-1,m})$, where C_0 is the self capacitance and C is the neighboring capacitance. The TJJ ring has four relevant energy scales: E_J, E_M, and the charging energies $E_C = \mathrm{e}^2/(2C)$ and $E_0 = \mathrm{e}^2/(2C_0)$. We assume that the dominant energy scale is either E_M or E_J, and that $E_C \ll E_0$ [42]. In this case, the TJJ ring is described by almost well defined superconducting condensate phases with small fluctuations controlled by E_C.

For $E_C = 0$, the Hamiltonian of the system becomes $H^{cl}_{TJJ} = H_J + H_M + E_0\frac{Q^2}{N}$, with $Q = \sum_n Q_n$. The superconducting phases become well-defined classical variables [64, 65]. Moreover the eigenstates of H^{cl}_{TJJ} must have well defined occupations of the fermionic modes c_n. Since the occupation of the c_n fermions is defined modulo 2 [66, 67], a given phase configuration corresponds to two distinct eigenstates of H^{cl}_{ring} distinguished by their fermionic parity $\mathcal{P}_{TJJ} = (-1)^Q$ [1]. As shown in 3.A, this leads to the following

[1]To simplify the notation we measure the charge Q in units of the electron charge e.

condition on the phases:

$$\sum_n \theta_n = 2\pi m \text{ with } \begin{cases} m \text{ even} & \text{if } \mathcal{P}_{TJJ} = -1 \\ m \text{ odd} & \text{if } \mathcal{P}_{TJJ} = 1 \end{cases}, \qquad (3.2.2)$$

where $\theta_n = \phi_{n+1} - \phi_n + 2\pi c_n^\dagger c_n \mod 4\pi$. The energy of a configuration of phase differences $\boldsymbol{\theta} = (\theta_1, ..., \theta_N)$ can be written as $E(\boldsymbol{\theta}) = -\sum_n V(\theta_n + \delta_\Phi)$, where $V(\theta)$ is the single junction potential $V(\theta) = -E_J \cos\theta - \frac{E_M}{2}\cos\frac{\theta}{2}$.

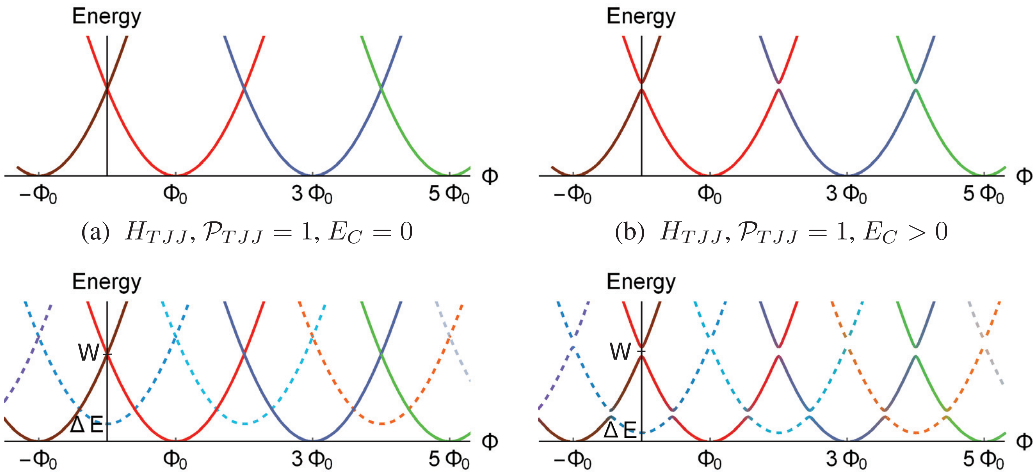

(a) $H_{TJJ}, \mathcal{P}_{TJJ} = 1, E_C = 0$ (b) $H_{TJJ}, \mathcal{P}_{TJJ} = 1, E_C > 0$

(c) $H, E_C = 0$ (d) $H, E_C > 0$

Figure 3.2: Schematic of our results for 'long' TJJ rings. In this case, the $2\Phi_0$ periodic terms become dominant. (a) Without phase fluctuations, the lowest energy bands of the even parity TJJ ring ($\mathcal{P}_{TJJ} = 1$) consist of parabolas centered around odd multiples of Φ_0, each corresponding to a different winding of the superconducting phase across the TJJ ring. (b) Phase fluctuations in the TJJ ring create avoided crossings making the spectrum $2\Phi_0$ periodic. The corresponding spectrum for the odd parity TJJ ring ($\mathcal{P}_{TJJ} = -1$) is that of panels (a) and (b) with a Φ_0 shift in the flux. (c) Once the TJJ ring is coupled to the dot, the energy spectrum includes states with $\mathcal{P}_{TJJ} = 1$ (solid lines) and states with $\mathcal{P}_{TJJ} = -1$ (dashed lines). Due to charging costs, the energies of states with $\mathcal{P}_{TJJ} = -1$ and $\mathcal{P}_{TJJ} = 1$ are offset by ΔE. (d) Phase fluctuations lead to avoided crossings. The groundstate energy behavior depends on how ΔE compares to the bandwidth of the $\mathcal{P}_{TJJ} = 1$ sector W.

The TJJ ring has a translational symmetry, i.e. the system is unchanged by circular shifts of the islands. Because of this, we expect configurations with uniform phase differences, i.e. $\theta_n = \theta$, to have the lowest energy. While this is true when $E_J = 0$, for non zero E_J the competition between 2π and 4π periodic tunneling may favor non uniform phase configurations. Nonetheless, we find that uniform phase configurations minimize the energy whenever

$$NE_J\left(1-\cos\frac{2\pi}{N}\right)+\frac{NE_M}{2}\left(1-\cos\frac{\pi}{N}\right)<E_M. \tag{3.2.3}$$

For $N \gtrsim 6$ this condition becomes

$$\frac{NE_M}{\pi^2} > 2E_J + \frac{E_M}{4}. \tag{3.2.4}$$

As a result of the presence of 2π periodic tunneling TJJ rings exhibit local minima at even (odd) Φ_0 for $\mathcal{P}_{TJJ} = 1(-1)$ if condition (3.2.3) is not met. Increasing N reduces the role of the 2π periodic components in the lowest energy bands. For the remainder of this work, we refer to the TJJ ring as 'long' if the condition (3.2.3) is met and as 'short' if it is not.

Since a TJJ ring with all equal junctions is a highly idealized situation, it is worth discussing how disorder in the couplings may affect the reduction of the role of 2π periodic components with increasing number of islands N. For $N \gtrsim 6$ and relatively small disorder the condition (3.2.3) becomes

$$\sum_{n=1}^{N}\frac{1}{E_{Jn}+\frac{E_{Mn}}{8}} > \frac{2\pi^2}{\min\left(E_{Mn}\right)}, \tag{3.2.5}$$

where E_{Jn} and E_{Mn} are the Josephson and Majorana couplings for the nth junction, respectively. The above condition reduces to (3.2.4) for even couplings. If we assume the couplings E_{Jn} and E_{Mn} to be uniformly distribution on the intervals $(E_J - \sigma_J, E_J + \sigma_J)$

and $(E_M - \sigma_M, E_M + \sigma_M)$, taking the average of (3.2.5) results in

$$\frac{N}{\pi^2}\left(E_M - \sigma_M \frac{N-1}{N+1}\right) > 2E_J + \frac{E_M}{4}. \tag{3.2.6}$$

We conclude that some disorder in the E_{Jn} couplings is not likely to affect our results. On the other hand, a large spread of E_{Mn} couplings increases the likelihood of finding local minima on the TJJ ground-state energy. Despite this, the left hand size of (3.2.6) grows with N as long as $\sigma_M < E_M$. Thus we conclude that the enhancement of the 4π periodic effects with increasing N is stable to small disorder in the couplings.

In the following, we focus on long TJJ rings. Taking into account the constraint, Eq. (3.2.2), the possible constant phase configurations are given by $\theta = 2\pi m/N$, where m is an odd(even) integer if $P_{TJJ} = 1(-1)$. We label these configurations by $|m\rangle$ and their energy by $\epsilon_m = NV(2\pi(m + \Phi/\Phi_0)/N)$. These different states correspond to different angular momentum values and can be distinguished by their persistent currents. The low-energy part of the spectrum of the states $|m\rangle$ for $\mathcal{P}_{TJJ} = 1$ is shown in Fig. 3.2a. For $N \gtrsim 6$ these states are essentially parabolas centered around $-m\Phi_0$.

For $E_C > 0$, the main types of phase fluctuations for the TJJ ring are plasmons and phase slips. Plasmons are harmonic fluctuations around the $|m\rangle$ states. They add a zero point motion energy to ϵ_m. We find that plasmons in the TJJ behave similarly to plasmons in non-topological JJ rings with the plasma frequency: $\hbar\omega_p = \sqrt{8E_J E_C + E_M E_C}$, as opposed to the non-topological frequency $\hbar\omega_p = \sqrt{8E_J E_C}$. Phase slips lead to quantum tunneling between the $|m\rangle$ states [64], causing the avoided crossings in Fig. 3.2b. For instance, the states $|m\rangle$ and $|m+2\rangle$ are connected trough 4π phase slips. Since H_{TJJ} conserves $\mathcal{P}_{TJJ}$ phase slips occur only in multiples of 4π, i.e. in long TJJ rings 2π phase slips are suppressed, as in topological superconducting wires [5, 68].

3.3 TJJ ring-quantum dot architecture

To control the parity of the TJJ ring, we couple the ring to a quantum dot, enabling electrons to tunnel between the TJJ and dot (together referred to as TJJ+D). In the simplest case of a single electronic level available to the dot, its Hamiltonian takes the form $H_D = E_D(d^\dagger d - \frac{1}{2})$, where d and $d^\dagger$ annihilate and create an electron in the dot. We consider a setup where electron tunneling from the quantum dot is into MZM modes on TJJ islands 1 and N with amplitudes w_1 and w_N, respectively. The Hamiltonian of the system is then $H = H_{ring} + H_D + H_{int}$, with the interaction between the TJJ ring and the dot given by:

$$H_{int} = \frac{w_N e^{-\frac{i\phi_N}{2}}}{2} i\gamma_N^r d^\dagger + \frac{w_1 e^{-\frac{i\phi_1}{2}}}{2} \gamma_1^l d^\dagger + \text{h.c.} \tag{3.3.1}$$

Assuming that no magnetic flux is enclosed by the loop formed between the dot and the two islands, the phase difference between w_1 and w_N is $\frac{\delta_\Phi}{2}$. The total parity is conserved in the TJJ+D system while it is not in the TJJ ring portion.

To proceed with the TJJ+D analysis, we denote by $|\boldsymbol{\theta}, Q; n_d\rangle$ a state of the system where 1) the TJJ has well defined phase differences $\boldsymbol{\theta}$ and well defined total charge Q and 2) the charge in the dot is n_d. H_{int} induces a 2π shift in the Nth junction when moving a particle from the TJJ to the dot. Thus, it connects the states $|\boldsymbol{\theta}, Q; 0\rangle$ and $|\boldsymbol{\theta} - 2\pi\vec{e}_N, Q-1; 1\rangle$, where $\boldsymbol{\theta} - 2\pi\vec{e}_N = (\theta_1, ..., \theta_{N-1}, \theta_N - 2\pi)$. When $E_C = 0$, both $|\boldsymbol{\theta}, Q; 0\rangle$ and $|\boldsymbol{\theta} - 2\pi\vec{e}_N, Q-1; 1\rangle$ are eigenstates of $H_{TJJ} + H_D$. As shown in 3.C, H is then diagonalized by superpositions of the form

$$\alpha_\pm |\boldsymbol{\theta}, Q; 0\rangle + \beta_\pm |\boldsymbol{\theta} - 2\pi\vec{e}_N, Q-1; 1\rangle \tag{3.3.2}$$

with the following energies:

$$E_{\pm}(\boldsymbol{\theta}) = \sum_{n=1}^{N-1} V\left(\theta_n + \delta_\Phi\right) + V_{\pm}\left(\theta_N + \delta_\Phi\right), \tag{3.3.3a}$$

with,

$$\begin{aligned} V_{\pm}(\theta) &= -E_J \cos\theta \pm \sqrt{\left(\frac{E_M}{2}\cos\frac{\theta}{2} + \frac{\Delta E}{2}\right)^2 + w_\theta}, \\ w_\theta &= \frac{|w_N|^2 + |w_1|^2}{4} + \frac{|w_N|\,|w_1|}{2}\cos\frac{\theta}{2}, \quad \text{and} \\ \Delta E &= E_D - E_0\left(2Q - 1\right)/N. \end{aligned} \tag{3.3.3b}$$

The offset, ΔE, originates from the charging costs of the dot and the TJJ ring.

The TJJ+D groundstate energy, ϵ, is obtained minimizing $E_{-}(\boldsymbol{\theta})$. The interaction breaks the translational symmetry of the TJJ ring making the values of $\boldsymbol{\theta}$ that minimize $E_{-}(\boldsymbol{\theta})$ flux dependent. Fortunately, the TJJ+D groundstate is well approximated by flux independent states which we label $|\psi_m\rangle$. The states $|\psi_m\rangle$ are obtained when taking Eq. 3.3.2 and choosing the phase configuration of the first term to be uniform with each junction having a phase difference $2\pi m/N$ and the appropriate charge on the dot. Furthermore, $|\psi_m\rangle$ is dominated by its component with constant phase differences in the TJJ ring, with the phase difference and occupation of the dot which match the overall parity and flux threaded. The energies of the states $|\psi_m\rangle$, ϵ_m, shown in Fig. 3.2c, are essentially parabolas centered around even and odd multiples of Φ_0, offset by ΔE. The greatest deviation between the energies ϵ_m and ϵ is at half-integer flux values for small numbers of islands. Comparing the energies ϵ_m with ϵ obtained numerically for $N = 2$ and $\Phi = \Phi_0/2$, we find that ϵ and the lowest ϵ_m differ by less than $0.05E_M$ for $|w_1|, |w_N| < E_M/2$. Increasing the number of islands to $N = 3$ reduces such difference to less than $0.001E_M$. The ϵ_m are then good approximations to ϵ as long as

$|w_1|, |w_N| \lesssim E_M$. Further details are given in 3.E.

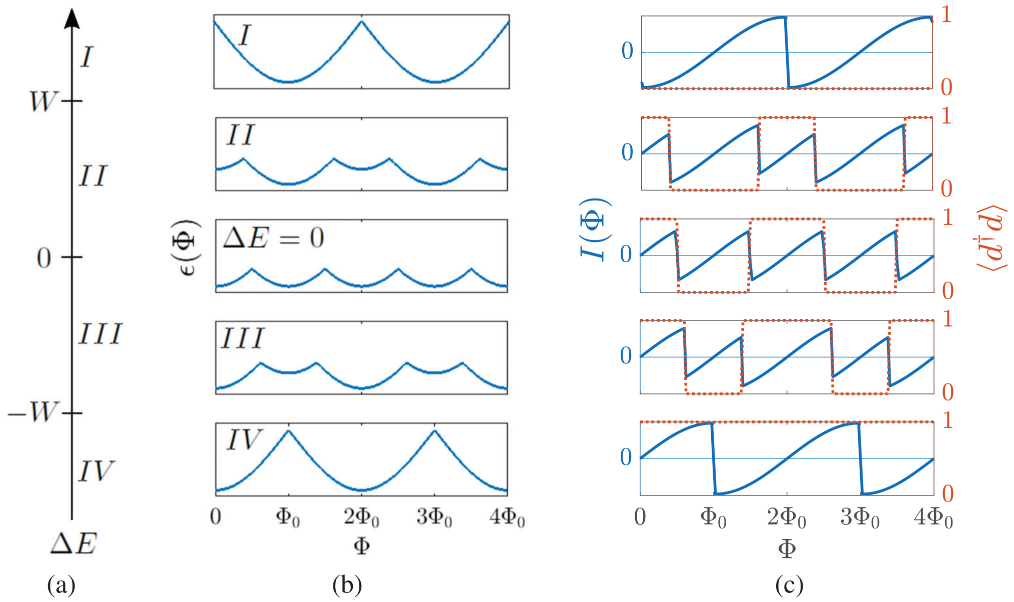

Figure 3.3: The energy and current profile of the TJJ+D system in different regions of energy offset ΔE relative to the band width W. The different behavior provides a signature of the Majorana assisted tunneling. (a) The energy offset ΔE compares to the bandwidth of the even/odd sector, W. (b) The dependence of the groundstate energy on the magnetic flux for the TJJ+D system for the different regions in (a). (c) The flux dependence of the persistent current (solid blue) and the average occupation of the quantum dot (dashed red). Figures (b) and (c) show numerical results for $N = 2$, $E_J = 0$, $E_M = 1$, $Q = 100$, $E_0 = 0.001 = 10E_C$, $w_1 = w_N = 0.1$ and (top to bottom) $\Delta E = 1.1$, $\Delta E = 0.25$, $\Delta E = 0$, $\Delta E = -0.25$ and $\Delta E = -1.1$.

Turning on E_C leads to avoided crossings where the energies of the states $|\psi_m\rangle$ cross. The states $|\psi_m\rangle$ and $|\psi_{m\pm1}\rangle$ are now connected by 2π phase slips enabled by breaking the parity of the TJJ ring through the interaction with the dot. The behavior of the energy and that of the persistent current is then determined by where and whether the states $|\psi_m\rangle$ and $|\psi_{m\pm1}\rangle$ cross. This depends on how the energy offset between the even and the odd $|\psi_m\rangle$ states, ΔE, compares to the bandwidth of the even (or odd) $|\psi_m\rangle$ states, W. To provide a more accurate analysis, we perform numerical simulations for small island numbers. These were done through exact diagonalization of the TJJ+D Hamiltonian limiting the charge on each island to some maximum charge Q. Examples of the different types of behavior of the energy and the persistent current obtained numerically are shown in Fig. 3.3b and in Fig. 3.3c, respectively. The corresponding groundstate occupation of the dot (red line in Fig. 3.3c) is also shown. The rapid changes in the dot groundstate occupation could be measured as peaks in the conductance as suggested by Ref. [60] in a similar setting. For $|\Delta E| > W$ (regions I and IV in Fig. 3.3), the first energy crossing occurs between states $|\psi_m\rangle$ and $|\psi_{m\pm2}\rangle$. In this case, the energy has global minima at either even or odd multiples of Φ_0. On the other hand, for $|\Delta E| < W$ (regions II and III in Fig. 3.3), the first energy crossing occurs between states $|\psi_m\rangle$ and $|\psi_{m\pm1}\rangle$, leading to both local and global energy minima.

The results shown in Fig. 3.3 describe the qualitative behavior of the TJJ+D architecture when the TJJ ring is long. For short TJJ rings, the competition between 2π and 4π periodic tunneling leads to local minima in the energy-flux relation even when $\mathcal{P}_{TJJ}$ is conserved. In this case, the energy of the TJJ+D system in the regions I and IV of Fig. 3.3 would still present local minima, reducing the visibility of the transition between the two parity sectors.

The ability to tune between $2\Phi_0$ and Φ_0 periodicity through controlling the occupation energy of the dot allows our setup to rule out other explanations of $2\Phi_0$ periodicity. For instance, $2\Phi_0$ periodicity may arise in small metallic or semi-conducting systems [69–71]. If such were the case, the $2\Phi_0$ periodicity would be unchanged by the occupation energy of the dot. If the $2\Phi_0$ periodicity was caused Andreev bound-states, the contact with a dot having small occupation energy would aid rather than suppress the $2\Phi_0$ periodicity [41].

3.4 Conclusions

The proposed Josephson ring-quantum dot hybrid architecture can be realized in Josephson junction rings with Majorana nanowires [8, 9] or with chains of magnetic atoms deposited on the surface of superconductors [11, 63]. Additionally, the TJJ ring can be understood as a coarse grained model of a 1D topological superconductor. Since the TJJ ring accounts for phase fluctuations, it could be used to shed some light into the effects of phase fluctuations, and number conservation, in topological superconductors. Crucially, the combination of 4π periodic tunneling and the ability to manipulate the parity of the TJJ ring using the quantum dot as a knob cannot be explained through trivial Andreev bound states. Quasi-particle poisoning and 2π periodic tunneling may obscure the MZM signature. These effects can be prevented increasing the self-charging energy of the superconducting islands and increasing the number of superconducting islands, respectively. Thus, while the Josephson junction-quantum dot hybrid architecture proposed in this paper cannot in itself enable the braiding MZMs, it can provide a solid signature of their existence. Future work would involve connecting the principles and geometry proposed here with the current scope of device capabilities in experiment.

3.5 Acknowlegments

The authors thank D. Van Harlingen for useful discussion. This material is based upon work supported by NSERC, FQRNT (RRM, TPB), the Secretary of Public Education and the Government of Mexico (RRM) and the National Science Foundation under Grant No. 1745304 (SV).

3.A Proof of Eqn. 3.2.2

Due to the topological nature of each the island, for any constant phase configuration with $0 \leq \phi_n < 2\pi$ there are two superconducting ground states that can be distinguished by their fermionic parity. These groundstates will be labeled as $|\phi_{n\mathcal{P}}\rangle$. The action of the operators γ_n^l and γ_n^r on the states $|\phi_{n\mathcal{P}}\rangle$ is

$$\begin{aligned} \gamma_l \left|\phi_{n\pm}\right\rangle &= \left|\phi_{n\mp}\right\rangle \\ i\gamma_r \left|\phi_{n\pm}\right\rangle &= \mp \left|\phi_{n\mp}\right\rangle . \end{aligned} \tag{3.A.1}$$

The Majorana operators associated with the superconducting island n are given by

$$\begin{aligned} \gamma_n^l &= \int\limits_{x\in n} dx \left(e^{-\frac{i\phi}{2}} f_n^l(x)\psi^\dagger(x) + e^{\frac{i\phi}{2}} f_n^l(x)^* \psi(x)\right) \\ \gamma_n^r &= \int\limits_{x\in n} dx \left(ie^{-\frac{i\phi}{2}} f_n^r(x)\psi^\dagger(x) - ie^{\frac{i\phi}{2}} f_n^r(x)^* \psi(x)\right), \end{aligned} \tag{3.A.2}$$

with $f_n^{l(r)}(x)$ a function localized around the left (right) edge of the n island and $\psi(x)$ the field operator. Under the gauge transformation $\phi_n \to \phi_n + 2\pi$ [2], the operators $\gamma_n^{l(r)}$ pick up a minus sign resulting in $c_n \to -c_n^\dagger$ and $c_{n-1} \to c_{n-1}^\dagger$. This implies that the occupation of the c_n fermions is defined modulo 2 and care must be taken to avoid over-counting the states in the Hilbert space [66].

Following Ref. [72] we define the following $N-1$ independent variables

$$\theta_n = \phi_{n+1} - \phi_n + 2\pi c_n^\dagger c_n \mod 4\pi, \tag{3.A.3}$$

for $n = 1, ..., N-1$, which are invariant under $\phi_n \to \phi_n + 2\pi$. Writing H_J and H_M in

[2]Note that the gauge transformation $\phi_n \to \phi_n + 2\pi$, which is a change in how we are looking at the system, differs from changing the phase ϕ_n by 2π adiabatically, which is a physical change in the system.

terms of the θ_ns results in

$$\begin{aligned}
H_M &= -\sum_{n=1}^{N-1} \frac{E_M}{2} \cos\left(\frac{\theta_n + \delta_\Phi}{2}\right) \\
&- \frac{E_M}{2} \cos\left(\frac{-\sum_{n=1}^{N-1}\theta_n - 2\pi\sum_{n=1}^{N} c_n^\dagger c_n + \delta_\Phi}{2}\right) \\
H_J &= -\sum_{n=1}^{N-1} E_J \cos\left(\theta_n + \delta_\Phi\right) \\
&- E_J \cos\left(-\sum_{n=1}^{N-1}\theta_n + \delta_\Phi\right),
\end{aligned} \tag{3.A.4}$$

The operators θ_n defined by Eqn. (3.A.3) are not enough to determine the state of the TJJ since the variables ϕ_1 and the $(-1)^{\sum_{n=1}^{N} c_n^\dagger c_n}$ are independent of them. To address this we define the θ_0 as

$$e^{\frac{i\theta_0}{2}} = \gamma_1^l e^{\frac{i\phi_1}{2}}. \tag{3.A.5}$$

Under the above definition θ_0 remains invariant when $\phi_1 \rightarrow \phi_1 + 2\pi$, and we have $[\theta_n, \theta_k] = 0$ for all $n, k = 0, ..., N-1$. The operator θ_0 obeys the following commutation relation with the total charge $Q = \sum_n Q_n$:

$$\left[Q, e^{\frac{i\theta_0}{2}}\right] = e^{\frac{i\theta_0}{2}}. \tag{3.A.6}$$

The fact that θ_0 does not appear in H_M and H_J indicates that both H_M and H_J conserve the total charge Q of the TJJ. Additionally for $n = 1, ..., N-1$ we also have

$$\left[\frac{\theta_n}{2}, Q\right] = 0 \quad \text{and} \quad \left[\frac{\theta_n}{2}, Q_k\right] = i\left(\delta_{n+1,k} - \delta_{n,k}\right), \tag{3.A.7}$$

hence it is possible to describe the state of the TJJ using either the states $|\theta_0, \theta_1, ..., \theta_{N-1}\rangle$ or the states $|Q, \theta_1, ..., \theta_{N-1}\rangle$. In the following we will use the later since $[H_{TJJ}, Q] = 0$.

To make the TJJ ring translational symmetry evident, it is convenient to rewrite H_M and H_J in terms of N constrained phase differences. This results in

$$\begin{aligned} H_M &= -\sum \frac{E_M}{2} \cos\left(\frac{\theta_n + \delta_\Phi}{2}\right) \\ H_J &= -\sum_n E_J \cos\left(\theta_n + \delta_\Phi\right), \end{aligned} \tag{3.A.8}$$

with the constraint

$$\sum_n \theta_n = \begin{cases} 4\pi m & \text{if} \quad (-1)^{\sum_n c_n^\dagger c_n} = 1 \\ 2\pi(2m+1) & \text{if} \quad (-1)^{\sum_n c_n^\dagger c_n} = -1 \end{cases}. \tag{3.A.9}$$

It is also possible to relate $(-1)^{\sum_n c_n^\dagger c_n}$ to Q by noting that $(-1)^{Q_n} = i\gamma_n^r \gamma_n^l$ and $(-1)^{c_n^\dagger c_n} = i\gamma_{n+1}^l \gamma_n^r$. The relation between $(-1)^{\sum_n c_n^\dagger c_n}$ and Q is then

$$\begin{aligned} (-1)^{\sum_n c_n^\dagger c_n} &= \prod_{n=N}^{1} i\gamma_{n+1}^l \gamma_n^r = \gamma_1^l \left(\prod_{n=N}^{2} i\gamma_n^r \gamma_n^l\right) i\gamma_1^r \\ &= -\prod_{n=N}^{1} i\gamma_n^r \gamma_n^l = -(-1)^Q. \end{aligned} \tag{3.A.10}$$

Combining Eqns. (3.A.9) and (3.A.10) leads to Eqn. (3.2.2).

We will use $|\boldsymbol{\theta}\rangle_Q$ to denote the state with charge Q and phase differences given by $\boldsymbol{\theta} = (\theta_1, ..., \theta_N)$.

3.B Quantifying the decrease of the 2π periodic tunneling contribution and its stability against junction disorder

In the main text, we showed that local minima in the ground-state energy vs flux relation of the TJJ can be removed by increasing the number of islands in the TJJ. Since the local minima arise due to the contribution of 2π periodic tunneling, we used this fact to argue that increasing N reduces the role of 2π periodic terms. In this appendix, we provide an additional way to quantify such decrease and use it to study the stability of this effect with respect to disorder.

The energy of the TJJ ring $E(\Phi)$ can be written as a Fourier series:

$$E(\Phi) = \sum_{n=0}^{\infty} E_n \cos(\pi n \Phi). \tag{3.B.1}$$

Using such decomposition, we can quantify the role of 2π periodic terms on the energy as

$$r = \frac{\sum_{n=1}^{\infty} |E_{2n}|^2}{\sum_{n=1}^{\infty} |E_n|^2}. \tag{3.B.2}$$

If only Φ_0 periodic terms are present in the energy vs flux relation, i.e. $E_M \to 0$, then $r = 1$.

Fig. 3.4a shows r as a function of the number of junctions in the ring for different rations of E_J with respect E_M. The results where obtained minimizing the classical energy vs. flux relation of the TJJ ring numerically. As expected, $r = 1$ when $E_M = 0$. On the contrary, Φ_0 periodic components do not fully disappear when the Cooper pair tunneling is absent, i.e. $E_J = 0$. This is due to shape of the ground-state energy dependence on the flux for $E_C = 0$, which is non-sinusoidal (see Fig. 3.2a). Nonetheless,

r provides a measure for the effects of the 2π periodicity on the ground-state energy. For $E_M = E_J$ (blue squares) r decreases with N at first, r starts increasing after it goes below the value of $r(E_J = 0)$ (gray up triangles) and then it continues to approach this value. This result agrees with our claim that the groundstate-energy dispersion for 'long' TJJ rings resembles that of rings with no 2π periodic tunneling, i.e. $E_J = 0$. The r dependence on N for $E_M = 0.1E_J$ (down red triangles) and $E_M = 0.5E_J$ (yellow diamonds) seem to follow a similar trend, but the range of N in Fig. 3.4a is not large enough to appreciate the full behavior.

Figure 3.4b shows the behavior of r with respect to N for $E_J = E_M = 1$ and different values of disorder. To obtain this figure, we calculated the average of r considering that the Josephson and Majorana couplings of the islands uniformly distributed on $(E_J - \sigma_J, E_J + \sigma_J)$ and $(E_M - \sigma_M, E_M + \sigma_M)$, respectively. In Fig. 3.4b we see that the qualitative behavior of r is unchanged by disorder in Josephson and Majorana couplings. We also find that for N up to 10, disorder in the Majorana hybridization energy, increases r. This is in agreement with the effects of disorder stated in the main text: the role of 2π periodic contributions is relatively insensitive to disorder in the Josephson couplings, on the other hand disorder on the Majorana hybridization energy increases the role of 2π periodic contributions overall. The fact that the role of 2π periodic contributions is decreased by increasing the number of islands N, is insensitive to relatively small disorder on both types of tunneling.

3.C Proof of Eqn. 3.3.3

Here we obtain the energies of the TJJ+D system for $E_C = 0$, described by $H^{cl}_{TJJ} + H_D + H_{int}$. We start by writing H_{int} in terms of the operators defined in the previous

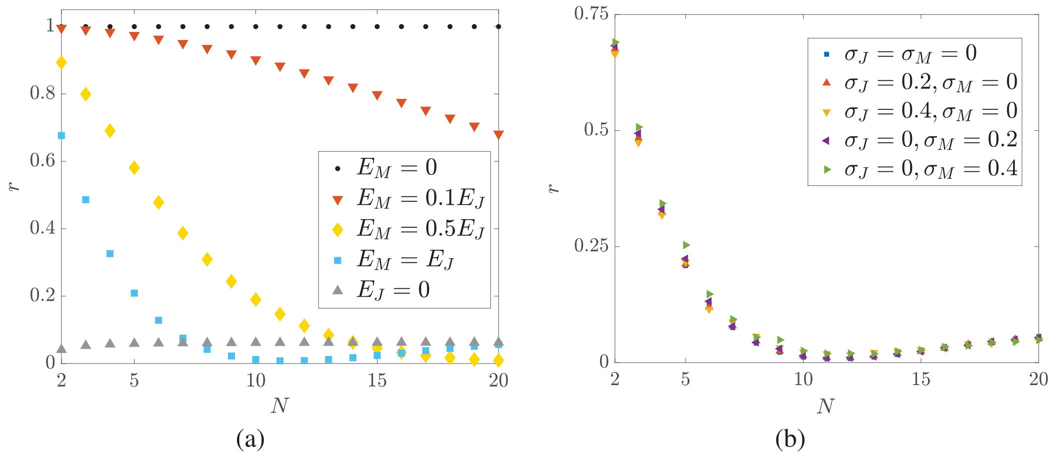

Figure 3.4: (a) Strength of the 2π periodic contribution to the ground-state energy as a function of N for different rations of E_J/E_M. (b) Average strength of the 2π periodic contribution to the ground-state energy as a function of N for $E_J = E_M = 1$ and different amounts of disorder.

section:

$$\begin{aligned} H_{int} =& \frac{w_N e^{-\frac{i\phi_N}{2}}}{2} i\gamma_N^r d^\dagger + \frac{w_1 e^{-\frac{i\phi_1}{2}}}{2} \gamma_1^l d^\dagger + \text{h.c.} \\ =& \left[-\frac{w_N}{2} e^{\frac{i}{2}\sum\limits_{n=1}^{N-1}\theta_n} (-1)^Q + \frac{w_1}{2} \right] e^{\frac{-i\theta_0}{2}} d^\dagger \\ &+ \text{h.c.}. \end{aligned} \tag{3.C.1}$$

From the above equation we obtain that H_{int} connects the states $|Q, \theta_1, ..., \theta_{N-1}\rangle$ and $d^\dagger |Q-1, \theta_1, ..., \theta_{N-1}\rangle$ as follows:

$$\begin{aligned} &H_{int} |Q, \theta_1, ..., \theta_{N-1}\rangle = -td^\dagger |Q-1, \theta_1, ..., \theta_{N-1}\rangle \\ &H_{int} d^\dagger |Q-1, \theta_1, ..., \theta_{N-1}\rangle = -t^* |Q, \theta_1, ..., \theta_{N-1}\rangle \\ &\text{with} \quad t = \frac{1}{2}\left(w_N e^{\frac{i}{2}\sum_{n=1}^{N-1}\theta_n} (-1)^Q + w_1 \right). \end{aligned} \tag{3.C.2}$$

Alternatively, we can write

$$
\begin{aligned}
H_{int}\left|\boldsymbol{\theta}\right\rangle_Q &= \text{-}\left[\frac{w_N}{2}e^{\frac{-i\theta_N}{2}}+\frac{w_1}{2}\right]d^\dagger\left|\boldsymbol{\theta}-2\pi\vec{e}_N\right\rangle_{Q-1}\\
H_{int}d^\dagger\left|\boldsymbol{\theta}-2\pi\vec{e}_N\right\rangle_{Q-1} &= \text{-}\left[\frac{w_N^*}{2}e^{\frac{i\theta_N}{2}}+\frac{w_1^*}{2}\right]\left|\boldsymbol{\theta}\right\rangle_Q .
\end{aligned}
\tag{3.C.3}
$$

The states $\left|\boldsymbol{\theta}\right\rangle_Q$ and $d^\dagger\left|\boldsymbol{\theta}-2\pi\vec{e}_N\right\rangle_{Q-1}$ are eigenstates of $H_{ring}+H_d$ with

$$
\begin{aligned}
(H_{TJJ}+H_D)\left|\boldsymbol{\theta}\right\rangle_Q &= \left[E(\boldsymbol{\theta})+\frac{E_0Q^2}{N}-\frac{E_D}{2}\right]\left|\boldsymbol{\theta}\right\rangle_Q\\
(H_{TJJ}+H_D)d^\dagger\left|\boldsymbol{\theta}-2\pi\vec{e}_N\right\rangle_{Q-1} &= \left[E(\boldsymbol{\theta}-2\pi\vec{e}_N)\right.\\
&\left.+\frac{E_D}{2}+\frac{E_0(Q-1)^2}{N}\right]d^\dagger\left|\boldsymbol{\theta}-2\pi\vec{e}_N\right\rangle_{Q-1}
\end{aligned}
\tag{3.C.4}
$$

where $E\left(\boldsymbol{\theta}\right)=-\sum_n V\left(\theta_n+\delta_\Phi\right)$, $V(\theta)=-E_J\cos\theta-\frac{E_M}{2}\cos\frac{\theta}{2}$.

Then $H = H_{TJJ}+H_D+H_C$ is diagonalized by states of the form $\alpha_\pm\left|\boldsymbol{\theta}\right\rangle_Q + \beta_\pm d^\dagger\left|\boldsymbol{\theta}-2\pi\vec{e}_N\right\rangle_{Q-1}$ with energies $E_\pm\left(\boldsymbol{\theta}\right)$ given by Eqns. (5) and (6) of the main text.

3.D Numerical Simulations.

In order to simulate the system numerically, it is convenient to describe the system in terms of charges rather than phases. For simplicity, we will focus on the case $N=2$. We want to find out the action of $H=H_C+H_J+H_M+H_D+H_{int}$ on a state with well defined charges on the islands and the dot, i.e., $\left|Q_1,Q_2,d\right\rangle$. States with well defined charge are eigenstates of H_C and H_D:

$$\begin{aligned}(H_C{+}H_D)\left|Q_1,Q_2,0\right\rangle = \\ \left(\frac{\mathrm{e}^2}{2}\sum_{n,m=1}^{2}Q_nC_{nm}^{-1}Q_m-\frac{E_D}{2}\right)\left|Q_1,Q_2,0\right\rangle \\ (H_C{+}H_D)\left|Q_1,Q_2,1\right\rangle = \\ \left(\frac{\mathrm{e}^2}{2}\sum_{n,m=1}^{2}Q_nC_{nm}^{-1}Q_m+\frac{E_D}{2}\right)\left|Q_1,Q_2,1\right\rangle .\end{aligned} \tag{3.D.1}$$

Now we proceed to find the effect of the H_J, H_M and H_{int} on the constant charge states. In order to do this, we first note that for the nth superconducting island the constant charge state $|Q_n\rangle$ can be constructed in terms of the states $|\phi_{n\mathcal{P}}\rangle$:

$$|Q_n\rangle = \frac{1}{2\pi}\int_0^{2\pi} d\phi e^{i\phi_n\frac{Q_n}{2}}\left|\phi_{\mathcal{P}}\right\rangle,\ \text{with}\ \mathcal{P}=(-1)^{Q_n}. \tag{3.D.2}$$

Using Equations 3.A.1 and 3.D.2 we can obtain the effect of the operators $e^{\pm\frac{i\phi_n}{2}}\gamma_n^{r(l)}$ on a state of the island n with well defined charge:

$$\begin{aligned}e^{\pm\frac{i\phi_n}{2}}\gamma_n^l\left|Q_n\right\rangle &= \left|Q_n\pm 1\right\rangle \\ e^{\pm\frac{i\phi_n}{2}}i\gamma_n^r\left|Q_n\right\rangle &= -\left(-1\right)^{Q_n}\left|Q_n\pm 1\right\rangle .\end{aligned} \tag{3.D.3}$$

Hence, we can write the states $|Q_1,Q_2,d\rangle$ as follows:

$$\left|Q_1,Q_2,d\right\rangle = \left(e^{\frac{i\phi_1}{2}}\gamma_1^l\right)^{Q_1}\left(e^{\frac{i\phi_2}{2}}\gamma_2^l\right)^{Q_2}(d^\dagger)^d\left|0\right\rangle \tag{3.D.4}$$

Using the above definition we find the action of H_M, H_J and H_{int} on the states

$|Q_1, Q_2, d\rangle$:

$$\begin{aligned} H_M |Q_1, Q_2, d\rangle = \frac{E_M}{4} \times \\ \left[\left((-1)^{Q_1+Q_2} e^{-\frac{i\delta_\Phi}{2}} - e^{\frac{i\delta_\Phi}{2}}\right) |Q_1 - 1, Q_2 + 1, d\rangle + \\ \left((-1)^{Q_1+Q_2} e^{\frac{i\delta_\Phi}{2}} - e^{-\frac{i\delta_\Phi}{2}}\right) |Q_1 + 1, Q_2 - 1, d\rangle\right], \end{aligned} \tag{3.D.5}$$

$$\begin{aligned} H_J |Q_1, Q_2, d\rangle = -E_J \cos\delta_\Phi |Q_1 - 2, Q_2 + 2, d\rangle \\ -E_J \cos\delta_\Phi |Q_1 + 2, Q_2 - 2, d\rangle, \end{aligned} \tag{3.D.6}$$

and

$$\begin{aligned} H_{int} |Q_1, Q_2, 0\rangle = -\frac{|w_2|}{2} e^{\frac{i\delta_\Phi}{4}} |Q_1, Q_2 - 1, 1\rangle + \\ (-1)^{Q_1+Q_2} \frac{|w_1|}{2} e^{-\frac{i\delta_\Phi}{4}} |Q_1 - 1, Q_2, 1\rangle \\ H_{int} |Q_1, Q_2, 1\rangle = -\frac{|w_2|}{2} e^{\frac{i\delta_\Phi}{4}} |Q_1, Q_2 + 1, 0\rangle + \\ (-1)^{Q_1+Q_2} \frac{|w_1|}{2} e^{-\frac{i\delta_\Phi}{4}} |Q_1 + 1, Q_2, 0\rangle. \end{aligned} \tag{3.D.7}$$

Since $Q_1 + Q_2 + n_d = Q$ is conserved by the Hamiltonian, we can write the Hamiltonian for a given Q sector:

$$\begin{aligned} H = \sum_{d,d'=0}^{1} \sum_{Q_1,Q_1'=0}^{Q-d,Q-d'} H_{Q_1,d}^{Q_1',d'} \times \\ |Q_1, Q_1 - Q - d, d\rangle \langle Q_1', Q_1' - Q - d', d'| \end{aligned} \tag{3.D.8}$$

where $H_{Q_1,d}^{Q_1',d'}$ is the matrix element between the states $|Q_1, Q_1 - Q - d, d\rangle$ and $|Q_1', Q_1' - Q - d', d'\rangle$ and can be obtained from Eqns. (3.D.1), (3.D.5), (3.D.5) and (3.D.7). The numeric results shown in the main text were obtained from the above Hamiltonian using exact diagonalization.

The above description can be readily extended to an arbitrary number of islands N, as the action of H on a state $|Q_1, ..., Q_N, d\rangle$ can be found by considering

$$|Q_1, ..., Q_N, d\rangle = \left(e^{\frac{i\phi_1}{2}}\gamma_1^l\right)^{Q_1} ... \left(e^{\frac{i\phi_N}{2}}\gamma_N^l\right)^{Q_N} \times (d^\dagger)^d |0\rangle . \tag{3.D.9}$$

3.E TJJ+D ground-state energy approximation.

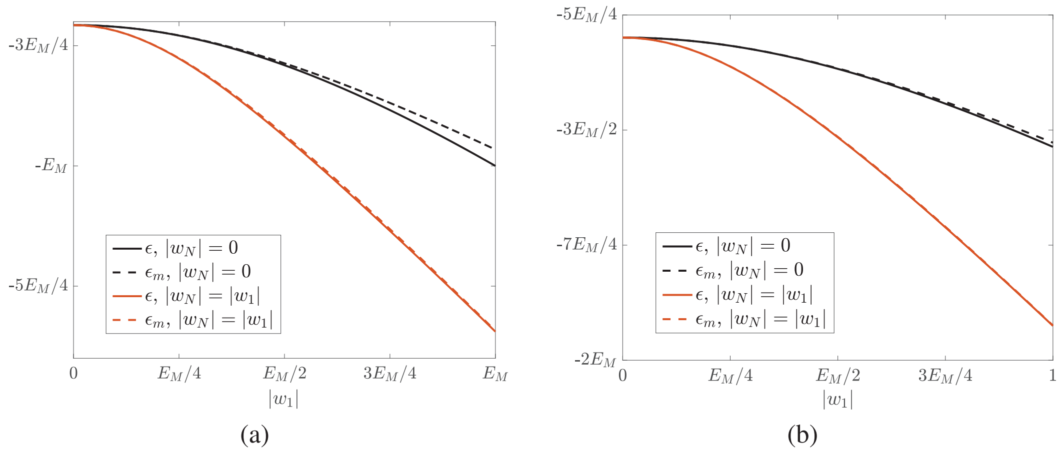

Figure 3.5: The ground-state energy of the TJJ+D, ϵ (solid lines), and ϵ_m with $m = -1$ (dashed lines) at $\Phi = \Phi_0/2$ are shown for $E_J, E_C = 0$ and $N = 2$ in panel (a), and $N = 3$ in panel (b).

In the main text it was argued that the TJJ+D groundstate energy ϵ was well approximated by the energies ϵ_m of flux independent states $|\psi_m\rangle$. It was also argued that such approximation works best a) close to integer flux quantum and b) when we increase the number of islands. Here we provide some details to support such arguments. First, we note that the reason the approximation of $\epsilon \approx \min(\epsilon_m)$ works best close to integer flux quantum is that the state $|\psi_m\rangle$ corresponds to the ground-state of the system when $\Phi = -m\Phi_0$.

On the other hand, the approximation improves when N increases since when the flux can be distributed in more junctions the ground-state configurations for different flux values are separated by smaller phase differences. Fig. 3.5 shows how the considerable improvement in the approximation obtain by increasing N from $N = 2$ to $N = 3$. The ground-state energy ϵ in Fig. 3.5 was obtained minimizing $E_{-}(\boldsymbol{\theta})$ with respect the phase differences vector $\boldsymbol{\theta}$ numerically.

References

[1] J. Alicea, Reports on Progress in Physics **75**, 076501 (2012).

[2] C. W. J. Beenakker, Rev. Mod. Phys. **87**, 1037–1066 (2015).

[3] M. Leijnse, and K. Flensberg, Semiconductor Science and Technology **27**, 124003 (2012).

[4] C. Beenakker, Annual Review of Condensed Matter Physics **4**, 113–136 (2013).

[5] A. Y. Kitaev, Physics-Uspekhi **44**, 131 (2001).

[6] C. Nayak, S. H. Simon, A. Stern, M. Freedman, and S. Das Sarma, Rev. Mod. Phys. **80**, 1083–1159 (2008).

[7] J. Alicea, Y. Oreg, G. Refael, F. von Oppen, and M. P. A. Fisher, NATURE PHYSICS **7**, 412–417 (2011).

[8] R. M. Lutchyn, J. D. Sau, and S. Das Sarma, Phys. Rev. Lett. **105**, 077001 (2010).

[9] Y. Oreg, G. Refael, and F. von Oppen, Phys. Rev. Lett. **105**, 177002 (2010).

[10] F. Pientka, Y. Peng, L. Glazman, and F. von Oppen, Physica Scripta **2015**, 014008 (2015).

[11] S. Nadj-Perge, I. K. Drozdov, B. A. Bernevig, and A. Yazdani, Phys. Rev. B **88**, 020407 (2013).

[12] S. Nadj-Perge, I. K. Drozdov, J. Li, H. Chen, S. Jeon, J. Seo, A. H. MacDonald, B. A. Bernevig, and A. Yazdani, Science **346**, 602–607 (2014).

[13] H. O. H. Churchill, V. Fatemi, K. Grove-Rasmussen, M. T. Deng, P. Caroff, H. Q. Xu, and C. M. Marcus, Phys. Rev. B **87**, 241401 (2013).

[14] A. D. K. Finck, D. J. Van Harlingen, P. K. Mohseni, K. Jung, and X. Li, Phys. Rev. Lett. **110**, 126406 (2013).

[15]V. Mourik, K. Zuo, S. M. Frolov, S. R. Plissard, E. P. A. M. Bakkers, and L. P. Kouwenhoven, Science **336**, 1003–1007 (2012).

[16]M. T. Deng, C. L. Yu, G. Y. Huang, M. Larsson, P. Caroff, and H. Q. Xu, Nano Letters **12**, PMID: 23181691, 6414–6419 (2012).

[17]L. P. Rokhinson, X. Liu, and J. K. Furdyna, NATURE PHYSICS **8**, 795–799 (2012).

[18]M. T. Deng, C. L. Yu, G. Y. Huang, M. Larsson, P. Caroff, and H. Q. Xu, SCIENTIFIC REPORTS **4** (2014).

[19]J. Wiedenmann, E. Bocquillon, R. S. Deacon, S. Hartinger, O. Herrmann, T. M. Klapwijk, L. Maier, C. Ames, C. Bruene, C. Gould, A. Oiwa, K. Ishibashi, S. Tarucha, H. Buhmann, and L. W. Molenkamp, NATURE COMMUNICATIONS **7** (2016).

[20]A. Das, Y. Ronen, Y. Most, Y. Oreg, M. Heiblum, and H. Shtrikman, NATURE PHYSICS **8**, 887–895 (2012).

[21]R. S. Deacon, J. Wiedenmann, E. Bocquillon, F. Domínguez, T. M. Klapwijk, P. Leubner, C. Brüne, E. M. Hankiewicz, S. Tarucha, K. Ishibashi, H. Buhmann, and L. W. Molenkamp, ArXiv e-prints (2016).

[22]H.-Y. Hui, J. D. Sau, and S. Das Sarma, Phys. Rev. B **90**, 174206 (2014).

[23]J. D. Sau, and S. Das Sarma, Phys. Rev. B **88**, 064506 (2013).

[24]A. M. Lobos, R. M. Lutchyn, and S. Das Sarma, Phys. Rev. Lett. **109**, 146403 (2012).

[25]P. Neven, D. Bagrets, and A. Altland, New Journal of Physics **15**, 055019 (2013).

[26]D. Rainis, L. Trifunovic, J. Klinovaja, and D. Loss, Phys. Rev. B **87**, 024515 (2013).

[27]D. I. Pikulin, J. P. Dahlhaus, M. Wimmer, H. Schomerus, and C. W. J. Beenakker, New Journal of Physics **14**, 125011 (2012).

[28]J. Liu, A. C. Potter, K. T. Law, and P. A. Lee, Phys. Rev. Lett. **109**, 267002 (2012).

[29]D. Bagrets, and A. Altland, Phys. Rev. Lett. **109**, 227005 (2012).

[30]D. Roy, N. Bondyopadhaya, and S. Tewari, Phys. Rev. B **88**, 020502 (2013).

[31]T. D. Stanescu, and S. Tewari, Phys. Rev. B **89**, 220507 (2014).

[32]G. Kells, D. Meidan, and P. W. Brouwer, Phys. Rev. B **86**, 100503 (2012).

[33]E. J. H. Lee, X. Jiang, R. Aguado, G. Katsaros, C. M. Lieber, and S. De Franceschi, Phys. Rev. Lett. **109**, 186802 (2012).

[34]E. J. H. Lee, X. Jiang, M. Houzet, R. Aguado, C. M. Lieber, and S. De Franceschi, NATURE NANOTECHNOLOGY **9**, 79–84 (2014).

[35]C. Moore, T. D. Stanescu, and S. Tewari, ArXiv e-prints (2017).

[36]H.-J. Kwon, K. Sengupta, and V. M. Yakovenko, The European Physical Journal B - Condensed Matter and Complex Systems **37**, 349–361 (2004).

[37]L. Fu, and C. L. Kane, Phys. Rev. B **79**, 161408 (2009).

[38]H.-J. Kwon, V. M. Yakovenko, and K. Sengupta, Low Temperature Physics **30**, 613–619 (2004).

[39]D. M. Badiane, L. I. Glazman, M. Houzet, and J. S. Meyer, Comptes Rendus Physique **14**, 840–856 (2013).

[40]J. D. Sau, E. Berg, and B. I. Halperin, ArXiv e-prints (2012).

[41]J. D. Sau, and F. Setiawan, Phys. Rev. B **95**, 060501 (2017).

[42]R. Fazio, and H. van der Zant, Physics Reports **355**, 235–334 (2001).

[43]I. M. Pop, I. Protopopov, F. Lecocq, Z. Peng, B. Pannetier, O. Buisson, and W. Guichard, NATURE PHYSICS **6**, 589–592 (2010).

[44]D. B. Haviland, and P. Delsing, Phys. Rev. B **54**, R6857–R6860 (1996).

[45]E. Chow, P. Delsing, and D. B. Haviland, Phys. Rev. Lett. **81**, 204–207 (1998).

[46]D. B. Haviland, K. Andersson, and P. Ågren, Journal of Low Temperature Physics **118**, 733–749 (2000).

[47]S. Rubbert, and A. R. Akhmerov, Phys. Rev. B **94**, 115430 (2016).

[48]T. Hyart, B. van Heck, I. C. Fulga, M. Burrello, A. R. Akhmerov, and C. W. J. Beenakker, Phys. Rev. B **88**, 035121 (2013).

[49]K. Flensberg, Phys. Rev. Lett. **106**, 090503 (2011).

[50]P. Bonderson, and R. M. Lutchyn, Phys. Rev. Lett. **106**, 130505 (2011).

[51]B. van Heck, A. R. Akhmerov, F. Hassler, M. Burrello, and C. W. J. Beenakker, New Journal of Physics **14**, 035019 (2012).

[52]D. Aasen, M. Hell, R. V. Mishmash, A. Higginbotham, J. Danon, M. Leijnse, T. S. Jespersen, J. A. Folk, C. M. Marcus, K. Flensberg, and J. Alicea, Phys. Rev. X **6**, 031016 (2016).

[53]T. Karzig, C. Knapp, R. M. Lutchyn, P. Bonderson, M. B. Hastings, C. Nayak, J. Alicea, K. Flensberg, S. Plugge, Y. Oreg, C. M. Marcus, and M. H. Freedman, Phys. Rev. B **95**, 235305 (2017).

[54]K. Gharavi, D. Hoving, and J. Baugh, Phys. Rev. B **94**, 155417 (2016).

[55]S. Hoffman, C. Schrade, J. Klinovaja, and D. Loss, Phys. Rev. B **94**, 045316 (2016).

[56]E. Vernek, P. H. Penteado, A. C. Seridonio, and J. C. Egues, Phys. Rev. B **89**, 165314 (2014).

[57]M. T. Deng, S. Vaitiekenas, E. B. Hansen, J. Danon, M. Leijnse, K. Flensberg, J. Nygård, P. Krogstrup, and C. M. Marcus, Science **354**, 1557–1562 (2016).

[58]J. Li, T. Yu, H.-Q. Lin, and J. Q. You, SCIENTIFIC REPORTS **4** (2014).

[59]S. Plugge, A. Rasmussen, R. Egger, and K. Flensberg, New Journal of Physics **19**, 012001 (2017).

[60]D. E. Liu, and H. U. Baranger, Phys. Rev. B **84**, 201308 (2011).

[61]D. J. Clarke, ArXiv e-prints (2017).

[62]E. Prada, R. Aguado, and P. San-Jose, Phys. Rev. B **96**, 085418 (2017).

[63]B. E. Feldman, M. T. Randeria, J. Li, S. Jeon, Y. Xie, Z. Wang, I. K. Drozdov, B. A. Bernevig, and A. Yazdani, Nat. Phys. **13** (2016).

[64]K. A. Matveev, A. I. Larkin, and L. I. Glazman, Phys. Rev. Lett. **89**, 096802 (2002).

[65]G. Rastelli, I. M. Pop, and F. W. J. Hekking, Phys. Rev. B **87**, 174513 (2013).

[66]L. Fu, Phys. Rev. Lett. **104**, 056402 (2010).

[67]B. van Heck, F. Hassler, A. R. Akhmerov, and C. W. J. Beenakker, Phys. Rev. B **84**, 180502 (2011).

[68]D. Pekker, C.-Y. Hou, D. L. Bergman, S. Goldberg, İ. Adagideli, and F. Hassler, Phys. Rev. B **87**, 064506 (2013).

[69]L. P. Lévy, G. Dolan, J. Dunsmuir, and H. Bouchiat, Phys. Rev. Lett. **64**, 2074–2077 (1990).

[70]A. C. Bleszynski-Jayich, W. E. Shanks, B. Peaudecerf, E. Ginossar, F. von Oppen, L. Glazman, and J. G. E. Harris, Science **326**, 272–275 (2009).

[71]H. Bary-Soroker, O. Entin-Wohlman, and Y. Imry, Phys. Rev. B **82**, 144202 (2010).

[72]C. Xu, and L. Fu, Phys. Rev. B **81**, 134435 (2010).

Preface to Chapter 4

This final chapter takes one of the main ingredients of the systems discussed in Chapter 3– a topological Josephson junction–and focuses on obtaining effective models to describe this system. We find that the commonly made assumption that phase slips only occur in multiples of 4π in topological junctions is not always valid. We also find an appropriate description of the system when this is the case. Our results have important consequences for the dissipative phase transition expected in the system, which are discussed. Similarly to Chapter 3, this chapter translates many of the concepts often used to describe Josephson junction and Josephson junction arrays to a topological context.

4

Revisiting 2π phase slip suppression in topological Josephson junctions

Rosa Rodríguez-Mota[1], Smitha Vishveshwara[2] and T. Pereg-Barnea[1]

[1]Department of Physics and the Centre for Physics of Materials, McGill University, Montreal, Quebec, Canada H3A 2T8

[2]Department of Physics, University of Illinois at Urbana-Champaign, Urbana, Illinois 61801-3080, USA

This chapter will be submitted for publication in Physical Review B.

Abstract

Current state of the art devices to detect and manipulate Majoranas commonly consist of networks of Majorana wires and tunnel junctions. In this work, we study a key ingredient of these networks – a topological Josephson junction in the presence of charging energy. The phase dependent tunneling term contains both 4π and 2π periodic terms corresponding to single and pair particle tunneling. The single particle tunneling is allowed due to the Majorana modes in the edges of the junction while the pair tunneling is the usual Josephson tunneling. For small values of the charging energy, the low energy physics of conventional Josephson junctions is described by 2π phase slips. In a topological junction, it is usually expected that only 4π phase slips are possible while 2π phase slips are suppressed. However, we find that if the ratio between the strengths of the Majorana assisted tunneling and the Josephson tunneling is small – as is likely to be the case for many setups – 2π phase slips occur and may even dominate. We provide an effective descriptions of the system in terms of 2π and 4π phase slips valid for all values of the ratio between the strengths of the 4π and the 2π periodic tunneling. Finally, we discuss the implications of our results on the dissipative phase transitions expected in such a system.

4.1 Introduction

In recent years, there has been a lot of scientic effort to understand, realize and manipulate topological states in condensed matter.[1, 2] Particularly, Majorana wires [3, 4], in which strong spin-orbit coupling, superconductivity and a Zeeman gap give rise to a non-trivial topology causing Majorana modes at the edges of the wires, have gathered much attention. Interest in Majorana wires is motivated by the possibility of using the non-Abelian nature of Majorana modes for quantum computation schemes [5, 6] and is sustained by encouraging experimental results [7–15]. Hence, networks of Majorana wires have been proposed as tools to manipulate Majorana modes with quantum information purposes [16–21] or to create more exotic matter [22, 23]. In this work, we study a phenomenon commonly relevant to this type of networks, charge induced quantum fluctuations in topological Josephson junctions.

In Josephson junctions, charging effects induce quantum fluctuations, mainly in the form macroscopic tunneling processes.[24, 25] In a non-topological Josephson junction, the tunneling processes are known as phase slips and are essentially 2π jumps in the phase difference between the superconductors. The delocalization of the phase induced by these fluctuations can be prevented with dissipation. As a result, Josephson junctions present a dissipative phase transition [26, 27]. In a tunnel junction made of two topological superconductors, i.e. a topological Josephson junction, there are Majorana modes at both edges of the junction. The presence of these modes leads to coherent single particle tunneling between the superconductors, commonly referred to as the 4π periodic Josephson effect. [3, 4, 6, 28–31] The change of periodicity in the overall tunneling current, suppresses 2π phase slips in topological Josephson junctions. [32] Both the 2π phase slip suppression [32–34], and its effects on the dissipative phase transition [34] have been proposed as a probe for topological superconductivity. Most studies of 2π phase slip suppression focus on having a sufficiently strong single particle tunneling. [32–34] This is despite the fact that the single particle tunneling may be a small component of the overall tunneling current, as is the case for 3D topological insulator based Josephson junctions [35, 36]. As a result, there are currently no studies which describe the 2π phase slip suppression throughout the transition from a non-topological to a topological junction.

In this work, we develop a theory for the effect of charging induced quantum fluctuations in the low energy spectrum of a topological Josephson junction, valid for any value of the ratio between the strengths of the single particle and the Cooper pair tunneling. Our results show that a description of the low energy physics of the topological junction in terms of 4π phase slips may be insufficient if the strength of the 4π periodic tunneling is small. In the presence of both 2π and 4π periodic components of the tunneling current, the potential energy of the junction as a function of the phase difference between the superconductors, θ, may have one or two minima in $[0, 4\pi)$ (see Figs. 4.1b and 4.1c). If only one minimum exists, the description in terms of 4π phase slips works as long as the phase fluctuations are small. In the presence of two minima, this description may break down even for small phase fluctuations if they are relatively large compared to the strength of the 4π periodic tunneling. In this case, a description of the junction in terms of coupled 2π phase slips is more appropriate. This is shown schematically in Fig. 4.1a where E_J and E_M correspond to the energy scale of the 2π and 4π periodic tunneling, respectively, and E_C to the strength of the phase fluctuations. The junction potential has only one minimum for $E_M > 8E_J$ and two otherwise.

This paper is organized as follows. In Sec. 4.2, we give a small review of the effects of charging induced phase fluctuations in Josephson junctions. This is followed by a qualitative discussion of the effects of phase fluctuations for different regimes of a topological Josephson junction in Sec. 4.3. The main results of this work are stated in Sec. 4.4 where we introduce effective models to describe the low-energy physics of topological Josephson junctions. In Sec. 4.5 we discuss the implications of our results on the dissipative phase transition. Finally, our conclusions are stated in Sec. 4.6.

4.2 Review of the effects of quantum phase slips in Josephson junctions

We begin with a quick review of the effects of small phase fluctuations in the spectrum of a (non-topological) Josephson junction. The junction consists of a weak link between two superconductors with capacitance C described by the Hamiltonian

$$\hat{H} = E_C \left(\hat{n} - n_g\right)^2 - E_J \cos\hat{\theta}, \tag{4.2.1}$$

where E_J is the Josephson energy associated with the tunneling of Cooper pairs between the two superconductors, $E_C = \mathrm{e}^2/(2C)$, the charging energy of the weak link and n_g the offset charge. The operator $\hat{n}$ measures the charge excess and the operator $\hat{\theta}$, measures the phase difference between the superconductors. To simplify the comparison with the following sections, we measure $\hat{n}$ (and n_g) in units of the electron charge e, rather than in the more conventional units of $2\mathrm{e}$. This means that the operators $\hat{n}$ and $\hat{\theta}$ follow the commutation relation $[\hat{\theta}, \hat{n}] = 2i$. Several examples of superconducting circuits, such as the ones used in the Cooper pair box [37, 38], quantronium [39] and transmon [40] qubits, can be mapped to Eq. (4.2.1). In these circuits, n_g is tuned using gate voltages, while the ratio of E_J and E_C is tuned either using split junctions or adding additional capacitances (see e.g. Ref. [41]).

In the basis of phase eigenstates, the wave-function $\Psi(\theta) = \langle\theta|\Psi\rangle$ describing the

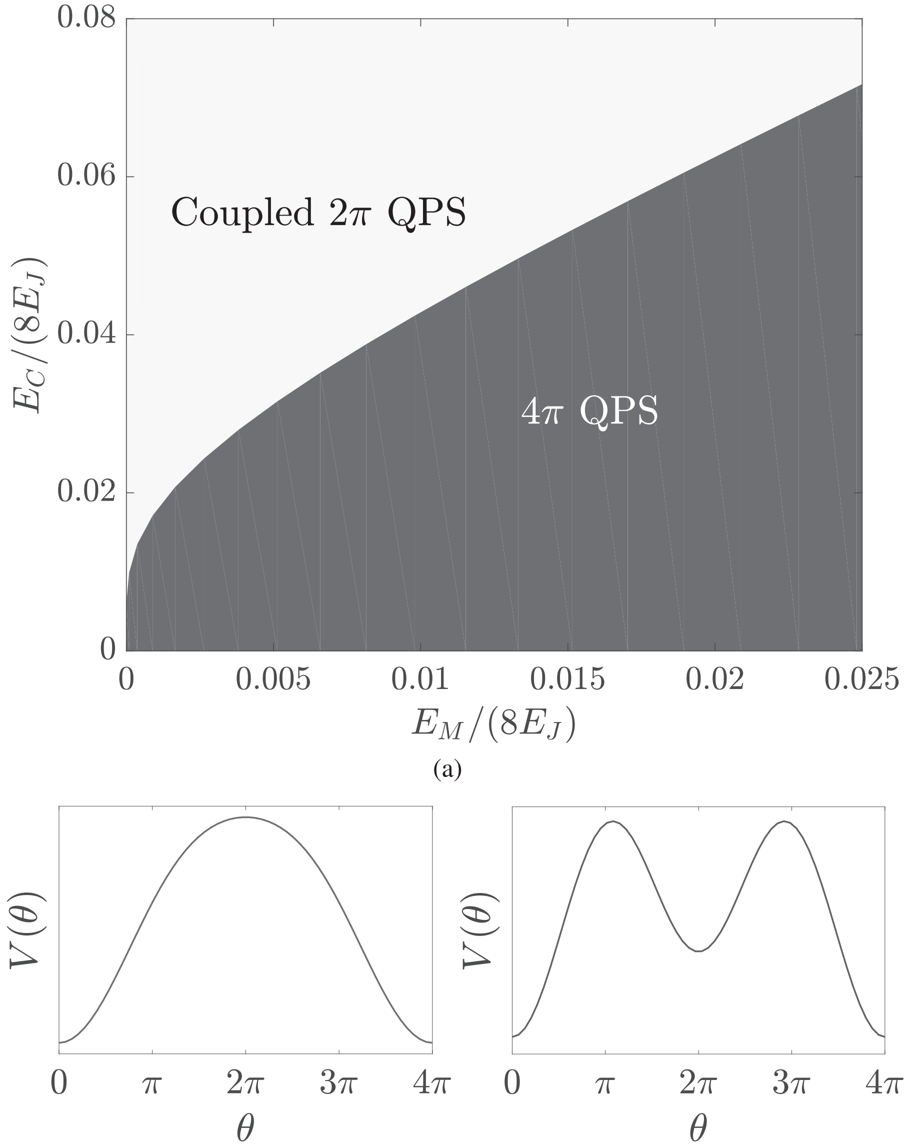

(b) $E_M/(8E_J) > 1$ (c) $E_M/(8E_J) < 1$

Figure 4.1: Depending on the relative strength between the single-particle (set by E_M) and the pair tunneling (set by E_J) the potential of the topological Josephson junction may be minimized when: (b) the phase difference across the junction is an integer multiple of 4π only, or (c) the phase difference across the junction is any integer multiple of 2π. In (c) the minima at odd 2π are local minima. (a) In (c), the strength of phase fluctuations (set by E_C) decides whether oscillations around the local minima contribute to the ground-state (Coupled 2π QPS) or not (4π QPS).

Josephson junction follows the equation

$$\left[E_C\left(-2i\frac{d}{d\theta}-n_g\right)^2-E_J\cos\theta\right]\Psi(\theta)=E\Psi(\theta) \tag{4.2.2a}$$

with the boundary condition

$$\Psi(\theta+2\pi)=\Psi(\theta). \tag{4.2.2b}$$

The dependence of the system on the offset charge n_g can be transferred from the Schrödinger's equation to the boundary condition via the transformation $\hat{n}\to\hat{n}+n_g$, i.e. $\Psi(\theta)\to e^{in_g\theta/2}\Psi(\theta)$ and

$$\left[E_C\left(-2i\frac{d}{d\theta}\right)^2-E_J\cos\theta\right]\Psi(\theta)=E\Psi(\theta) \tag{4.2.3a}$$

$$\Psi(\theta+2\pi)=e^{i\pi n_g}\Psi(\theta). \tag{4.2.3b}$$

The above equations can be solved using Mathieu functions. Nonetheless, expansions for different parameter regimes have been developed to provide more intuition. Since we are interested in studying phase fluctuations, we focus on the parameter region with $E_C \ll E_J$. This corresponds to the regime of interest of transmon qubits [40].

When $E_C \ll E_J$ the potential energy $-E_J\cos\theta$ dominates the energy of the system. Around the potential energy minima, i.e. $2\pi n$ with integer n, equation (4.2.3a) can be mapped onto an harmonic oscillator with frequency $\hbar\omega=\sqrt{8E_JE_C}$. The low energy levels of the Josephson junction therefore correspond to harmonic oscillator levels. Deep inside the potential well, these harmonic oscillations do not depend on the boundary conditions given by (4.2.3b). To find the junction dependence on n_g, we need to account for quantum tunneling between the different potential minima.

Denoting the amplitude for quantum tunneling between the mth harmonic oscillator level of one of the potential minima and its nearest neighbors by ν_m, it is possible to write an effective tight-binding Hamiltonian for the junction:

$$\hat{H} = \sum_{m=0}^{\infty} \sum_{j} \Big[\epsilon_m \Psi_m^\dagger(j) \Psi_m(j) \\ -\nu_m \Psi_m^\dagger(j+1) \Psi_m(j) + \text{H. c.}\Big] \tag{4.2.4}$$

Here $\Psi_m^\dagger(j)$ is the creation operator for mth level of an harmonic oscillator around $2\pi j$, and $\epsilon_m = \hbar\omega(m + 1/2)$ the energy of the a level. The tight-binding Hamiltonian (4.2.4) is diagonalized using the operators $\Psi_m(k) = \sum_j e^{-ikj} \Psi_m(j)$:

$$\hat{H} = \sum_m \sum_k \left(\epsilon_m - 2\nu_m \cos k\right) \Psi_m(k)^\dagger \Psi_m(k). \tag{4.2.5}$$

Comparing with (4.2.3b) leads to the identification $k = \pi n_g$, which allows us to conclude that for $E_C \ll E_J$ the dispersion of the mth level of the junction will be given by

$$E_m(n_g) = \epsilon_m - 2\nu_m \cos\left(\pi n_g\right), \tag{4.2.6}$$

which holds when $\nu_m \ll \hbar\omega$.

The tunneling amplitudes ν_m can be calculated using semi-classical methods. Here we briefly outline the calculation for ν_0 using the dilute instanton gas approximation in the path integral imaginary time formalism (see e.g. Ref. [42]). In this formalism, the amplitude to propagate from 0 to 2π during an imaginary time interval of length $2L$ is written as a weighted sum over all the paths that start at 0 at time $\tau = -L$ and finish at 2π at $\tau = L$:

$$(0, -L|2\pi, L) = \int [\mathcal{D}\theta] e^{-\frac{1}{\hbar}\int_{-L}^{L} \mathcal{L}(\theta(\tau)) d\tau}, \tag{4.2.7}$$

where

$$\mathcal{L}(\theta) = \frac{\hbar^2 (\partial_\tau \theta)^2}{16E_C} + E_J (1 - \cos\theta), \tag{4.2.8}$$

commonly known as the sine-Gordon Lagrangian, is the Lagrangian of the Josephson junction modeled by (4.2.1).

For $L \to \infty$, it is possible to find a "classical" solution, i.e. a path that extremizes the action $S = \int \mathcal{L} d\tau$ with $\theta(-\infty) = 0$ and $\theta(\infty) = 2\pi$. This path is known as a 2π-kink or instanton, and it is given by $\theta_{2\pi}^{cl}(\tau) = 4\arctan\left(e^{\omega(\tau-\tau_0)}\right)$ where ω coincides with the frequency for harmonic oscillations around $2\pi j$. Conversely, the model also has a classical solution with $\theta(-\infty) = 2\pi$ and $\theta(\infty) = 0$ known as an anti-kink. In the dilute instanton gas approximation, the path integration of Eq. (4.2.7) is done over combinations of kinks and anti-kinks and Gaussian fluctuations around them. Furthermore, it is assumed that the kinks and anti-kinks are separated enough (in imaginary time) that the interactions between them are negligible. This yields the result

$$\nu_0 = \sqrt{2(\hbar\omega)^3/(\pi E_C)} e^{-\hbar\omega/E_C}, \tag{4.2.9}$$

where $\hbar^2\omega/E_C = \hbar\sqrt{8E_J/E_C}$ is to the action of a 2π kink.

To test the validity of (4.2.9) we ask whether the gas of kinks and anti-kinks is in fact dilute. This can be done by comparing the width of the kinks, $2/\omega$, with the expected average separation among them, $\hbar/\nu_0$. The gas is dilute, and Eq. (4.2.9) is self-consistent, as long as $\nu_0 \ll \hbar\omega/2$.

This formalism can be extended to calculate the n_g-dependence of higher levels through the use of periodic instantons (see e.g. Ref. [43]). The decision to focus on ν_0 was made for the sake of simplicity.

4.3 Phase fluctuations in a topological Josephson junction

To study the effects of small phase fluctuations in a topological Josephson junction, we consider a simple model of a Josephson junction with capacitance C made of two topological superconductors. Since the two superconductors coupled by the junction are topological, each of them presents a Majorana mode which is close to the the junction. We denote these by γ_1 and γ_2, and ignore the other two Majorana modes which are far from the junction. The coupling of these Majorana modes adds a 4π periodic term to the tunneling current [3, 4, 6, 28–31]. The topological junction can then be modeled by the following Hamiltonian:

$$\hat{H} = E_C \left(\hat{n} - n_g\right)^2 - E_J \cos\hat{\theta} - i\gamma_1\gamma_2 \frac{E_M}{2} \cos\frac{\hat{\theta}}{2} \tag{4.3.1}$$

with $i\gamma_1\gamma_2$ the parity of the fermionic mode caused by the hybridization of the Majorana modes on both sides of the junction. When the local parity is conserved, this fermionic mode can be integrated out and we can substitute $i\gamma_1\gamma_2$ by either one of its two eigenvalues ±1. From now on, we assume $i\gamma_1\gamma_2 = +1$. As long as the local parity is conserved, our results do not rest on this assumption.

As in the previous section, after a charge translation the wave-function in phase basis follows an n_g independent Schrödinger's equation

$$\left[E_C \left(-2i\frac{d}{d\theta}\right)^2 - E_J \cos\theta - \frac{E_M}{2}\cos\frac{\theta}{2}\right]\Psi = E\Psi \tag{4.3.2a}$$

and a boundary condition

$$\Psi(\theta + 4\pi) = e^{i2\pi n_g}\Psi(\theta). \tag{4.3.2b}$$

where all the dependence on n_g is encoded.

For small E_C, the potential energy of the junction dominates. The low energy levels of the junction consist of linear combinations of harmonic oscillator levels at the different potential minima, as in the previous section. However in the topological Josephson junction, the competition between the pair and single particle tunneling creates two different regimes depending whether the junction potential has a single minimum or a two minima for $0 \leq \theta < 4\pi$.

When $E_M/(8E_J) > 1$, the junction potential has a single minimum in the $[0, 4\pi)$ interval. Hence, the potential is minimized when $\theta = 4\pi m$ with m an integer, and all the minima are degenerate. The frequency of harmonic oscillations around these minima, obtained by expading Eq. (4.3.2a) around these values, is $\hbar\omega = \sqrt{8E_J E_C + E_M E_C}$. This is exemplified in Fig. 4.2a where the first few harmonic oscillator levels and the ground-state wave-function amplitude are shown for $E_M = 2 = 10E_J$ and $E_C = 0.001$. The junction potential and the tunneling processes between the degenerate levels are also shown in Fig. 4.2a. As E_C increases, the spacing between the levels and tunneling amplitude increases and the harmonic wave-functions widen, as shown in Fig. 4.2b for $E_M = 2 = 10E_J$ and $E_C = 0.1$. However, the tunneling processes that give rise to the n_g dispersion remain unchanged by the increase of E_C. In this regime, the topological junction behaves qualitatively similar to the non-topological junction from the previous section with half the n_g periodicity and 4π phase slips taking the role of 2π phase slips.

On the other hand, if $E_M/(8E_J) < 1$, the junction potential has two minima in the $[0, 4\pi)$ interval. Hence, the potential has two kinds of minima with two different frequencies for harmonic oscillations around them: $\theta = 4\pi m$ with frequency $\hbar\omega_+ = \sqrt{8E_J E_C + E_M E_C}$, and $\theta = 4\pi m + 2\pi$ with frequency $\hbar\omega_- = \sqrt{8E_J E_C - E_M E_C}$. In addition to the effects discussed in the previous paragraph, changing E_C may also change the tunneling processes that contribute to each energy level. This is shown in

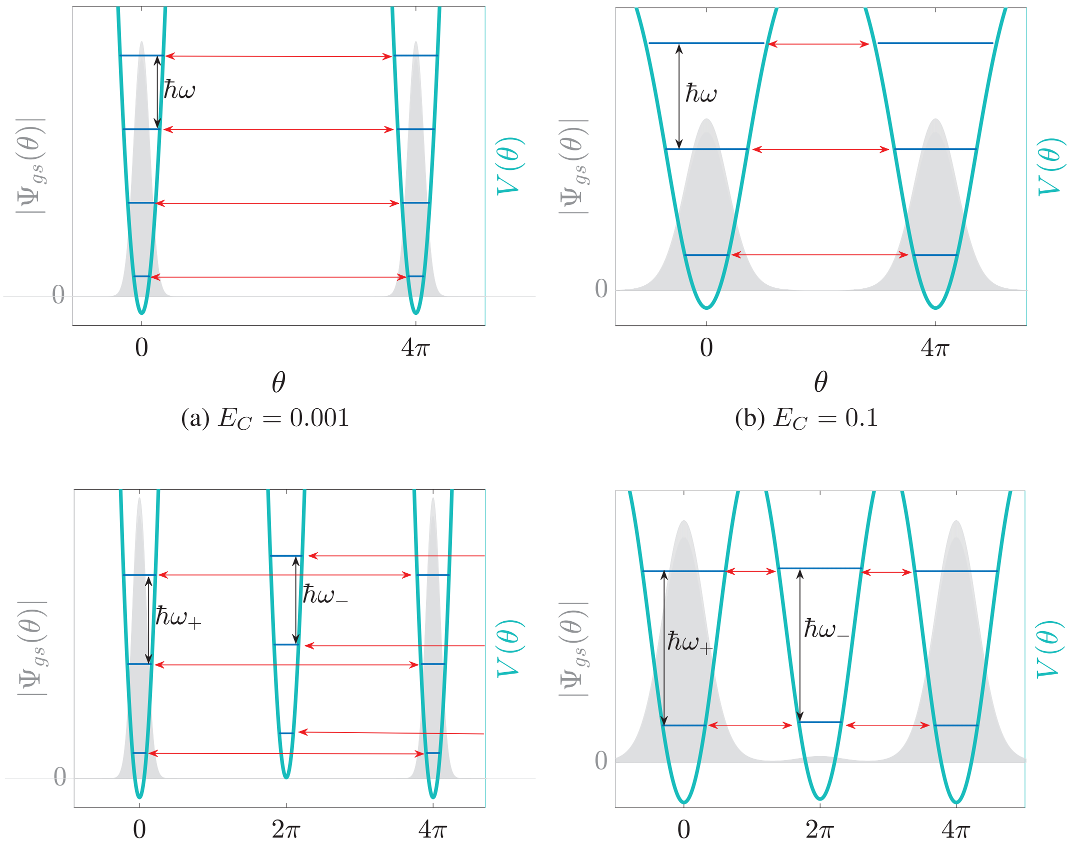

(a) $E_C = 0.001$ (b) $E_C = 0.1$

(c) $E_C = 0.001$ (d) $E_C = 0.1$

Figure 4.2: Phase fluctuations in the single-minimum and double-minimum regimes of a topological Josephson junction. The first harmonic levels (blue lines) and the junction potential (green line)are shown for a junction with $E_M = 2 = 10E_J$ and (a) $E_C = 0.001$ and (b) $E_C = 0.1$, and a junction with $E_J = 1 = 50E_M$ and (c) $E_C = 0.001$ and (d) $E_C = 0.1$. The ground-state wave-functions, whose amplitudes are shown in grey, correspond to linear superpositions of harmonic oscillations around the potential minima. The tunneling processes that give rise to the n_g dispersion of each level are shown in red. In the double-minimum regime ((c) and (d)), increasing E_C can change which are the dominant tunneling processes. The ground-state wave-function in (d) shows an additional (small) peak around 2π.

Figs. 4.2c and 4.2d. The ground-state wave-function in Fig. 4.2c is peaked around 0 and 4π, whereas the ground-state wave-function in Fig. 4.2d shows additional contributions from oscillations around 2π.

4.4 Effective models

As discussed in the previous section, the tunneling processes which contribute to each energy level in the topological Josephson junction depend on the system parameters. In this section, we will discuss two different effective models for the junction ground-state: one in which only oscillations between $4\pi m$ minima contribute and one in which oscillations around all $2\pi m$ minima contribute to the ground-state. We calculate the effective tunneling parameters of each model and discuss the their regions of validity.

4.4.1 4π QPS model

We can write an effective Hamiltonian for the ground-state of the junction as a combination of harmonic oscillations around $4\pi n$ plus tunneling between such minima:

$$\hat{H} = \sum_n \left(\frac{\hbar\omega}{2} \Psi_{2n}^\dagger \Psi_{2n} - \nu_{4\pi} \Psi_{2n+2}^\dagger \Psi_{2n} + \text{H. c.} \right), \tag{4.4.1}$$

where ω the frequency of harmonic oscillations around the minima at $4\pi n$ and is given by $\hbar\omega = \sqrt{8E_J E_C + E_M E_C}$. Accounting for the boundary condition (4.3.2b) results in the following ground-state energy dispersion

$$E_{gs}(n_g) = \frac{\hbar\omega}{2} - 2\nu_{4\pi} \cos\left(2\pi n_g\right). \tag{4.4.2}$$

This model gives an effective description of the system in the single-minimum regime and in the double-minimum regime for small enough E_C (see Fig. 4.2).

The tunneling amplitude $\nu_{4\pi}$ can be calculated following the procedure outlined in Sec. 4.2. The imaginary time Lagrangian of the topological junction,

$$\mathcal{L}(\theta) = \frac{\hbar^2 (\partial_\tau \theta)^2}{16 E_C} + E_J (1 - \cos\theta) + \frac{E_M}{2}\left(1 - \cos\frac{\theta}{2}\right), \tag{4.4.3}$$

is known as the double sine-Gordon Lagrangian and its semi-classical dynamics have been widely studied.[44] Interestingly, the 4π kink in the DSG model can be written as a sum over two 2π SG kinks

$$\theta_{4\pi}^{cl} = 4 \arctan e^{\omega(\tau-\tau_0)-R} + 4 \arctan e^{\omega(\tau-\tau_0)+R} \tag{4.4.4a}$$

separated by an imaginary time interval $2R/\omega$ where R is fixed by the ratio of E_M and $8E_J$:

$$R = \operatorname{arccosh}\left(\sqrt{1 + \frac{8E_J}{E_M}}\right). \tag{4.4.4b}$$

When $E_M \to 0$, the separation between the two 2π kinks diverges ($R \to \infty$) meaning that the 4π kinks effectively decouple into two separate 2π kinks as the DSG Lagrangian reduces to the SG Lagrangian.

Using the dilute instanton gas approximation, as before, we find

$$\nu_{4\pi} = \sqrt{\frac{8(\hbar\omega)^5}{\pi E_M E_C^2}} \exp\left(-\frac{\hbar\omega}{E_C} \times f\left(\frac{E_M}{8E_J}\right)\right) \tag{4.4.5a}$$

where

$$f(x) = 2 + \frac{2x}{\sqrt{1+x}} \coth^{-1}\left(\sqrt{1+x}\right) \tag{4.4.5b}$$

is an increasing function with $f(0) = 2$ and $f(\infty) = 4$. With the appropriate modifications, this result is in agreement with the result found by Ref. [45] in the context of statistical mechanics. A more detailed account of how Eq. (4.4.5) is obtained is shown in Appendix 4.A.1.

When $E_M \to 0$, $\nu_{4\pi}$ presents a square root divergence, i.e. $\nu_{4\pi} \sim 1/\sqrt{E_M}$. This divergence has different physical interpretations. First, it is indicative of a resonance in tunneling [46] when $E_M \to 0$. In our context, it is a sign that the validity of the model breaks down in this limit. In terms of the semi-classical formalism, the divergence arises because one of the eigenvalues of the operator for quadratic fluctuations around the 4π kink turns into a zero mode when $E_M \to 0$. The physical origin of this zero mode is the restoration of the 2π translation symmetry; i.e. the the two 2π kinks decouple in this limit.

The presence of this emergent zero mode for $E_M \to 0$ diminishes the range of the validity of the calculated expression for $\nu_{4\pi}$. This can be seen by noting that the dilute instanton gas approximation breaks down when $E_M \to 0$: the width of the 4π kinks $(2 + 2R)/\omega$ diverges as $-\log E_M$ whereas the average separation between the kinks $\hbar/\nu_{4\pi}$ goes to zero as $\sqrt{E_M}$. The assumption that the width of the 4π kinks is much smaller than the average separation between the kinks fails for $E_M \to 0$. We address this problem in the next subsection.

Emergent translational mode correction

One approach to increase the accuracy of the calculation is to account for a higher order of fluctuations in the direction of the emergent zero mode. [47, 48] Since the emergent zero mode is related to the decoupling of the two kinks, this is (roughly) equivalent to letting the distance between the two kinks fluctuate around its equilibrium value, $2R/\omega$.

The result of Ref. [48] can be written in terms of R as:

$$\nu_{4\pi} = \frac{4F(R)\,(\hbar\omega)^2}{\pi E_C}\,\mathcal{I}\left(R, \tfrac{\hbar\omega}{E_C}\right) \tag{4.4.6a}$$

where $F(R)$ is a numerical factor bounded by $\sqrt{2/5} \le F(R) \le 1$ and given by

$$F(R) = \frac{\sqrt{\cosh 2R - R\tanh R - 3R\coth R + 2}}{\sinh R\sqrt{2 - 8R^2\text{csch}^2 2R}}; \tag{4.4.6b}$$

and

$$\mathcal{I}\,(R, \alpha) = \int_0^\infty dr\sqrt{1 - 4r^2\text{csch}^2(2r)}e^{-\alpha S_R(r)} \tag{4.4.6c}$$

with

$$\begin{aligned} S_R(r) =& 1 + \frac{\tanh^2 R}{\tanh^2 r} + 2r\times \\ & \left(\frac{1}{\sinh 2r} + \frac{\coth r}{\cosh^2 R} - \frac{\tanh^2 R\coth r}{2\sinh^2 r}\right). \end{aligned} \tag{4.4.6d}$$

In the above expressions, $2r/\omega$ corresponds to the fluctuating distance between the two kinks and $S_R(r)$ is an r-dependent effective action. $S_R(r)$ is minimized at $r = R$ and behaves linearly for $r \gtrsim 5$, with a slope that decreases with increasing R. For more details on how this expression is obtained, we refer the reader to Appendix 4.A.2 and Ref. [48].

To the best of our knowledge, a closed form expression for $\mathcal{I}\,(R, \alpha)$ does not exist. Nonetheless, we can find approximate expressions for $\mathcal{I}\,(R, \alpha)$ for small and large R. For small R, the greatest contribution to $\mathcal{I}\,(R, \alpha)$ comes from the r values around R. A saddle point approximation of the integral $\mathcal{I}\,(R, \alpha)$ results in

$$\mathcal{I}\,(R, \alpha) \approx \sqrt{\frac{\pi}{2\alpha}\frac{\cosh R}{F(R)}}e^{-\alpha S_R(R)}. \tag{4.4.7}$$

This is a good approximation to $\mathcal{I}\left(R,\alpha\right)$ if $e^{2R} \ll 16\alpha$ (see Appendix 4.A.2). Substituting this in (4.4.6a) gives the expression for $\nu_{4\pi}$ obtained without including corrections due to the emergent translational mode, i.e. Eq. (4.4.5). Hence, Eq. (4.4.5) is valid when $E_M/(8E_J) \gg E_C/(4\hbar\omega)$.

When R is large, the integral is dominated by the linear large r behavior of $S_R(r)$. In Appendix 4.B.2, we find that for $16\alpha^2 \ll e^{2R}$

$$\mathcal{I}\left(R,\alpha\right) \approx \frac{\cosh^2(R)e^{-\alpha\left(\tanh^2(R)+1\right)}}{2\alpha}. \tag{4.4.8}$$

This leads to $\nu_{4\pi} \approx \nu_{4\pi}^{lr}$ with

$$\nu_{4\pi}^{lr} = \frac{f_2\left(\frac{E_M}{8E_J}\right)\left(\hbar\omega\right)^3}{\pi E_C E_M} \exp\left[-\frac{\hbar\omega}{E_C} \times f_1\left(\frac{E_M}{8E_J}\right)\right] \tag{4.4.9}$$

when $E_M/(8E_J) \ll 0.25E_C^2/(\hbar\omega)^2$. In the above equation, $f_1(x)$ and $f_2(x)$ are order 1 numerical factors which decrease with x; their exact form can be found in Appendix 4.B.2. Note that according to the above calculations $\nu_{4\pi}$ diverges for $E_M \to 0$ as $1/E_M$.

4.4.2 Coupled 2π QPS model

If the junction parameters are such that there are additional (local) minima at $2\pi m$ with m odd and oscillations around those minima contribute to the ground-state (see e.g. Fig. 4.2d), we can describe it by the following effective Hamiltonian:

$$\hat{H} = \sum_n \left(\epsilon_n \Psi_n^\dagger \Psi_n - \nu_{2\pi}\Psi_{n+1}^\dagger \Psi_n - \nu_{2\pi}\Psi_n^\dagger \Psi_{n+1}\right), \tag{4.4.10}$$

where $\nu_{2\pi}$ corresponds to tunneling amplitude between potential minima separated by 2π and the energies ϵ_n are given by:

$$\begin{aligned}\epsilon_{2n} =& \epsilon_e = \frac{\hbar\omega_+}{2} \\ \epsilon_{2n+1} =& \epsilon_o = E_M + \frac{\hbar\omega_-}{2} \\ \hbar\omega_\pm =& \sqrt{8E_J E_C \pm E_M E_C}.\end{aligned} \tag{4.4.11}$$

The dispersion of (4.4.10) is

$$\begin{aligned}E_\pm(n_g) =& \frac{1}{2}(\epsilon_o + \epsilon_e) \\ & \pm \frac{1}{2}\sqrt{(\epsilon_o - \epsilon_e)^2 + 8\nu_{2\pi}^2(1 + \cos(2\pi n_g))}.\end{aligned} \tag{4.4.12}$$

The hopping $\nu_{2\pi}$ can be calculated using the formula proposed by Ref. [49] for the tunneling through an asymmetric potential. Without loss of generality, we can focus on calculating the amplitude for tunneling between 0 and 2π. The minimum at 0 and the minimum at 2π are separated by a barrier which is largest at θ_{max}. Following Ref. [49] we define two potentials symmetric around θ_{max}, $V_L(\theta)$ and $V_R(\theta)$, such that $V_L(\theta)$ ($V_R(\theta)$) is equal to the junction potential for $0 < \theta < \theta_{max}$ ($\theta_{max} < \theta < 2\pi$). Then $\nu_{2\pi}$ can be written as:

$$\nu_{2\pi} = A\sqrt{\nu_L \nu_R}, \tag{4.4.13}$$

where ν_s, $s = L, R$, is the probability for tunneling from 0 to 2π through the potential V_s and

$$A = \frac{1}{2}\left[\left(\frac{V_{max} - \epsilon_e}{V_{max} - \epsilon_o}\right)^{1/4} + \left(\frac{V_{max} - \epsilon_o}{V_{max} - \epsilon_e}\right)^{1/4}\right]^{1/2}, \tag{4.4.14}$$

with $V_{max} = V(\theta_{max})$. The above expression for $\nu_{2\pi}$ clearly breaks down when $\epsilon_o > V_{max}$; at that point the zero point motion of the shallow minimum becomes larger than the potential barrier. The approximations leading to the above expression for $\nu_{2\pi}$ start failing before this point.

For our model of a topological Josephson junction, θ_{max} and V_{max} are given by:

$$\begin{aligned} \theta_{max} =& 4\arctan\left(\omega_+/\omega_-\right) \\ V_{max} =& 2E_J\left(E_M/(8E_J)+1\right)^2 . \end{aligned} \tag{4.4.15}$$

And the θ_{max}-symmetric potentials V_L and V_R are well approximated by

$$\begin{aligned} V_L(\theta) &\approx E_J\left(1+\frac{E_M}{8E_J}\right)^2\left(1-\cos\left(\frac{\pi\theta}{\theta_{max}}\right)\right) \\ V_R(\theta) &\approx E_M + \\ &E_J\left(1-\frac{E_M}{8E_J}\right)^2\left(1-\cos\left(\frac{\pi(\theta-2\pi)}{\theta_{max}-2\pi}\right)\right), \end{aligned} \tag{4.4.16}$$

which leads to the following tunneling amplitudes:

$$\nu_s = \frac{4}{\sqrt{P_s\pi}}\left(8E_s^3E_C\right)^{1/4} e^{-P_s\sqrt{\frac{8E_s}{E_C}}} \tag{4.4.17}$$

with $P_L = \theta_{max}/\pi = 2 - P_R$, $E_L = E_J(1+E_M/(8E_J))^2$ and $E_R = E_J(1 - E_M/(8E_J))^2$. P_s and E_s are, respectively, the period and amplitude of the potential V_s for $s = L, R$.

For $E_M \to 0$ the dispersion (4.4.12) becomes

$$E_\pm(n_g) \to \frac{\hbar\omega}{2} \pm \left|2\nu_0\cos\left(\pi n_g\right)\right| . \tag{4.4.18}$$

This is the expected result for the $E_M \to 0$ limit, as it corresponds to the breaking of the symmetry between the minima at even and odd multiples of 2π “folding" the n_g-Brillouin zone.

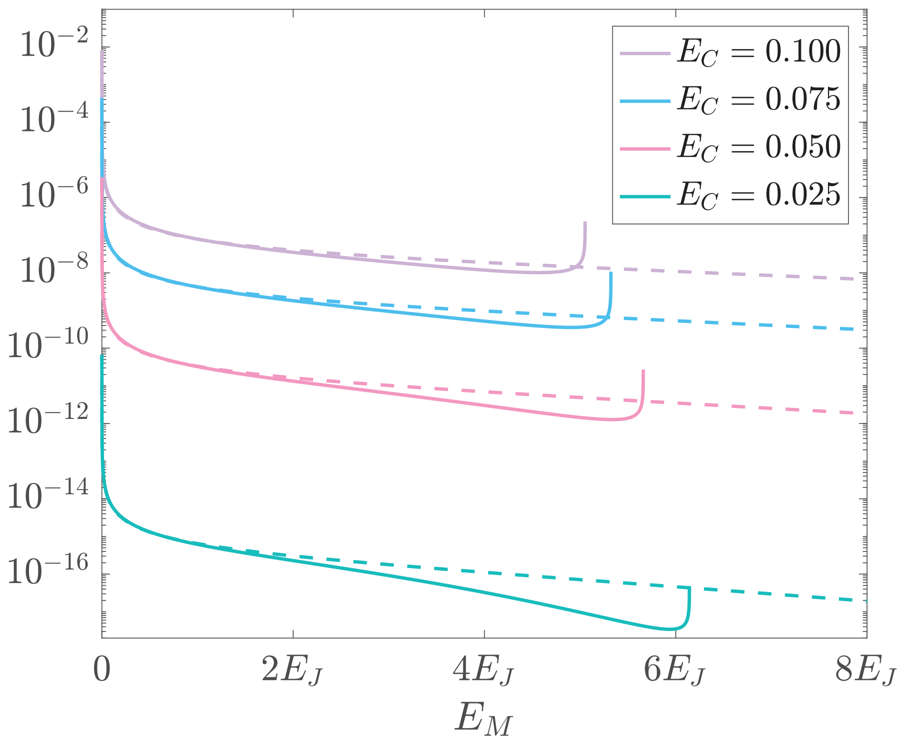

Figure 4.3: Comparison of $\nu_{2\pi}^2/|\epsilon_o - \epsilon_e|$ (solid line) and $\nu_{4\pi}^{lr}$ (dashed line) for $E_J = 1$. The $\nu_{2\pi}^2/|\epsilon_o - \epsilon_e|$ lines stop when the potential barrier is smaller than the zero point motion energy for oscillations around the shallow minima ϵ_o.

We also note that for $\nu_{2\pi} \ll |\epsilon_o - \epsilon_e|$ the lowest of the two bands becomes

$$E_-(n_g) \approx \epsilon_e - \frac{2\nu_{2\pi}^2}{|\epsilon_o - \epsilon_e|} - \frac{2\nu_{2\pi}^2}{|\epsilon_o - \epsilon_e|}\cos(2\pi n_g). \tag{4.4.19}$$

This dispersion would be equivalent to the dispersion found for the 4π phase slip model (4.4.2) if $\nu_{2\pi}^2/|\epsilon_o - \epsilon_e| \to \nu_{4\pi}$. As shown in Fig. 4.3, we find that $\nu_{2\pi}^2/|\epsilon_o - \epsilon_e| \approx \nu_{4\pi}^{lr}$. This allows us to interpret $\nu_{4\pi}^{lr}$ as arising from coupled but not confined 2π phase slips.

4.4.3 Validity of the effective models

The image that emerges from the results in this section and the previous energetic considerations is as follows. Given a junction with fixed E_M and E_J values, it is always possible to find E_C small enough such that the junction is well described by 4π QPS. On the other hand, given E_C we can always find a E_M small enough so 2π QPS are still present in the system. The range of E_C values in which the junction can be fully described by 4π QPS processes shrinks to 0 when $E_M \to 0$. To further clarify the range of parameters in which each picture is valid, we compare the different effective models for the topological Josephson junction with numerical result.

The spectrum of Eq. (4.3.1) is obtained numerically by truncating the Hilbert space in number basis, where the Hamiltonian becomes

$$\begin{aligned} H = \sum_{n=-\infty}^{\infty} \Big[& E_C\,(n-n_g)^2 \,|n\rangle\langle n| - \tfrac{E_M}{4}(|n\rangle\langle n+1| \\ & + |n\rangle\langle n-1|) - \tfrac{E_J}{2}(|n\rangle\langle n+2| + |n\rangle\langle n-2|)\Big]. \end{aligned} \tag{4.4.20}$$

The numerical results shown in this paper are obtained by taking the sum in the above equation from $-N$ to N with $N = 10^4$.

Comparisons between $E_{gs}(n_g)$ for the topological Josephson junction predicted by

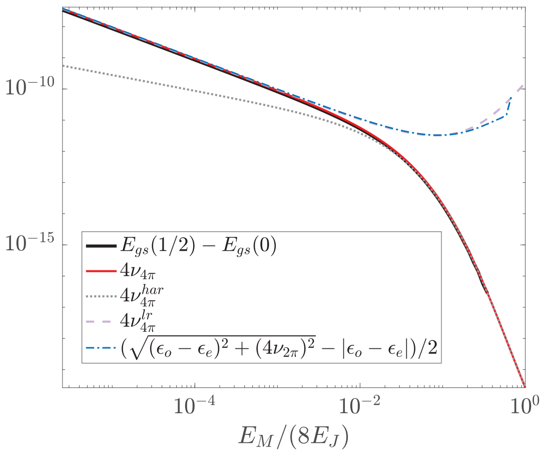

(a) $E_C = 0.005$

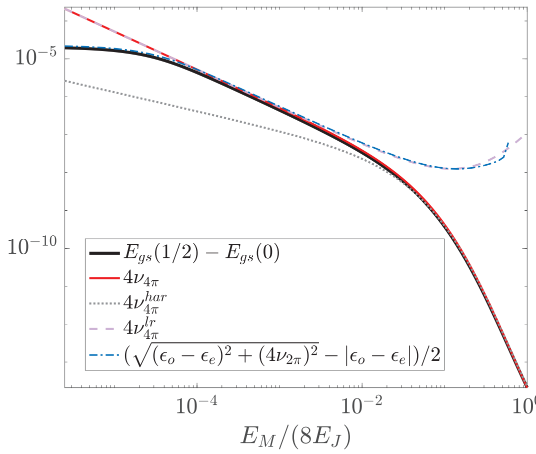

(b) $E_C = 0.01$

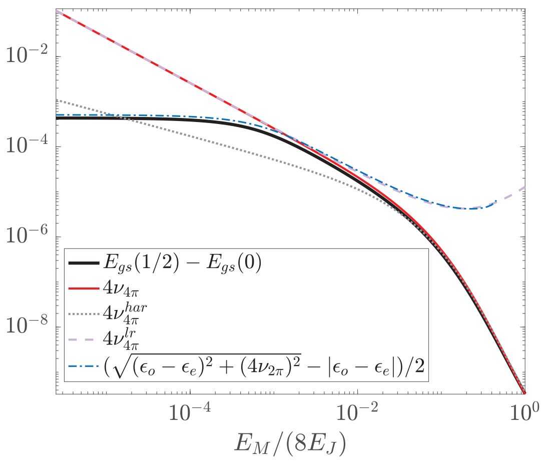

(c) $E_C = 0.02$.

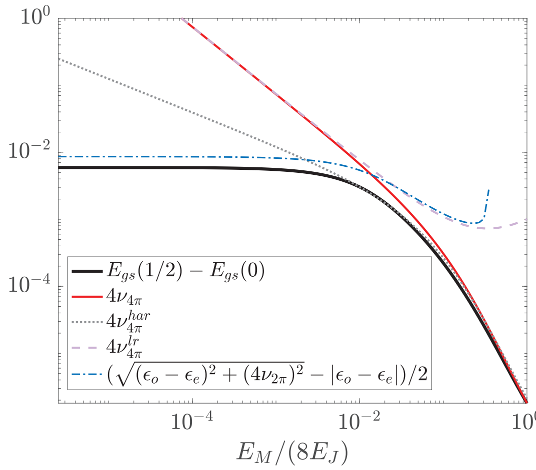

(d) $E_C = 0.05$.

Figure 4.4: Comparison between the effective models and numerical results. The numerically obtained value for $E_{gs}(1/2) - E_{gs}(0)$ (solid black line) is plotted along with its expected value from the effective models from Eqs. (4.4.1) (solid red line) and (4.4.10) (blue dashed-dotted line) as a function of $E_M/(8E_J)$ with $8E_J + E_M = 1$ and different E_C values. The approximate expressions found for the tunneling amplitude in Eq. 4.4.6 are also compared in this figure (dotted gray line and dashed purple line).

the effective models discussed previously and numerical results are shown in Fig. 4.4. The comparisons are done by plotting the difference $E_{gs}(1/2) - E_{gs}(0)$ as a function of $E_M/(8E_J)$ for different values of E_C. In Fig. 4.4 we fixed $8E_J + E_M = 1$ so $\hbar\omega$ is kept constant throughout each plot; this is done to show the entire range of $E_M/(8E_J)$ in the same plot. As expected, when $E_M/(8E_J) \to 0$ the numerical results (solid black line) agree with the 2π QPS description (dotted-dashed blue line) provided by the tight-binding Hamiltonian (4.4.10). While for larger values of $E_M/(8E_J)$ the 4π QPS description, i.e. that of (4.4.1), is closer to the numerical results. In addition, increasing E_C reduces the range of $E_M/(8E_J)$ in which the 4π QPS description is valid. For instance, in Fig. 4.4a the numerical results agree with the 4π QPS description for all the values $E_M/(8E_J)$ in the plot. While in Fig. 4.4b, this only occurs for $E_M/(8E_J) \in (10^{-4}, 1)$ and; in Fig. 4.4c and Fig. 4.4d for $E_M/(8E_J) \in (10^{-2}, 1)$ and $E_M/(8E_J) \in (0.1, 1)$, respectively.

Fig. 4.4 also shows the results of the 4π QPS description of the junction using the two approximations found for $\nu_{4\pi}$: the small E_M approximation given by Eq. (4.4.9) (purple dashed lines) and the large E_M approximation of Eq. (4.4.5) (gray dotted lines). Finally, Fig. 4.4 shows that as E_C increases the QPS descriptions of the topological Josephson junction become less accurate. This is expected, as all the expressions for the tunneling amplitudes are obtained using the dilute instanton gas approximation which relies on $E_C \ll \hbar\omega$ and thus becomes less accurate as E_C increases.

We can use the numerical results to figure out the range of parameters in which each picture is more appropriate. This is shown in Fig. 4.1a. As it was discussed previously, close to the boundary between the coupled 2π QPS and the 4π QPS regions, both descriptions give similar results.

4.5 Discussion

It is interesting to discuss the implications of our results in the dissipative transition that is expected in this system. [26, 27, 34] This transition was previously studied in Ref. [34], where it was found that the presence of 4π periodic tunneling would reduce the ohmic dissipation needed to restore superconductivity by a factor of 4. However, the results of Ref. [34] assumed that the topological junction could always be described by 4π QPS. In this work, we find that this is not necessarily the case. Consider a junction with fixed E_J and E_C, when $E_M = 0$ the junction is described by 2π QPS, turning on E_M leads to an increasing coupling of this 2π QPS until they become confined into pairs. Following the critical dissipation throughout this same path would lead to a continuous decrease in it until it reaches $1/4$ of the original value at the point where the 2π QPS are fully suppressed. We also find that the critical dissipation needed to stabilize the superconductivity in our model of a topological Josephson junction is dependent on E_C.

An important caveat about using the dissipative phase transition as a mechanism for detecting Majorana modes is that the dissipation induced by quasi-particle tunneling also reduces the critical resistance of non-topological Josephson junctions by a factor of 4. Furthermore, the effects of dissipation induced by quasi-particle tunneling in non-topological Josephson junctions are dependent on the ratio between the Josephson coupling and the charging energy. [27] This is because both the 4π periodic tunneling induced by Majoranas and the quasi-particle tunneling are single particle tunneling processes that break the same symmetry (the 2π periodicity of a non-topological Josephson junction), albeit the difference in coherence. A more careful analysis of dissipation in the topological Josephson junction is required to find whether there are signatures in the dissipative transition that would allow distinguishing between the 4π periodic tunneling induced by Majoranas and the quasi-particle tunneling.

The difference in the effects of 4π periodic vs. quasi-particle tunneling in the dissipative transition is unclear. However, the effects on the charge offset dispersion are clearly different. While both kinds of single particle tunneling turn the system from $2e$ periodic to e periodic, the 4π periodic tunneling opens up a gap (see Eq. 4.4.12), while the quasi-particle tunneling does not [27]. This could be a potential probe to distinguish between the two kinds of single-particle tunneling.

Finally, another important issue to consider is the effect of quasi-particle poising in this system. Since instanton techniques tend to be useful to describe systems coupled to external environments [50], the formalism used in this work could be useful to study the effects of quasi-particle poising.

4.6 Conclusions

We studied the effects of phase fluctuations induced by charging effects in a simple model of a topological Josephson junction. Our model considers both single particle tunneling and pair tunneling, which are, respectively, 4π and 2π periodic with respect to the superconducting phase difference across the junction. We found that when the single particle tunneling is a small component of the total tunneling current there are two possible ways to describe the ground-state of the junction: 1) in terms of 4π QPS or 2) in terms of coupled 2π QPS. We found the tunneling amplitudes for both effective descriptions and compared them to numerical results to determine the range of parameter in which each description is appropriate.

In addition, we discussed the possible implications that our results have for the dissipative phase transition expected in this system. As was previously found by Ref. [34], when the ground-state of the junction is described by 4π QPS we expect the critical resistance needed to make the junction superconducting to be 4 times smaller than the critical resistance needed to make a non-topological junction superconducting. In the regime where tunneling processes between minima separated by 2π are still present in the system we expect the critical transition to be somewhere between these two critical values. Given that increasing the charging energy of the junction may change the tunneling processes present in the system, our results also point towards a charging energy dependence of the critical resistance for the dissipative transition.

Several questions regarding the dissipative transition, particularly in relation to quasi-particle tunneling, remain unanswered. In the future, we will use the formalism developed in this work to obtain a quantitative description of this transition. It would be also interesting to figure out the relation between the results presented in this work and the dominant charging energy limit.

4.7 Acknowlegments

The authors thank D. Van Harlingen and S. Hegde for useful discussion. This material is based upon work supported by NSERC, FQRNT (RRM, TPB), the Secretary of Public Education and the Government of Mexico (RRM) and the National Science Foundation under Grant No. 1745304 (SV).

4.A Path Integral Calculations

4.A.1 4π phase slip amplitude

The calculation of the tunneling amplitude between the different potential minima can be performed using standard semi-classical methods. Despite this, we include the calculation here in detail for completeness, largely following Ref. [42].

We begin by calculating the amplitude to propagate from 0 to 4π in an imaginary time interval $2L$. This is given by the following path integral:

$$(0,-L|4\pi,L)=\int[\mathcal{D}\theta]e^{-\frac{1}{\hbar}\int_{-L}^{L}\mathcal{L}(\theta(\tau))d\tau}, \tag{4.A.1}$$

where $\mathcal{L}(\tau)$ is the Double sine-Gordon (DSG) Lagrangian given by Eq. (4.4.3), which can be rewritten as,

$$\mathcal{L}\left(\theta\right)=M\left(\frac{\left(\partial_{\tau}\theta\right)^{2}}{2}+V(\theta)\right) \tag{4.A.2}$$

with

$$V(\theta)=\omega^{2}\left[\tanh^{2}R\left(1-\cos\theta\right)+4\mathrm{sech}^{2}R\left(1-\cos\frac{\theta}{2}\right)\right] \tag{4.A.3}$$

and

$$\begin{aligned}&M=\hbar^{2}/(8E_{C})\\&\omega=\sqrt{E_{C}\left(8E_{J}+E_{M}\right)}/\hbar\\&\cosh\left(R\right)=\sqrt{(8E_{J}+E_{M})/E_{M}}.\end{aligned} \tag{4.A.4}$$

We expect the leading contribution to the path integral to be from paths of the form

$$\theta\left(\tau\right)=\theta^{cl}\left(\tau\right)+\chi(\tau) \tag{4.A.5}$$

where $\theta^{cl}\left(\tau\right)$ is the path that minimizes the action starting at 0 for $\tau=-L$ and ending at 4π for $\tau=L$, and $\chi(\pm L)=0$. This means $\theta^{cl}\left(\tau\right)$ fulfills the following equation:

$$\frac{dV}{d\theta}\left(\theta^{cl}\left(\tau\right)\right)=\frac{d^{2}\theta^{cl}}{d\tau^{2}}. \tag{4.A.6}$$

In the limit $L \to \infty$, $\theta^{cl}(\tau)$ is given by

$$\theta^{cl} = 4\arctan[e^{\omega(\tau-\tau_0)+R}] + 4\arctan[e^{\omega(\tau-\tau_0)-R}]. \tag{4.A.7}$$

Up to second order in $\chi(\tau)$ the Lagrangian for paths of the form (4.A.5) is

$$\begin{aligned}\mathcal{L}(\theta) =& \mathcal{L}\left(\theta^{cl}\right) + \frac{M}{2}\left(\partial_\tau \chi\right)^2 + \frac{M}{2}\frac{d^2V}{d\theta^2}\left(\theta^{cl}\right)\chi^2 \\ &+ M\partial_\tau(\chi\partial_\tau\theta^{cl}).\end{aligned} \tag{4.A.8}$$

This allows us to split the path integral in Eq. (4.A.1) into two parts:

$$(0, -L|4\pi, L) \approx F\exp\left(-\frac{S^{cl}}{\hbar}\right) \tag{4.A.9}$$

with S^{cl} the action of the instanton,

$$S^{cl} = \int_{-L}^{L} d\tau \mathcal{L}\left(\theta^{cl}\right) \tag{4.A.10}$$

and F contains the sum over Gaussian fluctuations around such instanton. F can be written as

$$F = \int [\mathcal{D}\chi]\exp\left(-\frac{M}{2\hbar}\int_{-L}^{L} d\tau \chi D\chi\right), \tag{4.A.11}$$

with D is the following differential operator:

$$D = -\frac{d^2}{d\tau^2} + \frac{d^2V}{d\theta^2}\left(\theta^{cl}(\tau)\right). \tag{4.A.12}$$

The path integral in Eq. (4.A.11) can be solved expanding χ in terms of the eigenfunctions of the operator D, i.e. taking

$$\chi(\tau) = \sum_n \chi_n y_n(\tau) \tag{4.A.13}$$

with

$$Dy_n(\tau) = \lambda_n y_n. \tag{4.A.14}$$

This leads to

$$F = \mathcal{N} \prod_n \int_{-\infty}^{\infty} \frac{d\chi_n}{\sqrt{2\pi\hbar/M}} e^{-\frac{M\lambda_n\chi_n^2}{2\hbar}} \tag{4.A.15}$$

with $\mathcal{N}$ a normalization constant. However, the above expression in not well defined since the operator D contains a zero mode, λ_0, which leads to a divergence in F. The time τ_0 at which the kink solution is centered is arbitrary which leads to $D\partial_\tau\theta^{cl} = 0$; i.e. the zero mode is a consequence of the time-translational invariance of the system. To deal with this divergence, we use the Fadeev-Popov method to transform the χ_0 integration to a τ_0 integration.

The Fadeev-Popov method consists of inserting

$$1 = \int d\tau_0 \left| \frac{\partial\chi_0}{\partial\tau_0}(\chi_0 = 0) \right| \delta(\chi_0), \tag{4.A.16}$$

into the expression for F given by Eq. 4.A.15:

$$\begin{aligned} F =& \mathcal{N} \prod_{n=1}^{\infty} \int_{-\infty}^{\infty} \frac{d\chi_n}{\sqrt{2\pi\hbar/M}} e^{-\frac{M\lambda_n\chi_n^2}{2\hbar}} \times \\ & \int d\tau_0 \left| \frac{\partial\chi_0}{\partial\tau_0}(\chi_0 = 0) \right| \int \frac{d\chi_0}{\sqrt{2\pi\hbar/M}} \delta(\chi_0) \\ =& \mathcal{N} \prod_{n=1}^{\infty} \int_{-\infty}^{\infty} \frac{d\chi_n}{\sqrt{2\pi\hbar/M}} e^{-\frac{M\lambda_n\chi_n^2}{2\hbar}} \times \\ & \int \frac{d\tau_0}{\sqrt{2\pi\hbar/M}} \left| \frac{\partial\chi_0}{\partial\tau_0}(\chi_0 = 0) \right|. \end{aligned} \tag{4.A.17}$$

The Jacobian $\left|\frac{\partial \chi_0}{\partial \tau_0}(\chi_0 = 0)\right|$ can be found rewriting the path θ so that fluctuations in the direction of the zero mode are traded for an explicit τ_0 dependence:

$$\theta(\tau) = \theta^{cl}\left(\tau - \tau_0\right) + \sum_{n=1}^{\infty} \chi_n y_n \left(\tau - \tau_0\right). \tag{4.A.18}$$

Comparing the above expression for the path with that of Eq. (4.A.5) leads to

$$\chi_0 = f(\tau_0) + \sum_{m=1}^{\infty} \xi_m r_n(\tau_0) \tag{4.A.19}$$

with

$$\begin{aligned} f(\tau_0) &= \int d\tau \left(\theta^{cl}(\tau - \tau_0) - \theta^{cl}(\tau)\right) y_0\left(\tau\right) \\ r_m(\tau_0) &= \int d\tau y_m\left(\tau - \tau_0\right) y_0\left(\tau\right). \end{aligned} \tag{4.A.20}$$

Furthermore, we note that the constraint $\chi_0 = 0$ corresponds to $\tau_0 = 0$ so we obtain:

$$\left|\frac{\partial \chi_0}{\partial \tau_0}(\chi_0 = 0)\right| = \left| f'(0) + \sum_{m=1}^{\infty} \xi_m r'_m(0)\right| \tag{4.A.21}$$

We know $\partial_\tau \theta^{cl} \propto y_0\left(\tau\right)$ since $D\partial_\tau \theta^{cl} = 0$. The proportionality constant can be found using the following expression:

$$\int_{-\infty}^{\infty} d\tau (\partial_\tau \theta^{cl})^2 = \frac{S^{cl}}{M}, \tag{4.A.22}$$

which stems from the fact that $\theta^{cl}(\tau)$ minimizes the action (Eq. (4.A.6)). We use this to find $f'(0)$:

$$f'(0) = -\int d\tau \partial_\tau \theta^{cl}(\tau)\, y_0(\tau) = -\sqrt{\frac{S^{cl}}{M}}. \tag{4.A.23}$$

The appropriate boundaries of integration for τ_0 are $-L$ and L since τ takes values in the interval $(-L, L)$. We then obtain

$$\begin{aligned} F =& \mathcal{N} \prod_{n=1}^{\infty} \int_{-\infty}^{\infty} \frac{d\chi_n}{\sqrt{2\pi\hbar/M}} e^{-\frac{M\lambda_n\chi_n^2}{2\hbar}} \times \\ & \int_{-L}^{L} \frac{d\tau_0}{\sqrt{2\pi\hbar/M}} \left(\sqrt{\frac{S^{cl}}{M}} - \sum_{m=1}^{\infty} \xi_m r'_m(0) \right) \\ =& \mathcal{N} 2L \sqrt{\frac{S^{cl}}{2\pi\hbar}} \frac{1}{\sqrt{\prod'_n \lambda_n}} \end{aligned} \tag{4.A.24}$$

where $\prod'_n$ indicates the product over the eigenvalues taking out the zero eigenvalue.

The normalization constant can be conveniently expressed in terms of the sum over harmonic fluctuations around 0 or 4π. If we define

$$F_0 = \int [\mathcal{D}\chi] \exp\left(-\frac{M}{2\hbar} \int_{-L}^{L} d\tau \chi D_0 \chi \right) \tag{4.A.25}$$

with

$$D_0 = -\frac{d^2}{d\tau^2} + \omega^2. \tag{4.A.26}$$

The normalization constant $\mathcal{N}$ can be written as

$$\mathcal{N} = F_0 \sqrt{\prod_n \lambda_n^0}, \tag{4.A.27}$$

where λ_n^0 are the eigenvalues of the differential operator D_0. F_0, the fluctuation contribution to the imaginary time harmonic oscillator propagator, is readily available in the literature (see e.g. Ref. [42]). For $L \to \infty$ its leading contribution is

$$F_0 = \sqrt{\frac{M\omega}{\pi\hbar}} e^{-\omega L}. \tag{4.A.28}$$

Our expression for F currently includes a ratio between the products of eigenvalues of the operators D_0 and D:

$$F = 2LF_0\sqrt{\frac{S^{cl}}{2\pi\hbar}}\sqrt{\frac{\prod_n \lambda_n^0}{\prod_n' \lambda_n}}, \tag{4.A.29}$$

which can be evaluated using the Gelfand-Yaglom formula. Following Ref. [42] we have

$$\frac{\prod_n \lambda_n^0}{\prod_n' \lambda_n} = \frac{2M\omega\eta^2}{S^{cl}}, \tag{4.A.30}$$

where η is defined by the asymptotic behavior of the classical solution:

$$\partial_\tau \theta^{cl} \to \eta e^{-\omega|\tau|} \quad \text{for } \tau \to \pm\infty. \tag{4.A.31}$$

To the leading order the amplitude to propagate from 0 to 4π in an imaginary time interval $2L$ is then:

$$(0, -L|4\pi, L) \approx 2LF_0\eta\sqrt{\frac{M\omega}{\pi\hbar}}e^{-\frac{S^{cl}}{\hbar}}. \tag{4.A.32}$$

However, the leading order contribution is not enough to obtain the level splitting. It is possible to obtain a more precise expression for the amplitude using the dilute instanton gas approximation.

Under the dilute instanton gas approximation, we sum over paths consisting of combinations of kinks and anti-kinks and quadratic fluctuations around them, i.e.

$$\theta(\tau) = \sum_{n=0}^{2N} \nu_n \theta^{cl}(\tau - \tau_n) + \chi(\tau) \tag{4.A.33}$$

where $\nu_n = \pm 1$ ($+$ for kinks and $-$ for anti-kinks) and $\sum_n \nu_n = 1$. The approximation consist of considering that the centers of the kinks and anti-kinks, i.e. τ_n are sufficiently spread out to make kink-kink interactions negligible. The obtained result is

$$\begin{aligned}(0,-L|4\pi,L) &= \sum_n \frac{F_0\left(2L\eta\sqrt{\frac{M\omega}{\pi\hbar}}e^{-\frac{S^{cl}}{\hbar}}\right)^{2n+1}}{(2n+1)!} \\ &= F_0\sinh\left(2L\eta\sqrt{\frac{M\omega}{\pi\hbar}}e^{-\frac{S^{cl}}{\hbar}}\right).\end{aligned} \tag{4.A.34}$$

The spectral representation of the amplitude (4.A.1) is

$$(0,-L|4\pi,L) = \sum_n \psi_n(0)\psi_n(4\pi)e^{-2LE_n/\hbar}. \tag{4.A.35}$$

Considering two groundstate levels of harmonic oscillators with frequency ω and mass M, one centered around 0 and other around 4π, which can tunnel to each other with amplitude ν, we have

$$\begin{aligned}\psi_1(\theta) &= \frac{1}{\sqrt{2}}\left(\psi_0(\theta)+\psi_{4\pi}(\theta)\right) \quad E_1 = \frac{\hbar\omega}{2}-\nu \\ \psi_2(\theta) &= \frac{1}{\sqrt{2}}\left(\psi_0(\theta)-\psi_{4\pi}(\theta)\right) \quad E_2 = \frac{\hbar\omega}{2}+\nu.\end{aligned} \tag{4.A.36}$$

In the above expression $\psi_0(\theta)$ and $\psi_{4\pi}(\theta)$ are the groundstate wavefunctions of harmonic oscillators centered around 0 and 4π, respectively, e.g.

$$\psi_0(\theta) = \left(\frac{M\omega}{\pi\hbar}\right)^{1/4} e^{-\frac{M\omega\theta^2}{2\hbar}}. \tag{4.A.37}$$

The amplitude (4.A.1) for such system would then be

$$(0,-L|4\pi,L) = \sqrt{\frac{M\omega}{\pi\hbar}}e^{-L\omega}\sinh\left(2L\nu/\hbar\right). \tag{4.A.38}$$

Comparing expressions (4.A.34) and (4.A.38) allows us to conclude

$$\nu = \hbar\eta\sqrt{\frac{M\omega}{\pi\hbar}}\exp\left(-\frac{S^{cl}}{\hbar}\right). \tag{4.A.39}$$

For the kink in equation (4.A.7) we have:

$$\begin{aligned} S^{cl} =& 16M\omega\left(1 + 2R\,\mathrm{csch}\,2R\right) \\ \eta =& 8\omega\cosh R. \end{aligned} \tag{4.A.40}$$

Substituting the values of M, ω and R from Eq. (4.A.4) we obtain

$$\nu_{4\pi} = \sqrt{\frac{8(\hbar\omega)^5}{\pi E_M E_C^2}}\exp\left(-\frac{\hbar\omega}{E_C}\times f\left(\frac{E_M}{8E_J}\right)\right) \tag{4.A.41}$$

with

$$f\left(x\right) = 2 + \frac{2x}{\sqrt{1+x}}\coth^{-1}\left(\sqrt{1+x}\right). \tag{4.A.42}$$

4.A.2 Emergent translational mode correction for the 4π phase slip amplitude.

Here, we follow the procedure outlined in Ref. [48] to introduce corrections to the previously found expression for $\nu_{4\pi}$. This section then follows the work done in Ref. [48] closely. We include the calculation here for clarity as the work in Ref. [48] was done in the context of classical statistical mechanics. We also note that Ref. [48] claims, incorrectly, that this procedure leads to a non-divergent expression. Here, we find otherwise.

When $E_M \to 0$, the expression for ν found in 4.A.1 diverges. This occurs because one of the eigenmodes of the operator D, which we will call λ_1 approaches 0 when $E_M \to 0$. Physically, the two 2π kinks decouple turning the distance between the two

2π kinks $2R$ into another translation mode. We must then have

$$y_1(\tau) \to \partial_R(\theta^{cl}) \text{ when } E_M \to 0 \tag{4.A.43}$$

This means that we can deal with the effects of the emergent translational mode by writing the path as

$$\begin{aligned}\theta(\tau) =& \theta^{cl}(\tau) + \sum_{n=0}^{\infty} \chi_n y_n(\tau) \\ =& \sigma(\tau - \tau_0, r) + \sum_{n=2}^{\infty} \chi_n y_n(\tau - \tau_0)\end{aligned} \tag{4.A.44}$$

with

$$\sigma(\tau, r) = 4\arctan[e^{\omega\tau + r}] + 4\arctan[e^{\omega\tau - r}]. \tag{4.A.45}$$

For $R = r$ we recover the classical solution, i.e. $\sigma(\tau, R) = \theta^{cl}(\tau)$. We should note that Eq. 4.A.44, and thefore the rest this appendix, relies on $y_1 \approx \partial_R(\theta^{cl})$. This is a valid assumption when $R > 1.25$.[47, 48]

Up to second order in $\chi = \sum_{n=2}^{\infty} \chi_n y_n(\tau - \tau_0) = 0$ the Lagrangian for the above path is given by:

$$\frac{\mathcal{L}(\sigma, \chi)}{M} = \frac{(\partial_\tau \sigma + \partial_\tau \chi)^2}{2} + V_0(\sigma) + \chi V_1(\sigma) + \chi^2 V_2(\sigma), \tag{4.A.46}$$

where $V_0(\sigma) = V(\sigma)$ is the potential of σ given by Eq. (4.A.3) and

$$\begin{aligned}V_1(\sigma) =& \frac{\omega^2}{\cosh^2(R)}\left(\sinh^2(R)\sin\sigma + 2\sin\frac{\sigma}{2}\right) \\ V_2(\sigma) =& \frac{\omega^2}{\cosh^2(R)}\left(\frac{1}{2}\sinh^2(R)\cos\sigma + \frac{1}{2}\cos\frac{\sigma}{2}\right).\end{aligned} \tag{4.A.47}$$

The action of this path can be written as

$$S(\sigma, \chi) = S_0(r) + S_1(\sigma, \chi) \tag{4.A.48}$$

with $S_0(r)$ and $S_1(\sigma, \chi)$ given by:

$$\begin{aligned} S_0(r) =& M \int d\tau \left(\frac{1}{2} (\partial_\tau \sigma)^2 + V_0(\sigma) \right) \\ =& 8M\omega \left(1 + \frac{\tanh^2 R}{\tanh^2 r} + \frac{2r}{\sinh 2r} + \right. \\ & \left. + \frac{2r \coth r}{\cosh^2 R} - \frac{r \tanh^2 R \coth r}{\sinh^2 r} \right) \\ S_1(\sigma, \chi) =& M \int d\tau \left(-\partial_\tau \sigma + V_1(\sigma) \right) \chi \\ & + M \int d\tau \left(\frac{1}{2} (\partial_\tau \chi)^2 + V_2(\sigma) \chi^2 \right). \end{aligned} \tag{4.A.49}$$

Using the Fadeev-Popov method to transform from the coordinates χ_0 and χ_1 to τ_0 and r leads to

$$\begin{aligned} (0, -L | 4\pi, L) =& \mathcal{N} \int \int \frac{d\tau_0 dr}{2\pi\hbar/M} \left| \frac{\partial \chi_0 \partial \chi_1}{\partial \tau_0 \partial r} \right| \Bigg|_{\chi_0, \chi_1 = 0} \\ & \prod_{n=2}^{\infty} \int \frac{d\chi_n}{\sqrt{2\pi\hbar/M}} e^{-S_0(r)/\hbar - S_1(\sigma,\chi)/\hbar} \end{aligned} \tag{4.A.50}$$

Following Ref. [48], we make the approximations:

$$\begin{aligned} & \left| \frac{\partial \chi_0 \partial \chi_1}{\partial \tau_0 \partial r} \right| \Bigg|_{\chi_0, \chi_1 = 0} \approx \sqrt{\int d\tau (\partial_\tau \sigma)^2 \times \int d\tau (\partial_r \sigma)^2} \\ & \int \prod_{n=2}^{\infty} \frac{d\chi_n}{\sqrt{2\pi\hbar/M}} e^{-S_1(\sigma,\chi)/\hbar} \approx \frac{1}{\sqrt{\prod_n'' \lambda_n}} \end{aligned} \tag{4.A.51}$$

where the λ_ns are the eigenmodes of the operator $\mathcal{D}$ from the Eq. 4.A.12, and the product $\prod_n''$ skips the 0 eigenmode and λ_1.

Under these approximations, we can write

$$(0, -L|4\pi, L) = F' K 2L \tag{4.A.52}$$

with,

$$F' = \frac{\mathcal{N}}{\sqrt{\prod_n'' \lambda_n}} = F_0 \sqrt{\frac{\prod_n \lambda_n^0}{\prod_n'' \lambda_n}} = F_0 \eta \sqrt{\frac{2M\omega}{S^{cl}}} \sqrt{\lambda_1} \tag{4.A.53}$$

and

$$\begin{aligned} K = \int_0^{L\omega} dr \frac{M\sqrt{\int d\tau (\partial_\tau \sigma)^2 \times \int d\tau (\partial_r \sigma)^2}}{2\pi\hbar} \\ e^{-S_0(r)/\hbar} \int_{-L+\frac{r}{\omega}}^{L-\frac{r}{\omega}} \frac{d\tau_0}{2L}. \end{aligned} \tag{4.A.54}$$

Using the following result from Ref. [47]:

$$\begin{aligned} \sqrt{\int d\tau (\partial_\tau \sigma)^2 \times \int d\tau (\partial_r \sigma)^2} = \\ 16\sqrt{1 - 4r^2 \mathrm{csch}^2 2r}. \end{aligned} \tag{4.A.55}$$

and performing the τ_0 integration gives

$$K = \int_0^{L\omega} dr \frac{16M(\omega L - r)\sqrt{1 - 4r^2 \mathrm{csch}^2 2r}}{2\pi\hbar\omega L} e^{\frac{-S_0(r)}{\hbar}}. \tag{4.A.56}$$

It is possible to calculate λ_1 by noting that calculating K using a quadratic approximation on $\rho = r - R$ gives

$$K_0 = \sqrt{\frac{S^{cl}}{2\pi\hbar}} \frac{1}{\sqrt{\lambda_1}} e^{-\frac{S^{cl}}{\hbar}} \tag{4.A.57}$$

Expanding $S_0(r)$ up to second order in ρ leads to

$$\begin{aligned} S_0(\rho) =& S^{cl} + 2M\omega\rho^2 \text{csch}^3 R \text{sech}^3 R \times \\ & (4\sinh 2R - 4R + \sinh 4R - 8R\cosh 2R) \end{aligned} \tag{4.A.58}$$

We then find

$$\begin{aligned} K_0 &= \int_{-\infty}^{\infty} d\rho \frac{M16\sqrt{1-4R^2\text{csch}^2 2R}}{2\pi\hbar} e^{-\frac{S_0(\rho)}{\hbar}} \\ &= \sqrt{\frac{M}{\hbar\omega\pi}} g(R) e^{-\frac{S^{cl}}{\hbar}} \end{aligned} \tag{4.A.59}$$

with

$$g(R) = \frac{\sinh 2R\sqrt{2-8R^2\text{csch}^2 2R}}{\sqrt{\cosh 2R - R\tanh R - 3R\coth R + 2}} \tag{4.A.60}$$

Note that the factor $(1-\frac{r}{L})$ from Eq. (4.A.56) goes to 1 in the Eq. (4.A.59) as we are taking the $L \to \infty$ limit. The vanishing eigenvalue λ_1 is then

$$\sqrt{\lambda_1} = \sqrt{\frac{S^{cl}}{2\pi\hbar}} \frac{e^{-\frac{S^{cl}}{\hbar}}}{K_0} = \sqrt{\frac{S^{cl}\omega}{2M}} \frac{1}{g(R)}, \tag{4.A.61}$$

which leads to

$$(0, -L|4\pi, L) = 2LF_0 \frac{\eta\omega}{g(R)} K \tag{4.A.62}$$

Using the dilute instanton gas approximation (see previous section), this result leads to the tunneling amplitude

$$\nu_{4\pi} = \hbar \frac{\eta\omega}{g(R)} K = \frac{8\hbar\omega^2\cosh R}{g(R)} K. \tag{4.A.63}$$

Taking L to infinity results in

$$K = \frac{8M}{\pi\hbar}\mathcal{I}\left(R, \tfrac{\hbar\omega}{E_C}\right) = \frac{\hbar}{\pi E_C}\mathcal{I}\left(R, \tfrac{\hbar\omega}{E_C}\right), \tag{4.A.64}$$

with $\mathcal{I}(R, \alpha)$ defined by Eq. (4.4.6c). Our final expression for ν is

$$\nu = \frac{8(\hbar\omega)^2 \cosh R}{g(R)\pi E_C}\mathcal{I}\left(R, \tfrac{\hbar\omega}{E_C}\right). \tag{4.A.65}$$

which corresponds to the expression in the main text (Eq. 4.4.6) since $F(R) = 2\cosh R/g(R)$.

4.B Approximate expressions for $\mathcal{I}(R, \alpha)$

4.B.1 Validity of the harmonic approximation

Taking $r = R + y/\sqrt{\alpha S_R''(R)}$ we can write the saddle point expansion of $\mathcal{I}(R, \alpha)$ as

$$\begin{aligned}
\mathcal{I}(R, \alpha) \approx \int_{-\infty}^{\infty} & \frac{dy\sqrt{1 - 4R^2\text{csch}^2 2R}e^{-\alpha S_R(R)}}{\sqrt{\alpha S_R''(R)}} \\
& \times e^{-y^2/2}\left(1 + \sum_{n=1}^{\infty}\frac{p_n(y, R)}{(\alpha S_R''(R))^{n/2}}\right) \\
=& e^{-\alpha S_R(R)}\sqrt{\frac{2\pi(1 - 4R^2\text{csch}^2 2R)}{\alpha S_R''(R)}} \\
& \times\left(1 + \sum_{n=1}^{\infty}\frac{C_n(R)}{(\alpha S_R''(R))^n}\right).
\end{aligned} \tag{4.B.1}$$

In the above equation the $p_n(y, R)$ are odd/even polynomials in y when n is even/odd, and the $C_n(R)$ are functions of R which can be expressed in terms of derivatives of $S_R(r)$ and $\sqrt{1 - 4r^2\text{csch}^2 2r}$ evaluated at $r = R$.

The expression for $\mathcal{I}\left(R,\alpha\right)$ in Eq. (4.4.7) corresponds to the first term in the above saddle point expansion; therefore, it is a valid approximation if $1/(\alpha S_R''(R)) \ll 1$. The function $1/S_R''(R)$ diverges for $R \to 0$ and for $R \to \infty$ making the approximation for both small and large R. However, since Eq. 4.4.6 was obtained to address the large R divergence, we only need to find the upper R limit for the validity of expression (4.4.7). Since

$$\frac{1}{\alpha S_R''(R)} = \frac{e^{2R}}{16\alpha} + \mathcal{O}(R), \tag{4.B.2}$$

Eq. (4.4.7) is valid when $e^{2R} \ll 16\alpha$. This condition makes the tunneling expression of Eq. 4.4.5 valid for $E_M/(8E_J) \gg E_C/(4\hbar\omega)$

4.B.2 Large *R* limit

To find an approximate expression for $\mathcal{I}\left(R,\alpha\right)$ in the large R limit, we note that $S_R(r)$ grows linearly with r for large r. Furthermore, the slope of the large r linear behavior as R increases. This means that, when R is large, the largest contribution to $\mathcal{I}\left(R,\alpha\right)$ will come from the large r linear behavior. We start by writing the following large r expansions:

$$\begin{aligned} S_R(r) &= 1 + \tanh^2 R + 2r\,\mathrm{sech}^2 R \\ &+ 4e^{-2r}\left(2r\mathrm{sech}^2 R + \tanh^2 R\right) + \mathcal{O}(e^{-4r}) \\ \sqrt{1 - 4r^2\mathrm{csch}^2 2r} &= 1 + \mathcal{O}(e^{-4r}) \end{aligned} \tag{4.B.3}$$

This means we can expand $\mathcal{I}\left(R,\alpha\right)$ as

$$\begin{aligned}\mathcal{I}\left(R,\alpha\right) = \int_0^\infty dr e^{-\alpha(1+\tanh^2 R + 2r\,\mathrm{sech}^2 R)}\,(1- \\ \alpha 4 e^{-2r}\left(2r\mathrm{sech}^2 R + \tanh^2 R\right) + \mathcal{O}(e^{-4r})\big) \\ = \mathcal{I}_0\left(R,\alpha\right) + \mathcal{I}_1\left(R,\alpha\right) + ...\end{aligned} \tag{4.B.4}$$

where

$$\mathcal{I}_0\left(R,\alpha\right) = \frac{\cosh^2 R e^{-\alpha\left(\tanh^2 R + 1\right)}}{2\alpha} \tag{4.B.5}$$

corresponds to the approximation to $\mathcal{I}\left(R,\alpha\right)$ cited in Eq. (4.4.8) and $\mathcal{I}_1\left(R,\alpha\right)$ is a leading order correction which we calculate to determine the range of validity of Eq. (4.4.8).

Performing the r interaction gives

$$\mathcal{I}_1(R,\alpha) = \frac{-2\alpha(\alpha\tanh^2 R\mathrm{sech}^2 R + 1)e^{-\alpha\tanh^2 R - \alpha}}{\left(\alpha\mathrm{sech}^2 R + 1\right)^2}, \tag{4.B.6}$$

and we obtain:

$$\frac{\mathcal{I}_1(R,\alpha)}{\mathcal{I}_0(R,\alpha)} \sim 16\alpha^2 e^{-2R} \sim 4\alpha^2 \frac{E_M}{8E_J}. \tag{4.B.7}$$

The approximation is valid when $16\alpha^2 e^{-2R} \ll 1$. For R given by Eq. (4.4.4b) and $\alpha = \hbar\omega/E_C$ this is equivalent to $E_M/(8E_J) \ll 0.25 E_C^2/(\hbar\omega)^2$.

For $\mathcal{I}\left(R,\alpha\right) \approx \mathcal{I}_0\left(R,\alpha\right)$ we obtain

$$\nu_{4\pi} = \frac{f_2\left(\frac{E_M}{8E_J}\right)\left(\hbar\omega\right)^3}{\pi E_C E_M} \exp\left[-\frac{\hbar\omega}{E_C} \times f_1\left(\frac{E_M}{8E_J}\right)\right] \tag{4.B.8}$$

with

$$\begin{aligned} f_1(x) =& \frac{2+x}{1+x} \\ f_2(x) =& \left[\frac{6(x+1)}{\frac{x}{\sqrt{x+1}} \log\left(\frac{\sqrt{x+1}+1}{\sqrt{x}}\right) + 1} \right. \\ & \left. + \frac{2}{\frac{x}{\sqrt{x+1}} \log\left(\frac{\sqrt{x+1}+1}{\sqrt{x}}\right) - 1} \right]^{1/2}. \end{aligned} \tag{4.B.9}$$

4.C Decoupling of 4π phase slips.

As it has been previously noted, the expression for $\nu_{4\pi}$ in Eq. (4.4.9) diverges when $E_M \to 0$. In this appendix, we will show that it is possible to recover the decoupling of the 4π phase slips into two 2π phase slips from Eq. (4.A.63). This is achieved by changing the order in which the limits $E_M \to 0$ and $L \to 0$ are taken.

Expanding F' and K around $x = E_M/(8E_J) = 0$ leads to

$$\begin{aligned} F' &= F_0\omega^2 \left(4 + x\left(3 - 2\log\left(\frac{x}{4}\right)\right) + \mathcal{O}(x^2)\right) \\ K &= \frac{4LM\omega e^{-\frac{16M\omega}{\hbar}}}{\pi\hbar} \\ &\quad - \frac{16x\left(2LM^2\omega^2(2L\omega - 3)e^{-\frac{16M\omega}{\hbar}}\right)}{3\left(\pi\hbar^2\right)} + \mathcal{O}\left(x^2\right) \end{aligned} \tag{4.C.1}$$

Then, when $E_M \to 0$,

$$(0, -L|4\pi, L) \to F_0 \frac{8(2L)^2 M\omega^3 e^{-\frac{16M\omega}{\hbar}}}{\pi\hbar} \tag{4.C.2}$$

The tunneling amplitude between 0 and 2π in a non-topological Josephson junction can be written as

$$\nu_{2\pi} = 4\omega\sqrt{\frac{\hbar M\omega}{\pi}}e^{-\frac{8M\omega}{\hbar}}. \tag{4.C.3}$$

This leads to

$$(0, -L|4\pi, L) \to F_0\frac{(2L)^2}{2}\left(\frac{\nu_{2\pi}}{\hbar}\right)^2 \tag{4.C.4}$$

which is the expected result for propagating between 0 to 4π through two uncoupled 2π phase slips. The $\frac{1}{2}$ factor arises from time ordering the phase slips, i.e.

$$\int_{-L}^{L} d\tau_1 \int_{\tau_1}^{L} d\tau_2 = \frac{(2L)^2}{2}. \tag{4.C.5}$$

References

[1]T. Senthil, Annual Review of Condensed Matter Physics **6**, 299–324 (2015).

[2]F. D. M. Haldane, Rev. Mod. Phys. **89**, 040502 (2017).

[3]R. M. Lutchyn, J. D. Sau, and S. Das Sarma, Phys. Rev. Lett. **105**, 077001 (2010).

[4]Y. Oreg, G. Refael, and F. von Oppen, Phys. Rev. Lett. **105**, 177002 (2010).

[5]S. D. Sarma, M. Freedman, and C. Nayak, Npj Quantum Information **1**, Review Article, 15001 (2015).

[6]A. Y. Kitaev, Physics-Uspekhi **44**, 131 (2001).

[7]S. M. Albrecht, A. P. Higginbotham, M. Madsen, F. Kuemmeth, T. S. Jespersen, J. Nygård, P. Krogstrup, and C. M. Marcus, Nature **531**, 206 (2016).

[8]H. Zhang, Ö. Gül, S. Conesa-Boj, K. Zuo, V. Mourik, F. K. de Vries, J. van Veen, D. J. van Woerkom, M. P. Nowak, M. Wimmer, D. Car, S. Plissard, E. P. A. M. Bakkers, M. Quintero-Pérez, S. Goswami, K. Watanabe, T. Taniguchi, and L. P. Kouwenhoven, ArXiv e-prints (2016).

[9]M. T. Deng, S. Vaitiekenas, E. B. Hansen, J. Danon, M. Leijnse, K. Flensberg, J. Nygård, P. Krogstrup, and C. M. Marcus, Science **354**, 1557–1562 (2016).

[10]A. D. K. Finck, D. J. Van Harlingen, P. K. Mohseni, K. Jung, and X. Li, Phys. Rev. Lett. **110**, 126406 (2013).

[11]A. Das, Y. Ronen, Y. Most, Y. Oreg, M. Heiblum, and H. Shtrikman, Nature Physics **8**, Article, 887 (2012).

[12]H. O. H. Churchill, V. Fatemi, K. Grove-Rasmussen, M. T. Deng, P. Caroff, H. Q. Xu, and C. M. Marcus, Phys. Rev. B **87**, 241401 (2013).

[13] M. T. Deng, C. L. Yu, G. Y. Huang, M. Larsson, P. Caroff, and H. Q. Xu, Nano Letters **12**, PMID: 23181691, 6414–6419 (2012).

[14] V. Mourik, K. Zuo, S. M. Frolov, S. R. Plissard, E. P. A. M. Bakkers, and L. P. Kouwenhoven, Science **336**, 1003–1007 (2012).

[15] L. P. Rokhinson, X. Liu, and J. K. Furdyna, Nature Physics **8**, 795 (2012).

[16] T. Hyart, B. van Heck, I. C. Fulga, M. Burrello, A. R. Akhmerov, and C. W. J. Beenakker, Phys. Rev. B **88**, 035121 (2013).

[17] K. Flensberg, Phys. Rev. Lett. **106**, 090503 (2011).

[18] P. Bonderson, and R. M. Lutchyn, Phys. Rev. Lett. **106**, 130505 (2011).

[19] B. van Heck, A. R. Akhmerov, F. Hassler, M. Burrello, and C. W. J. Beenakker, New Journal of Physics **14**, 035019 (2012).

[20] D. Aasen, M. Hell, R. V. Mishmash, A. Higginbotham, J. Danon, M. Leijnse, T. S. Jespersen, J. A. Folk, C. M. Marcus, K. Flensberg, and J. Alicea, Phys. Rev. X **6**, 031016 (2016).

[21] T. Karzig, C. Knapp, R. M. Lutchyn, P. Bonderson, M. B. Hastings, C. Nayak, J. Alicea, K. Flensberg, S. Plugge, Y. Oreg, C. M. Marcus, and M. H. Freedman, Phys. Rev. B **95**, 235305 (2017).

[22] F. Hassler, and D. Schuricht, New Journal of Physics **14**, 125018 (2012).

[23] A. Chew, A. Essin, and J. Alicea, Phys. Rev. B **96**, 121119 (2017).

[24] K. K. Likharev, and A. B. Zorin, Journal of Low Temperature Physics **59**, 347–382 (1985).

[25] D. V. Averin, A. B. Zorin, and K. K. Likharev, Zh. Eksp. Teor. Fiz **88**, 692–703 (1985).

[26]S. V. Panyukov, and A. D. Zaikin, Journal of Low Temperature Physics **73**, 1–32 (1988).

[27]G. Schön, and A. Zaikin, Physics Reports **198**, 237–412 (1990).

[28]H.-J. Kwon, K. Sengupta, and V. M. Yakovenko, The European Physical Journal B - Condensed Matter and Complex Systems **37**, 349–361 (2004).

[29]L. Fu, and C. L. Kane, Phys. Rev. B **79**, 161408 (2009).

[30]H.-J. Kwon, V. M. Yakovenko, and K. Sengupta, Low Temperature Physics **30**, 613–619 (2004).

[31]D. M. Badiane, L. I. Glazman, M. Houzet, and J. S. Meyer, Comptes Rendus Physique **14**, 840–856 (2013).

[32]D. Pekker, C.-Y. Hou, D. L. Bergman, S. Goldberg, İ. Adagideli, and F. Hassler, Phys. Rev. B **87**, 064506 (2013).

[33]Z.-T. Zhang, Z.-Y. Xue, and Y. Yu, ArXiv e-prints (2017).

[34]P. Matthews, P. Ribeiro, and A. M. García-García, Phys. Rev. Lett. **112**, 247001 (2014).

[35]C. Kurter, A. D. K. Finck, Y. S. Hor, and D. J. Van Harlingen, Nature Communications **6**, Article, 7130 (2015).

[36]J. Wiedenmann, E. Bocquillon, R. S. Deacon, S. Hartinger, O. Herrmann, T. M. Klapwijk, L. Maier, C. Ames, C. Brüne, C. Gould, A. Oiwa, K. Ishibashi, S. Tarucha, H. Buhmann, and L. W. Molenkamp, Nature Communications **7**, 10303 (2016).

[37]V. Bouchiat, D. Vion, P. Joyez, D. Esteve, and M. H. Devoret, Physica Scripta **1998**, 165 (1998).

[38]Y. Makhlin, G. Schön, and A. Shnirman, Rev. Mod. Phys. **73**, 357–400 (2001).

[39] D. Vion, A. Aassime, A. Cottet, P. Joyez, H. Pothier, C. Urbina, D. Esteve, and M. H. Devoret, Science **296**, 886–889 (2002).

[40] J. Koch, T. M. Yu, J. Gambetta, A. A. Houck, D. I. Schuster, J. Majer, A. Blais, M. H. Devoret, S. M. Girvin, and R. J. Schoelkopf, Phys. Rev. A **76**, 042319 (2007).

[41] S. M. Girvin, in *Quantum machines: measurement and control of engineered quantum systems: lecture notes of the les houches summer school: volume 96, july 2011* (Oxford University Press, 2014) Chap. 3.

[42] H. Kleinert, in *Path integrals in quantum mechanics, statistics, polymer physics, and financial markets*, 3rd (WORLD SCIENTIFIC, 2013) Chap. 17, pp. 1103–1202.

[43] H. J. W. Müller-Kirsten, in *Introduction to quantum mechanics*, 2nd (WORLD SCIENTIFIC, 2013) Chap. 26, pp. 783–822.

[44] G. Mussardo, V. Riva, and G. Sotkov, Nuclear Physics B **687**, 189–219 (2004).

[45] K. M. Leung, Phys. Rev. B **26**, 226–244 (1982).

[46] J. Singh, in *Quantum mechanics* (Wiley-VCH Verlag GmbH, 2007), pp. 126–169.

[47] C. R. Willis, M. El-Batanouny, S. Burdick, R. Boesch, and P. Sodano, Phys. Rev. B **35**, 3496–3505 (1987).

[48] C. R. Willis, M. El-Batanouny, R. Boesch, and P. Sodano, Phys. Rev. B **40**, 686–697 (1989).

[49] G. Rastelli, Phys. Rev. A **86**, 012106 (2012).

[50] A. J. Leggett, S. Chakravarty, A. T. Dorsey, M. P. A. Fisher, A. Garg, and W. Zwerger, Rev. Mod. Phys. **59**, 1–85 (1987).

5

Conclusions

5.1 Summary of results

This thesis studied Josephson junctions with unusual energy/phase difference relations, which arose from unconventional pairing symmetries (Chapter 2) or from topological superconductivity (Chapters 3 and 4). This work dealt with how such unusual energy/phase difference relations arise and how they can be probed via Josephson junction loops and architectures. Our work also translated many of the available concepts of conventional arrays of Josephson junctions to a topological context.

Chapter 2 of this work focused on deriving the energy/phase difference relation relation from a microscopic model. The model studied consisted of a tunnel junction between an $s_{\pm}$ superconductor and a single band s-wave superconductor. A key ingredient of this model was that it considered variations of the order parameter close to the junction. This was done using a self-consistent Bogoliubov-deGennes formalism. We found four different types of their energy/phase difference relation: (i) 0-junction, (ii) π-junction, (iii) ϕ-junction, and (iv) a double minimum junction. The main result of this work is that when the system was close to frustration, i.e. when the s superconductor interacted comparably with both parts of the $s_\pm$ Fermi surface, allowing the order parameter to vary close to the junction had striking consequences in the energy/phase difference relation of the junction. Particularly, the double minimum junction behavior only appeared when variations in the order parameter were accounted for. Although the focus of Chapter 2 was mainly on the derivation of the energy/phase difference relation, we also studied how to probe these relations by flux threading an $s_\pm$-s loop. In such case, the visibility of the effects of double-minimum junctions improved for loops with large inductance. This work highlights the role of the Josephson effect as a probe of unconventional pairing symmetries. It also speaks to the importance of using and developing microscopic models that take into account order parameter variations, particularly in systems with Josephson frustration.

Chapter 3 moved away from microscopic derivations of the energy/phase difference relation and focused on how this relation can be probed. To do this, we constructed a topological version of Josephson junction rings consisting of a flux threaded loop of N identical topological superconductors. We modeled the tunneling between the superconductors to include both pairs (conventional Josephson effect), and single particles (4π periodic Josephson effect) enabled by the topological nature of the superconductors. We showed that the visibility of the single particle tunneling can be increased by increasing the number of superconductors in the loop. This visibility enhancement is relatively insensitive to disorder in the couplings between the junctions. In addition, we studied a Josephson ring-quantum dot hybrid architecture in which the topological Josephson junction ring is tunnel coupled to a quantum dot. In this hybrid system, tuning the occupation energy of the quantum dot enables changes in its flux periodicity. Such tunneling cannot be explained through trivial Andreev bound-states. In addition, quasi-particle poisoning can be prevented in this system via increasing the energy cost of adding particles to the superconductors. Thus, the studied Josephson ring-quantum dot hybrid architecture addresses most of the caveats that prevent the identification of the 4π periodic tunneling.

Finally, in Chapter 4, we focused on studying small charging energy effects in a single topological junction. As in Chapter 3, the junction was modeled considering only the behavior of the macroscopic degrees of freedom – the superconducting phase and the particle number. Also as in Chapter 3, the model of the junction considered both single particle and pair tunneling. We found two possible effective models for the ground-state of the junction though identifying which macroscopic quantum tunneling processes contribute to its charge offset dispersion. We also calculated the effective tunneling amplitudes and discussed the parameter regimes in which each model is valid. The main result of this work is that if the single particle tunneling is a small component of the total current increasing the charging energy may change which macroscopic quantum tunneling processes contribute to the charge offset dispersion. This signals a likely charging energy dependence of the critical resistance for the dissipative transition expected in this system.

5.2 Future directions

This thesis presented three studies that exhibit 1) the Josephson effect as a probe for unconventional/topological superconductivity and 2) the importance of considering fluctuations and variations of the order parameter in such settings. Here, we will discuss some possible extensions of our work.

A main caveat of the work presented in Chapter 2 is that while it presents microcospic evidence of a phase originally predicted through a phenomenological Ginzburg-Landau theory (the double minimum junction), it fails to provide experimental ways to find such behavior. This is because the main microscopic controls to tune into this phase are the tunneling amplitude between the s superconductor and each of the $s_{\pm}$ bands and the strength of the superconducting pairing. Tuning these parameters in an experiment seems highly unrealistic. However, in iron-based superconductors pressure can be used to tune the ration between strength of the superconducting pairing and the bandwidth. It might then be worth considering whether pressure can be used as parameter to tune this behavior experimentally.

An interesting direction based on the results from Chapter 3 would be to modify the topological Josephson junction with the aim of making it a realistic model of a 1D topological superconductor. This could improve our understanding of the effects of phase fluctuations in 1D topological superconductors. Additionally, it would be interesting to study the behavior of the systems in Chapters 3 and 4 in the dominant charging energy limit.

The results of Chapter 4 highlight the importance to extend current studies of the dissipative transition on topological Josephson junction. Furthermore, the instanton formalism used in this Chapter is well suited to study dissipative effects such as quasi-particle poisoning. Hence, it would be interesting to study extended models of the junction studied in Chapter 4 that include ohmic dissipation, dissipation due to quasi-particle tunneling through the junction and/or quasi-particle poisoning. Finally, it would be interesting to see if the results of Chapter 4 can be used to assess the viability of some of the proposed schemes that use tunnel junctions to manipulate Majoranas.